

**ELECTRO-MECHANICAL STRESS ANALYSIS OF
CURRENT CARRYING CONDUCTORS**

BY

HAFIZUR RAHMAN



A THESIS

SUBMITTED TO THE

DEPARTMENT OF ELECTRICAL AND ELECTRONIC ENGINEERING
IN PARTIAL FULFILMENT OF THE REQUIREMENTS FOR THE

DEGREE OF

MASTER OF SCIENCE IN ELECTRICAL AND ELECTRONIC ENGINEERING.



DEPARTMENT OF ELECTRICAL AND ELECTRONIC ENGINEERING
BANGLADESH UNIVERSITY OF ENGINEERING AND TECHNOLOGY

DHAKA-1000, BANGLADESH.



CERTIFICATE

This is to certify that this work has been done by me and has not been submitted elsewhere for the award of any degree or diploma.

Signature of the candidate.



Hafizur Rahman.

The board of examiners hereby recommends to the Department of Electrical and Electronic Engineering, B.U.E.T, Dhaka, the acceptance of the thesis, "Electro-mechanical Stress Analysis of Current Carrying Conductors", submitted by Hafizur Rahman, Roll no.861319P as satisfactory in partial fulfilment of the requirements for the degree of Master of Science in Electrical and Electronic Engineering.

THE BOARD OF EXAMINERS:

m. a. Matin 5.1.90

 Dr. Md. Abdul Matin.
 Professor
 Department of Electrical and Electronic
 Engineering, B.U.E.T, Dhaka.

Chairman
 (Supervisor)

m. a. Matin 5.1.90

 Head of the Department,
 Department of Electrical and Electronic
 Engineering, B.U.E.T, Dhaka.

Member.

EBasher 5/1/90

 Dr. Enamul Basher.
 Associate Professor
 Department of Electrical and Electronic
 Engineering, B.U.E.T, Dhaka..

Member

Rhan 5/1/90

 Dr. Md. Rezwan Khan.
 Associate Professor
 Department of Electrical and Electronic
 Engineering, B.U.E.T, Dhaka.

Member

Shamsuddin 5/1/90

 Prof. Md. Shamsuddin Ahmed.
 Head, Department of Electrical and Electronic
 Engineering, Islamic Centre for Technical and
 Vocational Training and Research (ICTVTR).
 Board Bazar, Gazipur.

Member
 (External).

ACKNOWLEDGEMENT

It is of immense pleasure on the part of the author to express his profound gratitude and indebtedness to his supervisor, Dr. Md. Abdul Matin, Professor and Head, Department of Electrical and Electronic Engineering, Bangladesh University of Engineering and Technology (BUET), Dhaka for advice, guidance and constant supervision throughout the course of this research work.

The author is indebted to Dr. Md. Mujibur Rahman, Professor and Dean, Faculty of Electrical and Electronic Engineering, BUET for constant support and encouragement with this work.

The author also wishes to express his thanks and sincerest gratitude to Dr. Md. Rezwan Khan, Dr. Enamul Basher and Mr. A.H.M. Zahirul Alam of the Department of Electrical and Electronic Engineering, BUET, Dhaka for their timely help and invaluable suggestions.

Most of the computational works were performed at the computer centre, BUET. The author therefore, is also thankful to the Director and personnel of the computer centre, BUET for their co-operation.

ABSTRACT

Electrical conductors, while carrying currents are found to be stressed mechanically both for mechanical as well as for electrical causes. The present work has been devoted to calculating the stress and the resulting force developed on conductors due to electrical reasons only. On the basis of energy balance equation in a current carrying conductor, mathematical models are established for the different forms of stresses (viz; dielectric stress, stress due to magnetic field and that resulting from Joule-heating) developed on the conductor and using those mathematical models representative numerical examples are cited. Forces on overhead power lines due to these three reasons are calculated for steady-state, fault current and transient switching on conditions. Stress due to Joule-heating is much higher than that owing to the magnetic field, while a negligibly small amount of dielectric stress is caused by the electric field on a conductor. Stress distribution inside a cylindrical conductor is studied during steady-state operations. Nonuniform stress distribution owing to the 'Skin effect' in case of ac fields is vividly observed. With the increase in frequency all the three forms of stresses increase rapidly and become as high as several hundred times at MHz range of frequencies of that at power frequencies for the same amount of current flowing through a conductor. Current as well as the stress distribution inside a conductor during switching on condition is studied on the basis of a rigorous mathematical treatment of the diffusion equation. It is observed that transient switching current and the stress are maximum at the axis and minimum near the surface unlike the current distribution during steady-state operation.

I N D E X

	<u>Page</u>
CHAPTER -1	GENERAL INTRODUCTION
1.1	Introduction. 2
1.2	Historical Review. 2
1.3	Objective of the Research. 4
1.4	Thesis Layout. 4
CHAPTER -2	ELECTROMAGNETIC ENERGY AND STRESS IN CONDUCTING MEDIA
2.1	Introduction. 7
2.2	Electromagnetic Energy in Conducting Media. 7
2.3	Mechanical Stress in Elastic Media. 11
2.4	Electromagnetic Forces on Charges and Currents. 15
2.5	Electromechanical Stress in a Conducting Medium. 16
2.6	Discussion. 23
CHAPTER -3	ELECTROMAGNETIC FIELDS IN CONDUCTING MEDIA.
3.1	Introduction. 25
3.2	The Equations for Fields in a Conducting Medium. 25
3.3	Application in a Cylindrical Conductor. 27
3.3.1	Steady-state Current Distribution Inside the Conductor. 28
3.3.2	Transient Current Distribution Inside the Conductor. 33
3.4	Discussion. 43
CHAPTER -4	CALCULATION OF DIELECTRIC STRESS IN A CONDUCTOR DUE TO ELECTRIC FIELD.
4.1	Introduction. 45
4.2	Stress Distribution in a Cylindrical Conductor. 45
4.2.1	Stress under steady-state DC. 48
4.2.2	Stress under steady-state AC. 48
4.3	Numerical Example. 51

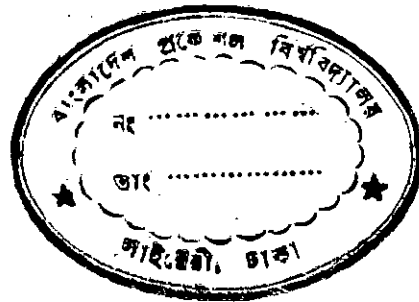
4.3.1	Steady-state Condition.	53
4.3.2	Fault Current Condition.	59
4.3.3	Transient Switching on.	60
4.4	Discussion.	63
CHAPTER -5	CALCULATION OF MECHANICAL STRESS IN A CONDUCTOR DUE TO MAGNETIC FIELD.	
5.1	Introduction.	65
5.2	Stress Distribution in a Cylindrical Conductor.	65
5.3	Numerical Example.	70
5.4	Discussion.	80
CHAPTER -6	CALCULATION OF STRESS DUE TO JOULE-HEATING IN A CONDUCTOR.	
6.1	Introduction.	82
6.2	Stress Distribution in a Cylindrical Conductor.	82
6.3	Numerical Example.	85
6.4	Discussion.	94
CHAPTER -7	COMPARATIVE STUDY OF THE THREE TYPES OF ELECTRO-MECHANICAL FORCES IN A CONDUCTOR.	
7.1	Introduction.	96
7.2	Variaton of the Forces with Current.	96
7.3	Variaton of the Forces with Coductor Specifications.	98
7.3.1	Variation with the Diameter of the Conductor.	99
7.3.2	Variation with the Resistivity of the Conductor.	100
7.4	Variation of the Forces with Frequency	102
7.5	Discussion.	104
CHAPTER -8	GENERAL DISCUSSION AND CONCLUSION AND NOTE FOR FURTHER RESEARCH.	105
APPENDIX		109
REFERENCES		132

List of Principal Symbols

- ϵ_0 = Electric permittivity of free space, 8.854×10^{-12} Farad/meter.
 μ_0 = Magnetic permeability of free space, $4\pi \times 10^{-7}$ Henry/meter.
 ϵ_r = Relative permittivity of the medium (=1 for good conductors)
 μ_r = Relative permeability of the medium (=1 for good conductors)
 ω = The angular frequency, rad/sec.
 f = operating frequency, Hz.
 \vec{D} = Electric flux density vector.
 \vec{E} = Electric field intensity.
 \vec{B} = Magnetic flux density vector, Weber/m²
 \vec{H} = Magnetic field intensity.
 \vec{J} = Current density, Ampere/m².
 σ = Conductivity of the medium (conductor), (Ohm-m)⁻¹.
 T_e = Total force (compression) due to dielectric stress, newton.
 T_m = Total force (tension) due to magneto-mechanical stress, newton.
 T_{th} = Total force (tension) due to Joule-heating, newton.

CHAPTER ONE

GENERAL INTRODUCTION



1.1 Introduction

Electrical conductors have got a wide range of applications from generation to distribution of electrical power. In course of almost all applications a conductor is subjected to mechanical stress arising from various causes. Thermal stress developed in a conductor due to Joule-heating is found to have considerable effect in damaging a conductor. Increment in sag of overhead conductors is not only due to the self load of the conductor, but also due to the eletro-mechanical stresses developed in a conductor during the flow of current. Stress analysis of electric wires is important from the stand-point of stringing of overhead lines as well as in selecting wires for winding of electrical apparatus.

1.2 Historical Review

A number of papers are available on studies on the thermal characteristics of current carrying conductors. House and Tuttle[1] are probably the first to develop a model to predict the real time conductor temperatures, associated thermal stress and resulting sag by knowing the conductor current, and approximate ambient conditions. But the model was restricted to steady state conditions only. However, the line current is a variable and weather conditions are rarely constant for more than a few minutes. All of these factors reduce the accuracy of a steady state ampacity program as suggested by House and Tuttle [1]. To encounter this problem a single-step linear integration of the House and Tuttle method was reported by Davidson and

others[2]. Yet several simplifying assumptions used in this model made it unusable in simulating a real-time operation.

Another model prescribed by Wong and others[3] linearizes convection, radiation and heat generation and combines these terms into a constant which had also an assumption of constant conductor current and constant weather conditions that limit its accuracy as real-time rating schemes. A real time ampacity model represented by Black [4] comes out of these constraints. The model considers convection and radiation from the surface of the conductor, energy generation inside the conductor due to I^2R heating and storage of energy within the conductor due to its thermal capacitance.

A current carrying conductor is not subjected to thermal stress only. There may be stresses due to its electric and magnetic fields. A general formula was established by Stratton [5] to calculate the stress resulting from electric and magnetic fields.

Begg[6] calculated the electromechanical stress distribution in insulators and found that it is as high as 1.8 kN/m^2 in a ferro-electric insulator placed between two parallel circular plates and subjected to an electric field of 10^6 V/m .

In the case of current carrying conductor, all the three types of stresses viz, Ohmic stress, magnetic and dielectric stresses need to be studied separately. In this thesis

the electro-mechanical stress analysis of a current carrying conductor has been carried out by paying attention chiefly to these three types of stresses.

1.3 Objective of the Research.

The stress developed in a current carrying conductor is different from that developed in a dead wire owing to the mechanical stress developed within the conductor due to its electromagnetic fields. The objective of this study is to calculate the amount of stress due to the electromagnetic fields in a conductor and to make a comparison among the variety of stresses developed in a current carrying conductor.

1.4 Thesis Layout:

On the basis of Poynting's theorem a general formula is established in chapter-2 to determine the electric, magnetic and Ohmic stresses for time varying fields. Since stress distribution is a function of current distribution, current distribution in a cylindrical conductor for both steady-state and transient switching conditions are studied in chapter-3. Equivalent mechanical stress distribution in a conductor resulting from a.c and d.c electric fields is studied in chapter-4. Steady state and transient conditions are verified through some representative numerical examples. Stress distribution inside a conductor due to the action of the magnetic field is placed in chapter-5, where both a.c and d.c cases are considered with numerical examples. Chapter-6 is equipped with the Ohmic stress

developed in conductor. In chapter-7, tables of comparison of the three types of stresses for different conductor specifications are illustrated. The thesis is concluded with a general discussion and future research proposals in chapter-8.

CHAPTER TWO

ELECTROMAGNETIC ENERGY AND STRESS
IN CONDUCTING MEDIA

2.1 Introduction

In this chapter a review has been carried out on electromagnetic energy and stress in conducting media. The energy flow has been shown to be governed by the well-known Poynting's theorem. A precise relationship between electromagnetic energy and electro-mechanical stress is found by mathematical reasonings and it is shown that the electromagnetic energy imparted in to a conductor manifests in the form of three different stresses viz, dielectric stress, magnetic stress, and thermal stress.

2.2 Electromagnetic energy in conducting media

When currents flow in a conductor as a result of the application of a suitable potential source, energy is expended by the source in maintaining the currents. The energy supplied by the source is stored in the electric and magnetic fields set up by the currents or propagated (radiated away) in the form of electromagnetic wave. Poynting's theorem introduces the energy balance equation among these different forms of energy. The time average power transmitted across a closed surface S is given by the integral of the real part of one-half of the real component of the complex Poynting vector, i.e

$$P = \text{Re} \left[\frac{1}{2} \oint_S \bar{\mathbf{E}} \times \bar{\mathbf{H}}^* \cdot d\bar{\mathbf{s}} \right] \dots \dots (2.1)$$

Which represents the power flow density.

The complex Poynting vector theorem may be derived from Maxwell's field equations which are :

$$\nabla \times \bar{E} + \frac{\partial \bar{B}}{\partial t} = 0 \quad \dots \quad (2.2)$$

$$\nabla \times \bar{H} - \frac{\partial \bar{D}}{\partial t} = \bar{J} \quad \dots \quad (2.3)$$

$$\nabla \cdot \bar{B} = 0 \quad \dots \quad (2.4)$$

$$\nabla \cdot \bar{D} = \rho \quad \dots \quad (2.5)$$

Now expanding the divergence of $\bar{E} \times \bar{H}^*$, we obtain,

$$\nabla \cdot (\bar{E} \times \bar{H}^*) = (\nabla \times \bar{E}) \cdot \bar{H}^* - (\nabla \times \bar{H}^*) \cdot \bar{E} \quad \dots \quad (2.6)$$

With the help of equations (2.2) and (2.3), the right hand side of equation (2.6) can be written for fields varying as $e^{j\omega t}$

$$\nabla \cdot (\bar{E} \times \bar{H}^*) = -j\omega \bar{B} \cdot \bar{H}^* + j\omega \bar{D}^* \cdot \bar{E} - \bar{E} \cdot \bar{J}^* \quad \dots \quad (2.7)$$

where ω is the angular frequency

The integration of this equation throughout a volume V bounded by a closed surface S gives ,

$$\begin{aligned} & \frac{1}{2} \int_V \nabla \cdot (\bar{E} \times \bar{H}^*) \, dV \\ &= \frac{1}{2} \oint_S \bar{E} \times \bar{H}^* \cdot d\bar{S} \\ &= -j\omega/2 \int_V (\bar{B} \cdot \bar{H}^* - \bar{E} \cdot \bar{D}^*) \, dV - \frac{1}{2} \int_V \bar{E} \cdot \bar{J}^* \, dV \quad \dots \quad (2.8) \end{aligned}$$

where the divergence theorem has been used on the left-hand-side integral. The above result may be rewritten as

$$\begin{aligned}
 & 1/2 \oint_S \bar{E} \times \bar{H}^* \cdot (-d\bar{S}) \\
 & = 2j\omega \int_V \left(\frac{\bar{B} \cdot \bar{H}^*}{4} - \frac{\bar{E} \cdot \bar{D}^*}{4} \right) dV + 1/2 \int_V \bar{E} \cdot \bar{J}^* dV \dots (2.9)
 \end{aligned}$$

where $-d\bar{S}$ is a vector element of area directed into the volume V . If the medium in V is characterized by the parameters, $\epsilon = \epsilon' - j\epsilon''$ and $\mu = \mu' - j\mu''$ and conductivity σ , the real and imaginary parts of equation (2.9) may be equated to give

$$\begin{aligned}
 \text{Re } & 1/2 \oint_S \bar{E} \times \bar{H}^* \cdot (-d\bar{S}) \\
 & = \omega/2 \int_V (\mu' \bar{H} \cdot \bar{H}^* + \epsilon'' \bar{E} \cdot \bar{E}^*) dV + 1/2 \int_V \sigma \bar{E} \cdot \bar{E}^* dV \dots (2.10a)
 \end{aligned}$$

$$\begin{aligned}
 \text{Im } & 1/2 \oint_S \bar{E} \times \bar{H}^* \cdot (-d\bar{S}) \\
 & = 2\omega \int_V \left(\frac{\mu'' \bar{H} \cdot \bar{H}^*}{4} - \frac{\epsilon' \bar{E} \cdot \bar{E}^*}{4} \right) dV \dots \dots (2.10b)
 \end{aligned}$$

Equation (2.10a) is interpreted to state that the real electromagnetic power transmitted through the closed surface S into V is equal to the power loss produced by conduction current $\sigma \bar{E}$, resulting in Joule-heating plus the power loss resulting from polarization damping forces. But in case of a conductor since ϵ'' and μ'' does not exist so no power loss will occur from polarization damping forces.

The time average energy stored in the magnetic field is given by

$$W_m = 1/4 \int \mu' \bar{H} \cdot \bar{H}^* dV \dots \dots (2.11)$$

and the time average energy stored in the electric field is

$$W_e = 1/4 \int_V \epsilon \bar{E} \cdot \bar{E}^* dV \dots \dots \dots (2.12)$$

Equation (2.10b) states that the imaginary part of the complex rate of energy flow into V is equal to 2w times the net reactive energy $W_m - W_e$ stored in the magnetic and electric fields in V. Now replacing the $j2w$ multiplier on the left hand side of equation (2.9) by the $\frac{\partial}{\partial t}$ operator and integrating with respect to time, the energy balance equation (2.9) will take the form :

$$\int_0^t \int_S \bar{E} \times \bar{H}^* \cdot (-d\bar{S}) dt$$

$$= 1/2 \int_V (\mu \bar{H} \cdot \bar{H}^* - \epsilon \bar{E} \cdot \bar{E}^*) dV + \int_V \bar{E} \cdot \bar{E}^* \sigma t dV \dots (2.13)$$

The first integral on the right hand side accounts for the electromagnetic energy storage and the second integral accounts for energy in the form of Joule-heating [7]

2.3 Mechanical Stress in Elastic Media:

Let us suppose that a given solid or fluid body of matter is in static equilibrium under the action of specified system of applied forces . Within this body we isolate a finite volume V by means of a closed surface S , as indicated in fig 2.1.

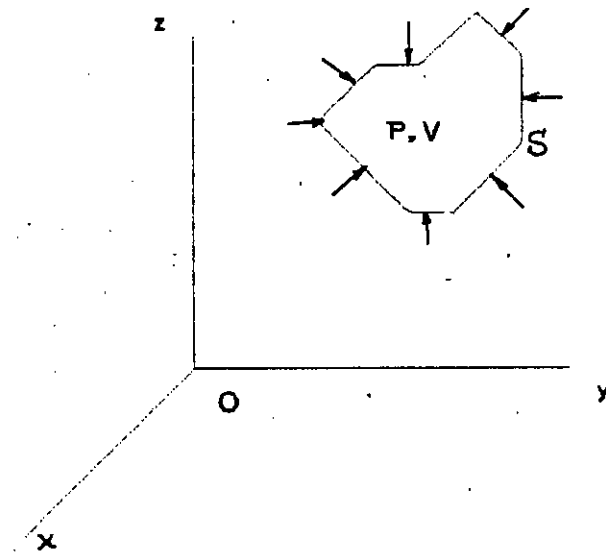


Fig. 2.1 A region V bounded by a surface S in an elastic medium under stress.

Since equilibrium has been assumed for the body and all its parts, the resultant force \bar{F} exerted on the matter within S must be zero. Contributing to this resultant are ~~volume~~ or body forces and surface forces exerted by elements of matter just outside the enclosed region on contiguous elements within.

Throughout V , therefore, we suppose it to be distributed with a density \bar{f} per unit volume, while the force exerted by matter outside S on a unit area of S will be represented by the vector \bar{t} . The components of \bar{t} are evidently normal pressures or

tensions and tangential shears [5].

The condition of translational equilibrium is expressed by the equation

$$\int_V \bar{f} \, dv + \int_S \bar{t} \, da = 0 \quad (2.14)$$

To ensure rotational equilibrium it is necessary also that the resultant torque be zero, or

$$\int_V \bar{r} \times \bar{f} \, dv + \int_S \bar{r} \times \bar{t} \, da = 0 \quad (2.15)$$

where \bar{r} is the radius vector from an arbitrary origin O to an element of volume or surface.

Let \bar{n} be the unit outward normal to an element of S . There are then three vectors \bar{X} , \bar{Y} , \bar{Z} which satisfy the equations

$$t_x = \bar{X} \cdot \bar{n}, \quad t_y = \bar{Y} \cdot \bar{n}, \quad t_z = \bar{Z} \cdot \bar{n} \quad (2.16)$$

The expansion of the scalar products in the form :

$$\begin{aligned} t_x &= X_x n_x + X_y n_y + X_z n_z \\ t_y &= Y_x n_x + Y_y n_y + Y_z n_z \\ t_z &= Z_x n_x + Z_y n_y + Z_z n_z \end{aligned} \quad (2.17)$$

may also be interpreted as a linear transformation of the component of \bar{n} into the components of \bar{t} , the components n_x, n_y, n_z being the direction cosines of \bar{n} with respect to the co-ordinate axes. The equilibrium of the x-components of forces acting on matter within S is now expressed by

$$\int_V f_x dv + \int_S \bar{X} \cdot \bar{n} da = 0 \quad (2.18)$$

which in virtue of the divergence theorem and the arbitrariness of V is equivalent to the condition that at all points within S.

$$\int_V f_x + \nabla \cdot \bar{X} = 0 \quad (2.19)$$

For the Y & Z components we have, likewise,

$$f_y + \nabla \cdot \bar{Y} = 0, \quad f_z + \nabla \cdot \bar{Z} = 0 \quad (2.20)$$

The rotational equilibrium expressed by (2.15) imposes further conditions upon the nine components of the three vectors $\bar{X}, \bar{Y}, \bar{Z}$. The x-component of this equation is for example,

$$\int_V (y f_z - z f_y) dv + \int_S (y t_z - z t_y) da = 0 \quad (2.21)$$

Introduction of the values of t_z and t_y defined in (2.16) leads to

$$\int_V (yf_z - zf_y) dv + \int_S (y\bar{Z} - z\bar{Y}) \cdot \bar{n} da = 0 \quad (2.22)$$

which again takes to the divergence theorem and the arbitraryness of V and is equivalent to

$$yf_z - zf_y + \nabla \cdot (y\bar{Z} - z\bar{Y}) = 0 \quad (2.23)$$

But,

$$\nabla \cdot (y\bar{Z}) = y \nabla \cdot \bar{Z} + z \cdot \nabla y = y \nabla \cdot \bar{Z} + Z_y \quad (2.24)$$

Equation(2.23), reduces to

$$y(f_z + \nabla \cdot \bar{Z}) - z(f_y + \nabla \cdot \bar{Y}) + Z_y - Y_z = 0 \quad (2.25)$$

or, on taking account of (2.20),

$$Z_y = Y_z \quad (2.26)$$

In like manner there may be derived from the y- & z-components of (2.15) the symmetry relations

$$X_y = Y_x, \quad X_z = Z_x \quad (2.27)$$

The nine components X_x, Y_y, \dots, Z_z , representing forces exerted on unit elements of area, are called stresses. In

diagonal terms X_x , Y_y , Z_z act in a direction normal to the surface element and are, therefore, pressures or tensions. The remaining six components are the shearing stresses acting in the plane of the element. These nine components constitute the components of a symmetrical tensor, as is evident from (2.17) and the fact that \bar{t} and \bar{n} are true vectors. Representing the components of the stress tensor by S_{jk} , where

$$\begin{aligned} X_x &= S_{11} \quad , \quad X_y = S_{12} \quad , \dots\dots \\ Y_x &= S_{21} \quad , \quad Y_z = S_{23} \quad \dots\dots \quad Z_z = S_{33} \end{aligned} \tag{2.28}$$

2.4 Electromagnetic Forces on Charges and Currents:

The electric field E at a point (in its vicinity) is defined as the force experienced by a unit point charge placed at that point. In vector notation the definition of \bar{E} becomes

$$\bar{E} = \bar{F}_e / q \quad \dots \quad \dots \tag{2.29}$$

Now if we suppose that the charge is distributed throughout a volume V with a macroscopically continuous charge density, then the net mechanical force acting on the charge is

$$\bar{F}_e = \int_V \rho \bar{E} \, dv \quad \dots \quad \dots \tag{2.30}$$

distributed with a volume density

$$\bar{f}_e = \rho \bar{E} \tag{2.31}$$

Again for the purpose of defining the magnetic induction

it is convenient to define \bar{f}_m the magnetic force per unit volume (frequently called the Lorentz force), as that part of a force exerted on moving charge density (coul/m³), which is neither electrostatic nor mechanical. The magnetic induction or magnetic flux density vector, \bar{B} is then defined as the vector which satisfies

$$\bar{f}_m = \rho \bar{v} \times \bar{B} \quad (2.32)$$

where, ρ = the charge density in coul/m³

\bar{v} = the velocity vector of the charge in m/sec.

hence, $\rho \bar{v} = \bar{i}$ = current density in A/m²

$$\text{Thus } \bar{f}_m = \bar{i} \times \bar{B} \quad (2.33)$$

Equation (2.33) represents the force exerted by the magnetic field on a unit volume element of current. Taking volume integral of equation (2.33) leads to

$$\bar{F}_m = \int_V \bar{i} \times \bar{B} \, dv \quad (2.34)$$

where, \bar{F}_m = the net force exerted on a volume distribution of current.

2.5 Electromagnetic Stress in a Conducting Medium:

Referred to the energy balance equation (2.13), deduced earlier in section 2.2, the first term within the integration sign on the right hand side, expresses the energy density stored per unit volume due to electric field. Dimensionally it is the force per unit area or a stress due to the electric forces within the system. Similarly the second term represents a stress due to

magnetic forces. The third term gives the volumetric energy density dissipated in the form of heat (as is known from Joule's law of electric heating); in other words this is the value of the thermal stress developed in a conductor due to the flow of electric current. The minus sign on the left hand side of equation (2.13) indicates that all the net energy term expressed by the right hand side of relation (2.13) must have been supplied externally. Thus the term on the left represents the energy flow into a unit volume of the system, where it is converted into electric, magnetic and thermal stresses. A detailed analysis is made by Stratton [5], where it is shown that the magnitude of the stress due to electric field is

$$|\bar{t}^{(e)}| = 1/2 \epsilon E^2 \quad (2.35)$$

and in vector notation it is given by,

$$\bar{t}^{(e)} = \bar{S}^{(e)} \cdot \bar{n} \quad (2.36)$$

where $\bar{S}^{(e)}$ = the electric stress tensor like that mentioned in article 2.3 and the elements of this tensor are shown in table 2.1

Table - 2.1 Components $S_{jk}^{(e)}$ of the Tensor $\hat{S}^{(e)}$

$j \backslash k$	1	2	3
1	$\epsilon(E_x^2 - 1/2E^2)$	$\epsilon E_x E_y$	$\epsilon E_x E_z$
2	$\epsilon E_y E_x$	$\epsilon(E_y^2 - 1/2E^2)$	$\epsilon E_y E_z$
3	$\epsilon E_z E_x$	$\epsilon E_z E_y$	$\epsilon(E_z^2 - 1/2E^2)$

The magnitude of the stress due to magnetic field is given by ,

$$|\vec{t}^{(m)}| = 1/2 \mu H^2 \quad (2.37)$$

and in vector notation it is given by,

$$\vec{t}^{(m)} = \hat{S}^{(m)} \cdot \vec{n} \quad (2.38)$$

where $\hat{S}^{(m)}$ = the magnetic stress tensor corresponding to magnetic field whose elements are shown in table 2.2

Table - 2.2 Components $S_{jk}^{(m)}$ of the Tensor $\hat{S}^{(m)}$

$j \backslash k$	1	2	3
1	$1/\mu (B_x^2 - 1/2B^2)$	$1/\mu B_x B_y$	$1/\mu B_y B_z$
2	$1/\mu B_y B_x$	$1/\mu (B_y^2 - 1/2B^2)$	$1/\mu B_y B_z$
3	$1/\mu B_z B_x$	$1/\mu B_z B_y$	$1/\mu (B_z^2 - 1/2B^2)$

Similarly from equation (2.13), the magnitude of the stress due to Joule-heating is

$$|\bar{E}^{(th)}| = \sigma E^2 t \quad (2.39)$$

and in vector notation it is given by,

$$\bar{E}^{(th)} = \hat{S}^{(th)} \cdot \bar{n} \quad (2.40)$$

where $\hat{S}^{(e)}$ = the stress tensor corresponding to Joule-heating whose elements are tabulated below:

Table - 2.3 Components S_{jk}^{th} of the Tensor $\hat{S}^{(th)}$.

$j \backslash k$	1	2	3
1	$2\sigma t(E_x^2 - 1/2E^2)$	$2\sigma t E_x E_y$	$2\sigma t E_x E_z$
2	$2\sigma t E_y E_x$	$2\sigma t(E_y^2 - 1/2E^2)$	$2\sigma t E_y E_z$
3	$2\sigma t E_z E_x$	$2\sigma t E_z E_y$	$2\sigma t(E_z^2 - 1/2E^2)$

From equation (2.40) it is observed that the stress due to Joule-heating (Ohmic dissipation) on the system increases steadily with time, t .

But as the Ohmic loss manifests in the form of heat, temperature of the system rises. This in turn expresses that the temperature as well as the elastic strain resulting from thermal stress will tend towards infinity for an unlimited period of energy transmission through the system. But it is not so in practice. What happens usually is that an energy balance occurs amongst the heat developed, convection and radiation from the surface of the system.

For example in case of a conductor, an energy balance on a unit volume of it results in a governing equation given by Black and Byrd [4],

$$mC_p \frac{dT}{dt} = Q_{gen} + Q_{sun} - Q_{rad} - Q_{conv} \quad (2.41)$$

where, Q_{gen} =the rate of heat generation per unit volume of the conductor due to the ohmic dissipation in it

$$= \bar{E} \cdot \bar{J} = \sigma \bar{E} \cdot \bar{E} = \sigma E^2 \quad (2.42)$$

Q_{sun} =the rate of heat absorbed by the conductor per unit volume from solar irradiation.

Q_{rad} =the rate of heat radiated away from the surface of the unit volume of the conductor.

Q_{conv} =the rate of heat passing away from the surface of the unit volume of the conductor by convection.

Putting the various representative data of the ambient condition, solar absorptivity of the conductor, solar flux, infrared emissivity convective heat transfer co-efficient in the first order ordinary non-linear differential equation (2.41) and solving the equation employing the standard numerical technique such as Runge-Kutta method, a value for the conductor temperature at discrete time intervals can be provided to plot a curve of the form shown in Fig. 2.2.

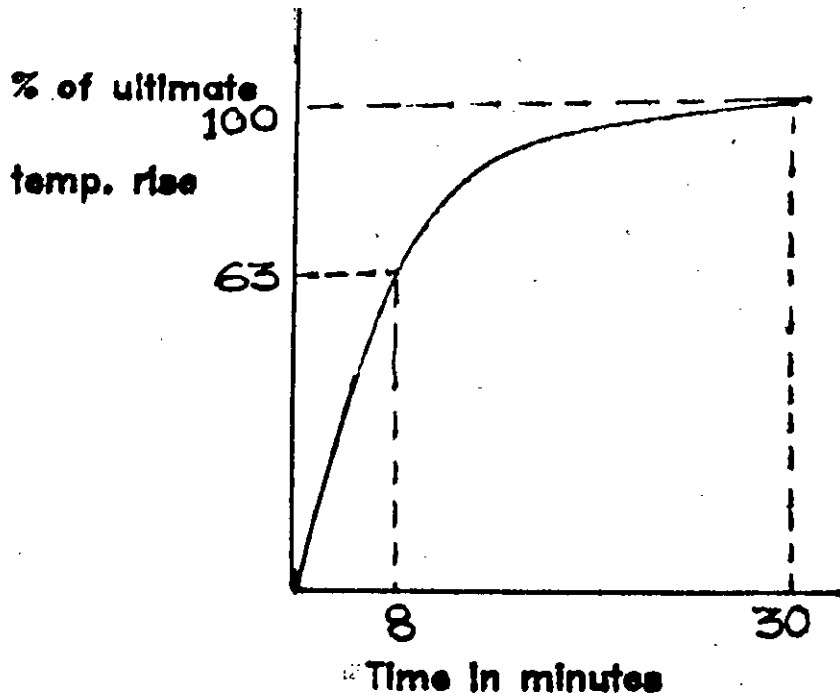


Fig. 2.2 Time constant of Linnet conductor

The time constant of the conductor is the time required for the conductor to reach 63% of its ultimate steady state temperature rise when subject to change in current. The time constant for a Linnet conductor is calculated to be approximately 8 minutes by Black and Byrd [4].

From the figure it is evident that the temperature starts rising with current but for a short duration; when it reaches a definite value, all the generated heat due to Ohmic

loss and absorbed heat from solar flux is dissipated in the surrounding atmosphere through radiation and convection processes.

2.6 Discussion

Energy stored in a system due to electric and magnetic field and so with the case of stress due to electric field and stress due to magnetic field is found to be independent of time. But the Ohmic loss, i.e. the stress due to Joule-heating is time dependent up to a certain interval after switching on and finally a steady state temperature is reached. In article 2.3 it is shown that the body forces and surface forces exerted by elements of matter on its contiguous elements within a material under static equilibrium, form stress tensors and their equivalent electromagnetic stresses are discussed in article 2.4 and 2.5.

CHAPTER THREE

**ELECTROMAGNETIC FIELDS IN
CONDUCTING MEDIA**

3.1 Introduction

Stress distribution inside a conductor is dependent on time as well as spatial distribution of current inside a conductor. Hence it is of practical importance to be familiar with the current distribution inside a conductor. It is well-known that the current distribution is not uniform throughout the conductor in case of alternating fields and it is of further interest to know the current distribution inside a conductor during switching period. Complete solution of diffusion equation is enough to have an idea of both spatial and time dependence of the current density inside a conductor. From the generalized wave equation electromagnetic field penetration and current diffusion is stated inside a cylindrical conductor of infinite length by solving the diffusion equation for it.

3.2 The Equations for Fields in a Conducting Medium

Electromagnetic fields in a conducting medium are governed by the equations:

$$\nabla \times \bar{E} = - \frac{\partial \bar{B}}{\partial t} \quad (3.1)$$

$$\nabla \times \bar{H} = \bar{i} + \frac{\partial \bar{D}}{\partial t} \quad (3.2)$$

$$\bar{D} = \epsilon \bar{E} \quad (3.3)$$

$$\bar{B} = \mu \bar{H} \quad (3.4)$$

$$\bar{i} = \sigma E \quad (3.5)$$

$$\nabla \cdot \bar{B} = 0 \quad (3.6)$$

$$\nabla \cdot \bar{D} = \rho \quad (3.7)$$

For a homogeneous medium μ , ϵ and σ are independent of

position so that

$$\nabla \cdot \bar{H} = 0 \quad (3.8)$$

$$\nabla \cdot \bar{D} = \epsilon \nabla \cdot \bar{E} \quad (3.9)$$

$$\nabla \cdot \bar{i} = \sigma \nabla \cdot \bar{E} \quad (3.10)$$

Taking divergence of equation (3.2)

$$\nabla \cdot \bar{i} + \frac{\partial}{\partial t} (\nabla \cdot \bar{D}) = 0 \quad (3.11)$$

Then by equation (3.3) and equation (3.7) it becomes

$$\frac{\partial \rho}{\partial t} + \frac{\sigma}{\epsilon} \rho = 0 \quad (3.12)$$

The solution is

$$\rho = \rho_0 e^{-\frac{\sigma}{\epsilon} t} \quad (3.13)$$

where ρ_0 is the initial charge density at $t = 0$.

As the factor σ/ϵ is very large for a conductor, then any charge concentration in the conductor dies out quickly. Hence in a conductor it is approximately such that

$$\rho = 0 \quad (3.14)$$

Then by equations (3.3), (3.7) and (3.14)

$$\nabla \cdot \bar{E} = 0 \quad (3.15)$$

However, this is exact for fields varying as $E = E_0 e^{j\omega t}$.

Taking curl of equation (3.1) and by equations (3.2), (3.3)

and (3.5)

$$\nabla \times \nabla \times \bar{E} = -\mu \frac{\partial}{\partial t} (\sigma \bar{E} + \epsilon \frac{\partial \bar{E}}{\partial t}) \quad (3.16)$$

The vector identity

$$\nabla \times \nabla \times \bar{E} = \nabla (\nabla \cdot \bar{E}) - \nabla^2 \bar{E} \quad (3.17)$$

is now used to obtain

$$\nabla (\nabla \cdot \bar{E}) - \nabla^2 \bar{E} = -\mu \sigma \frac{\partial \bar{E}}{\partial t} - \mu \epsilon \frac{\partial^2 \bar{E}}{\partial t^2} \quad (3.18)$$

Equation (3.15) is used to eliminate $\nabla \cdot \bar{E}$, and by

regrouping terms we obtain

$$\nabla^2 \bar{E} - \mu \epsilon \frac{\partial^2 \bar{E}}{\partial t^2} - \mu \sigma \frac{\partial \bar{E}}{\partial t} = 0 \quad (3.19)$$

Similar relationships can be obtained for magnetic field \bar{H} and current density, \bar{i}

$$\nabla^2 \bar{H} - \mu \epsilon \frac{\partial^2 \bar{H}}{\partial t^2} - \mu \sigma \frac{\partial \bar{H}}{\partial t} = 0 \quad (3.20)$$

$$\nabla^2 \bar{i} - \mu \epsilon \frac{\partial^2 \bar{i}}{\partial t^2} - \mu \sigma \frac{\partial \bar{i}}{\partial t} = 0 \quad (3.21)$$

Equations (3.19)-(3.21) are the generalized equations for fields in a conducting medium. For ac fields varying as $e^{j\omega t}$ and for a good conductor with $\sigma \gg \omega \epsilon$ the above equations reduce to

$$\nabla^2 \bar{E} = \mu \sigma \frac{\partial \bar{E}}{\partial t} \quad (3.22)$$

$$\nabla^2 \bar{H} = \mu \sigma \frac{\partial \bar{H}}{\partial t} \quad (3.23)$$

$$\nabla^2 \bar{i} = \mu \sigma \frac{\partial \bar{i}}{\partial t} \quad (3.24)$$

These are the familiar forms of equations describing a diffusion process indicating that medium and low frequency fields in a conductor are subject to diffusion.

3.3 Application to a Cylindrical Conductor

Equation (3.23) in cylindrical co-ordinates can be written as :

$$\frac{1}{r} \frac{\partial}{\partial r} \left(r \frac{\partial \bar{i}}{\partial r} \right) + \frac{1}{r^2} \frac{\partial^2 \bar{i}}{\partial \phi^2} + \frac{\partial^2 \bar{i}}{\partial z^2} = \mu \sigma \frac{\partial \bar{i}}{\partial t} \quad (3.25)$$

For axial symmetry $\frac{\partial \bar{i}}{\partial \phi} = 0$ and for an infinitely long conductor, there will be no variation of \bar{i} along the z-direction

i.e. $\frac{\partial i}{\partial z} = 0$, hence for straight cylindrical conductor of infinite length we can write,

$$\frac{1}{r} \frac{\partial}{\partial r} \left(r \frac{\partial i}{\partial r} \right) = \mu \sigma \frac{\partial i}{\partial t} \quad (3.26)$$

Equation (3.26) will have a solution of the form :

$$i = i_{s.s} + i_{tr.} \quad (3.27)$$

where $i_{s.s}$ = steady-state current density to be given by the particular solution of a differential equation.

$i_{tr.}$ = transient current density to be given by the complementary function of the differential equation.

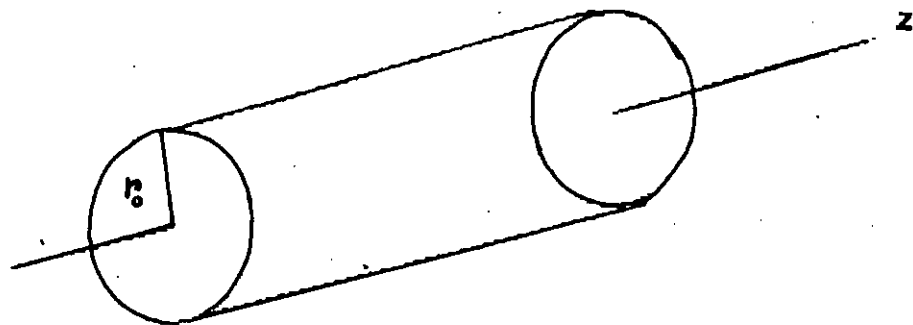


Fig. 3.1 A solid cylindrical conductor of circular cross-section with its axis along the z-direction and of radius r_0

3.3.1 Steady-state Current Distribution

Assuming sinusoidally time varying current of the form, $i = i_0 e^{i\omega t}$ equation (3.26) becomes,

$$\frac{\partial^2 i}{\partial r^2} + \frac{1}{r} \frac{\partial i}{\partial r} = j \omega \mu \sigma i$$

or,
$$\frac{\partial^2 i}{\partial r^2} + \frac{1}{r} \frac{\partial i}{\partial r} + T^2 i = 0 \quad (3.28)$$

where,

$$T = j^{-1/2} \sqrt{j \omega \mu \sigma} = j^{-1/2} \sqrt{2} / \delta$$

where,
$$\delta = \frac{1}{\sqrt{\pi f \mu \sigma}}$$

Equation (3.28) has exactly the form of the zero order Bessel equation although T is complex. A complete solution may be written as [2],

$$i = A J_0(Tr) + B N_0(Tr) \quad (3.29)$$

where J_0 and N_0 are zero order Bessel and Neuman functions respectively. Since Neuman function of order zero would become infinite at $r=0$, then

$$i = A J_0(Tr) \quad (3.30)$$

The arbitrary constant A may be evaluated in terms of current density at the surface. Let

$$i = i_0 \quad \text{at} \quad r = r_0$$

Then from equation (3.30)

$$A = i_0 / J_0(Tr_0) \quad (3.31)$$

and
$$i = i_0 J_0(Tr) / J_0(Tr_0) \quad (3.32)$$

Now expressing the Bessel's function of order zero of first kind as a series in ascending powers of the argument,

$$J_0(\text{Tr}) = 1 + \frac{j\omega\mu\sigma r^2}{2^2} - \frac{(\omega\mu\sigma)^2 r^4}{2^2 \times 4^2} + j\frac{(\omega\mu\sigma)^3 r^6}{2^2 \times 4^2 \times 6^2} \quad (3.33)$$

When the series (3.33) is separated into a series of real and a series of imaginary terms, each series is a modified form of Bessel's function. Separating the real and imaginary terms and substituting

$$m = \sqrt{\omega\mu\sigma} = \sqrt{2}/\delta \quad (3.34)$$

We obtain

$$\begin{aligned} J_0(\text{Tr}) &= \left[1 - \frac{(mr)^4}{2^2 \times 4^2} + \frac{(mr)^8}{2^2 \times 4^2 \times 6^2 \times 8^2} - \dots \right. \\ &\quad \left. + j \left[\frac{(mr)^2}{2^2} - \frac{(mr)^6}{2^2 \times 4^2 \times 6^2} \right] \right] \\ &= \text{Ber}(mr) + j\text{Bei}(mr) \quad (3.35) \end{aligned}$$

Where, the terms 'Ber' and 'Bei' are abbreviation for "Bessel real of order zero" and "Bessel imaginary" of order zero.

i.e.

$$\text{Ber}(mr) = 1 - \frac{(mr)^4}{2^2 \times 4^2} + \frac{(mr)^8}{2^2 \times 4^2 \times 6^2 \times 8^2} - \dots \quad (3.36)$$

$$\text{Bei}(mr) = \frac{(mr)^2}{2^2} - \frac{(mr)^6}{2^2 \times 4^2 \times 6^2} + \dots \quad (3.37)$$

Hence the steady state solution of the diffusion equation for a cylindrical conductor of infinite length and having circular cross section is given by

$$i_{ss}(r) = i_0 \frac{\text{Ber}(mr) + j\text{Bei}(mr)}{\text{Ber}(mr_0) + j\text{Bei}(mr_0)} \quad (3.38)$$

or,

$$i_{ss}(r) = i_0 \frac{\text{Ber}(\frac{\sqrt{2}r}{\delta}) + j\text{Bei}(\frac{\sqrt{2}r}{\delta})}{\text{Ber}(\frac{\sqrt{2}r_0}{\delta}) + j\text{Bei}(\frac{\sqrt{2}r_0}{\delta})}$$

$i_{ss}(r)$ represents the current density at a radial distance r from the axis of the conductor.

From equations (3.34) and (3.38) it is clear that the steady-state current distribution is a function of frequency of operation, depth of penetration ' δ ' and the radius of the cylindrical conductor. The radial distribution of steady-state current at different frequencies is shown in Fig 3.2.

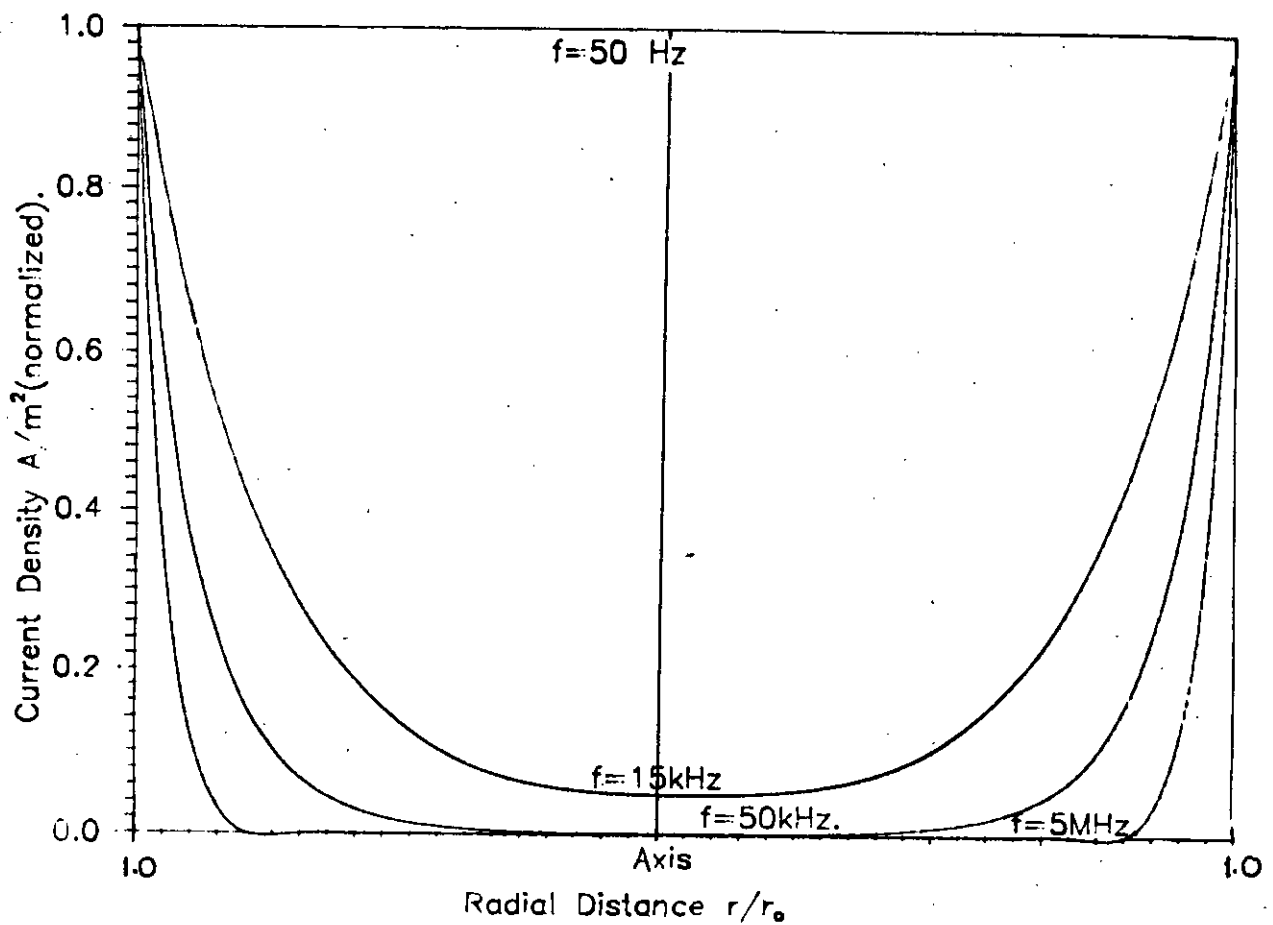


Fig. 3.2 Steady-state current distribution in cylindrical wire at different frequencies for 4 mm diameter aluminium wire of conductivity $\sigma = 3.58 \times 10^7 (\Omega\text{-m})^{-1}$

At low frequencies the current density is almost uniform throughout the cross-section but as the frequency is increased, the current distribution predominates towards the surface. This effect is more pronounced for thick conductors i.e, for higher values of the ratio r_0/δ .

3.3.2 Transient Current Distribution

Let the transient solution of diffusion equation be of the form:

$$i_{tr} = f(r) e^{-kt} \quad (3.39)$$

where, $f(r)$ is an arbitrary function representing the radial distribution and e^{-kt} represents the exponentially decaying nature of the transient current, k is an arbitrary constant.

Now substituting i from equation (3.39) in the diffusion equation (3.26) we get,

$$\frac{1}{r} \frac{\partial}{\partial r} \left\{ r \frac{\partial f(r)}{\partial r} \right\} = -k\mu\sigma f(r) \quad (3.40)$$

or, $\frac{\partial^2 f(r)}{\partial r^2} + \frac{1}{r} \frac{\partial f(r)}{\partial r} + \tau^2 f(r) = 0$

where,

$$\tau = \sqrt{k\mu\sigma} \quad \text{i.e., } K = \tau^2/\mu\sigma \quad (3.41)$$

A direct comparison of (3.40) with equation (3.28) shows that both have exactly the form of zero order Bessel equation, here τ is real ; hence the solution will be of the form:

$$f(r) = CJ_0(\tau r) + DY_0(\tau r) \quad (3.42)$$

With a similar reasoning as mentioned earlier D must be zero and hence,

$$f(r) = CJ_0(\tau r) \quad (3.43)$$

So , from equations (3.39) and (3.41)

$$\begin{aligned}
 i_{tr} &= C J_0 (\mathcal{T}r) e^{-kt} \\
 &= C J_0 (\mathcal{T}r) e^{-\tau^2/4\sigma t}
 \end{aligned}
 \tag{3.44}$$

The general solution of the diffusion equation is the sum of the transient solution and the steady state solution i.e.

$$i(r,t) = i_{tr}(r,t) + i_{ss}(r,t). \tag{3.45}$$

Now we assume a boundary condition that the total current density will be zero everywhere at $t=0$, except at the surface, where it is such that

$$i(r_0,0) = i_0.$$

comparing this with equations (3.45) and (3.38) it follows that

$$i_{tr}(r_0,0) = 0 \tag{3.46}$$

Also it is such that

$$i_{tr}(r,0) = -i_{ss}(r,0) \quad 0 < r < r_0 \tag{3.47}$$

$$= -i_0 \frac{J_0(\sqrt{-jA/4\sigma} r)}{J_0(\sqrt{-jA/4\sigma} r_0)}$$

Now applying the condition (3.46) in equation (3.44) we get,

$$J_0(\mathcal{T}r_0) = 0$$

$$\text{or, } \mathcal{T}r_0 = P_m$$

where , P_m is the m th root of the equation $J_0(v) = 0$

it readily follows that

$$\gamma = P_m/r_0 \tag{3.48}$$

So the transient current density will be given by the series.

$$i_{tr}(r) = \sum_{m=1}^{\infty} C_m J_0\left(\frac{P_m r}{r_0}\right) e^{-P_m^2 t / r_0^2 / 4\sigma} \quad (3.49)$$

This solution is analogous to the solution of heat diffusion equation for a cylindrical conductor [9].

Now at $t = 0$,

$$i_{tr}(r, 0) = \sum_{m=1}^{\infty} C_m J_0\left(\frac{P_m r}{r_0}\right) \quad (3.50)$$

The co-efficient C_m may be evaluated in a manner similar to that used for Fourier co-efficients by multiplying each term of (3.50) by $rJ_0(P_m r/r_0)$ and integrating from 0 to r_0 .

Then from the orthogonality of Bessel function

$$\int_0^{r_0} r J_0(P_m r/r_0) J_0(P_q r/r_0) dr = 0 \quad \text{for } (P_m \neq P_q) \quad (3.51)$$

all the terms on the right disappear except the m th term i.e.,

$$\int_0^{r_0} r i_{tr}(r, 0) J_0(P_m r/r_0) dr = \int_0^{r_0} C_m r [J_0(P_m r/r_0)]^2 dr \quad (3.52)$$

Again we can write, [10]

$$\int_0^{r_0} r J_0^2(P_m r/r_0) dr = \frac{r_0^2}{2} J_1^2(P_m)$$

so from equation (3.52)

$$\int_0^{r_0} r i_{tr}(r, 0) J_0(P_m r/r_0) dr = C_m r_0^2 J_1^2(P_m)$$

or, $C_m = \frac{2}{r_0^2 J_1^2(P_m)} \int_0^{r_0} r i_{tr}(r, 0) J_0(P_m r/r_0) dr$

Now substituting $i_{tr}(r,0)$ by equation (3.47)

$$C_m = \frac{-2i_0}{r_0^2 J_1^2(P_m) J_0(\sqrt{-j\omega\mu\sigma} r_0)} \int_0^{r_0} r J_0(\alpha r) J_0(\beta r) dr \quad (3.53)$$

$$\text{where, } \alpha = \sqrt{-j\omega\mu\sigma} \quad \text{and} \quad \beta = P_m/r_0 \quad (3.54)$$

Now applying the identity :

$$\int_0^1 v R_\nu(\alpha v) R_\nu(\beta v) dv = \frac{1}{\alpha^2 - \beta^2} [\beta R_\nu(\alpha) R_{\nu-1}(\beta) - \alpha R_{\nu-1}(\alpha) R_\nu(\beta)] \quad (3.55)$$

R_ν denotes J_ν , N_ν , $H_\nu^{(1)}$ or $H_\nu^{(2)}$, for the definite integral of the R.H.S of equation (3.53) we have

$$\int_0^{r_0} r J_0(\alpha r) J_0(\beta r) dr = \frac{r_0^2}{\alpha^2 - \beta^2} [\beta J_0(\alpha r_0) J_1(\beta r_0) - \alpha J_1(\alpha r_0) J_0(\beta r_0)] \quad (3.56)$$

$$\text{But } J_{-1}(x) = -J_1(x) \quad (3.57)$$

Hence the co-efficient C_m becomes :

$$C_m = \frac{-2i_0 r_0}{J_1^2(P_m) r_0^2 J_1^2(P_m) \times (\alpha^2 - \beta^2)} [\alpha J_1(\alpha r_0) J_0(\beta r_0) - J_0(\alpha r_0) J_1(\beta r_0)] \quad (3.58)$$

Now according to the definition of P_m and from equation

(3.54)

$$J_0(\beta r_0) = J_0(P_m) = 0.$$

$$\text{and } J_0(\alpha r_0) = J_0(j\sqrt{j\omega\mu\sigma} r_0) = I_0(\sqrt{j\omega\mu\sigma} r_0)$$

$$\text{and } J_1(\beta r_0) = J_1(P_m); \quad \alpha^2 - \beta^2 = -j\omega\mu\sigma - P_m^2/r_0^2$$

So substituting from equation (3.57) in equation (3.58).

$$C_m = \frac{-2i_0 P_m}{J_1(P_m) [P_m^2 + j\omega\mu\sigma r_0^2]}$$

Therefore the transient current density distribution becomes :

$$i_{tr} = -2i_0 \sum_{m=1}^{\infty} \frac{P_m J_0(P_m r/r_0) \exp[-(P_m r/r_0)^2 t/\mu\sigma]}{J_1(P_m) [P_m^2 + j\omega\mu\sigma r_0^2]} \quad \dots (3.59)$$

Considering an aluminium wire of radius 4mm, the transient current density at different time after switching is studied and is shown in fig 3.3

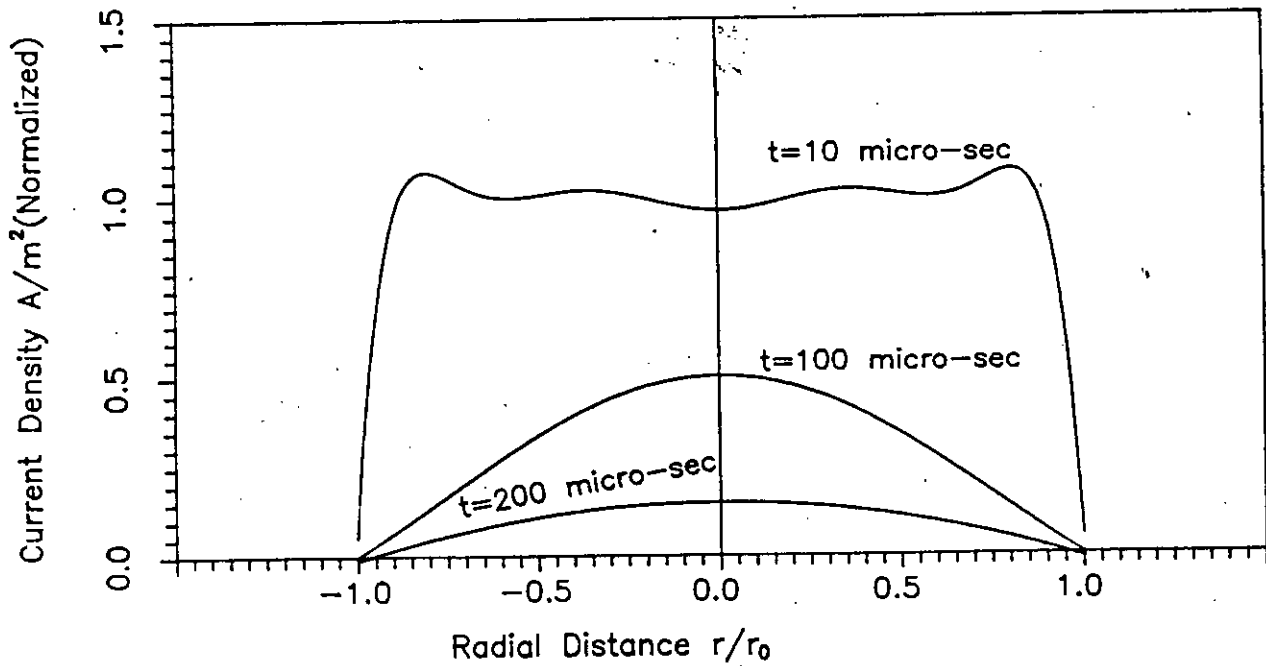


Fig. 3.3 Radial distribution of transient current

(ac 50 Hz) at different time after switching.

$$r = 4\text{mm}, \quad \sigma = 3.54 \times 10^7 (\Omega \cdot \text{m})^{-1}, \quad m = 21.$$

For AC at power frequency it is observed that the transient current die out within several hundred micro-sec .The transient current density at the surface remains zero but that at the axis is at a maximum till the dying out of the transient current except up to a few micro-sec after switching while it oscillates inside the conductor . In equation (3.60) the sum has been carried out for upto $m=21$ and for higher values of m the exponential term die out rapidly.As the frequency is increased the pattern of the transient current distribution changes widely. This can be observed from comparison of fig 3.3 with fig 3.4 .

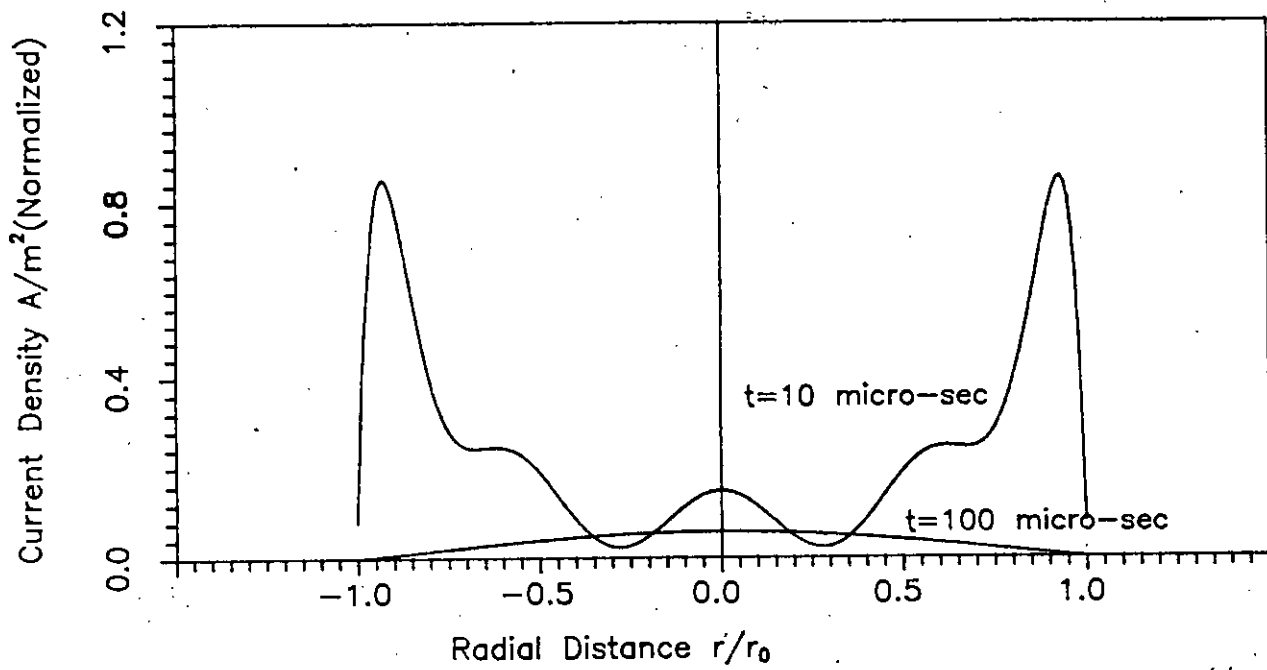


Fig. 3.4 Radial Distribution of Transient current (AC 15kHz)
At Different Time after Switching

It is found that the process of dying out of the transient current at higher frequencies occurs more rapidly than that for low frequency. Further for a few micro-sec after switching, the current distribution is found to be terminated towards the surface rather than near the axis.

Expression of total current density

Substitutions from equation (3.39) and equation (3.59) in equation (3.45) gives the expression for total current density as a function of time and radius.

$$i(r,t) = -2i_o \sum_{m=1}^{\infty} \left(\frac{P_m J_0(P_m r/r_o) \exp[-(P_m r/r_o)^2 t/\mu\sigma]}{J_1(P_m) [P_m^2 + j\omega\mu\sigma r_o^2]} \right) + i_o \frac{\text{Ber}(\pi r) + j\text{Bei}(\pi r)}{\text{Ber}(\pi r_o) + j\text{Bei}(\pi r_o)} e^{j\omega t} \quad (3.60)$$

The distribution of total current at different instants after switching is plotted in fig 3.5.

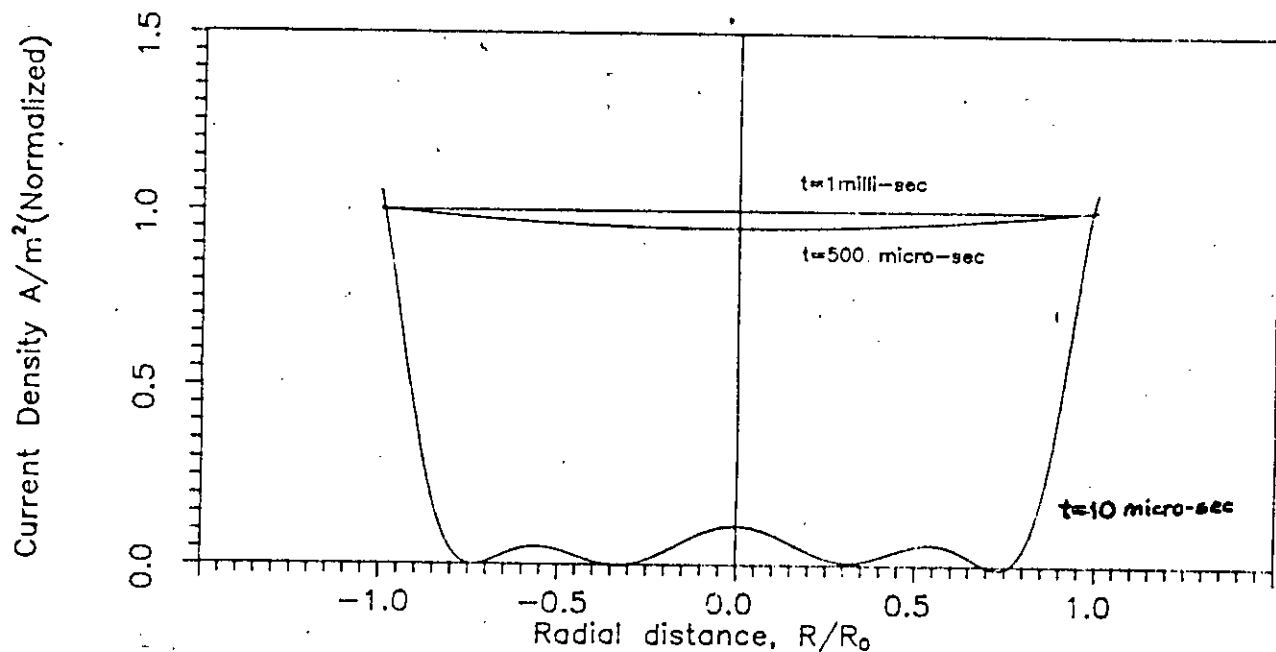


Fig. 3.5 Radial distribution of total current (ac 50 Hz) at different time after switching.

Since for AC 50 Hz the steady state current distribution is almost uniform throughout the cross-section of the conductor. The total current which is the algebraic sum of the transient current and the steady-state current is found to have similar pattern like the transient one elevated by unity. The surface current density remains unity throughout the period while the current distribution inside the conductor rises from zero to unity after a few hundreds of micro-sec.

Transient Current for Static Field(D.C):

In case of static, time invariant field it is quite evident that the operating frequency is zero i.e. putting $\omega=0$ in equation (3.59) we get the Bessel co-efficient

$$C_m = \frac{-2i_0 P_m}{P_m^2 J_1(P_m)} \quad (3.62)$$

Hence the transient current distribution will be given by:

$$i_{tr} = -2i_0 \sum_{m=1}^{\infty} \frac{J_0(P_m r/r_0) \exp[-(P_m r/r_0)^2 t/\mu\sigma]}{P_m J_1(P_m)} \quad (3.63)$$

Since the steady state current distribution is uniform through out the conductor for d.c, so if I be the total current, the surface current density is given by

$$i_0 = I/\pi r_0^2 \quad (3.64)$$

and transient current density as a function of time and radius is therefore:

$$i_{tr} = \frac{-2I}{\pi r_0^2} \sum_{m=1}^{\infty} \frac{J_0(P_m r/r_0) \exp[-(P_m r/r_0)^2 t/\mu\sigma]}{P_m J_1(P_m)} \quad (3.65)$$

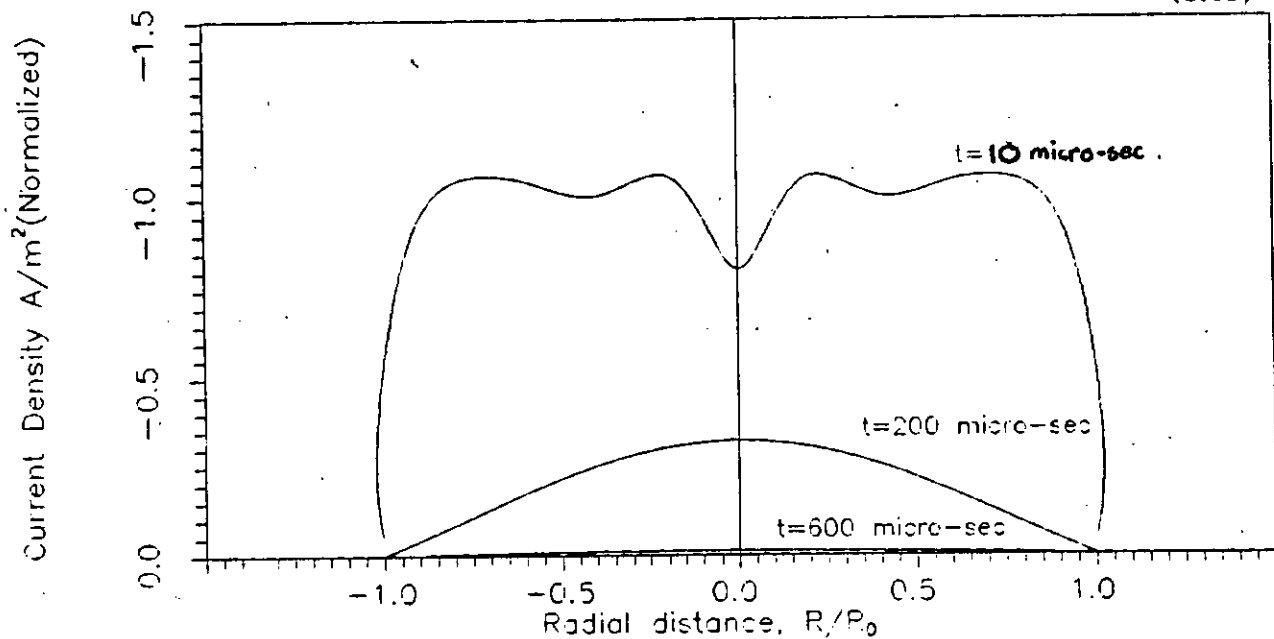


Fig. 3.6 Radial distribution of transient current dc at different time after switching.

In case of DC (fig 3.6) the process of dying out of the transient current is found to be slower than that in case of AC , but like AC up to few micro-sec after switching the transient current distribution is oscillatory inside the conductor remaining zero at the surface . Later on the oscillation ceases and the distribution pattern assumes the shape of a parabola with its vertex at the axis , i.e, the transient current density is maximum there .

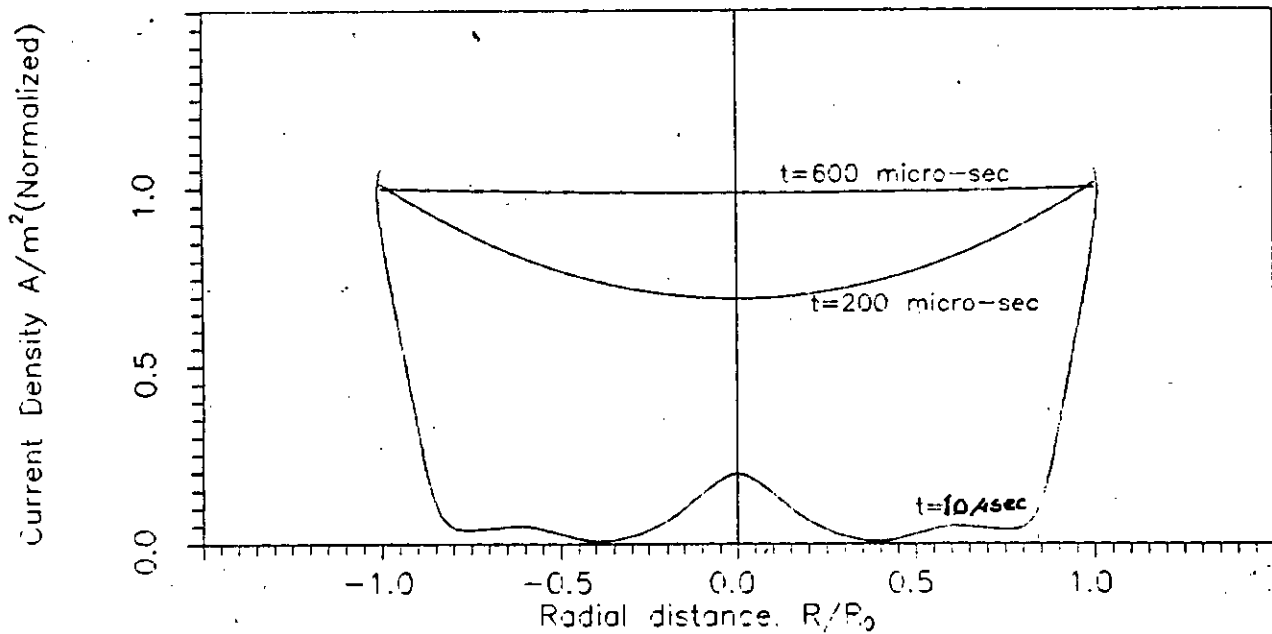


Fig. 3.7 Radial distribution of total current (DC) at different time after switching.

In fig 3.7 the total current distribution for DC is shown. The current distribution is found to increase with oscillations (initially) inside the conductor to unity while the surface current density is unity throughout the time. So several hundreds of micro-sec later the transient current dies out and the total current distribution becomes uniform all over the conductor cross-section.

3.6 Discussion

Electromagnetic field penetration in a conducting medium is characterized by diffusion equation and in article 3.2 it is demonstrated that the current density abide by the diffusion equation inside a conducting medium. So in two consecutive articles solution of diffusion equation is accomplished for cylindrical conductors of infinite length. In case of low frequency ac, the switching transient current density is found to be maximum near the axis and zero at the surface. With the increase in frequency the peak current density shifts towards the surface, yet the surface current density remains zero. Though direct current is distributed uniformly throughout the cross-section during steady state condition but switching (transient) current is distributed in a separate fashion as is shown in fig. 3.6. In the following chapters these current distributions will be used to observe the pattern of stress distributions.

CHAPTER FOUR

**CALCULATION OF DIELECTRIC STRESS
IN A CONDUCTOR DUE TO
ELECTRIC FIELD**

4.1 Introduction

A charge in an electric field experiences a force on it which depends on the strength of the field. Hence from the forces exerted by charges may be determined the work necessary to establish a field; from energy relations in turns it will be possible to deduce the forces exerted on ponderable elements of matter. The theory on Maxwell-Faraday's electromechanical stress in matter has been widely discussed by Stratton [5]. We outline below the method of utilizing the electromechanical stress tensor derived in section 2.5 to calculate the mechanical stress developed in conductors of different specifications due to the electric field.

4.2 Stress Distribution in a Cylindrical Conductor

The dielectric stress developed within a conductor due to the electric field can be calculated using relation (2.24),

$$t^{(e)} = \hat{S}^{(e)} \cdot \bar{n} \quad (4.1)$$

where $\hat{S}^{(e)}$ = the stress tensor.

the components of $\hat{S}^{(e)}$ are given in table -2.1 of section 2.5, and the components of $\bar{t}^{(e)}$ can be written as,

$$t_j^{(e)} = \sum_{k=1}^3 S_{jk} \cdot n_k \quad (j = 1, 2, 3) \quad (4.2)$$

If in equation (4.2) the components of $\hat{S}^{(e)}$ are substituted from table-2.1

$$\begin{aligned}
\vec{t}^{(e)} &= \bar{a}_x t_x^e + \bar{a}_y t_y^e + \bar{a}_z t_z^e \\
&= [\bar{a}_x \{ (E_x^2 - 1/2E^2)n_x + E_x E_y n_y + E_x E_z n_z \} \\
&\quad + \bar{a}_y \{ (E_y^2 - 1/2E^2)n_y + E_y E_x n_x + E_y E_z n_z \} \\
&\quad + \bar{a}_z \{ (E_z^2 - 1/2E^2)n_z + E_z E_y n_y + E_z E_x n_x \}] \\
&= [\bar{a}_x E_x (E_x n_x + E_y n_y + E_z n_z) \\
&\quad + \bar{a}_y E_y (E_x n_x + E_y n_y + E_z n_z) \\
&\quad + \bar{a}_z E_z (E_x n_x + E_y n_y + E_z n_z)] \\
&\quad - E^2 (\bar{a}_x n_x + \bar{a}_y n_y + \bar{a}_z n_z)
\end{aligned}$$

or,

$$\vec{t}^{(e)} = \epsilon (\vec{E} \cdot \vec{n}) \vec{E} - \frac{\epsilon}{2} E^2 \vec{n} \quad (4.3)$$

Let us consider a cylindrical conductor with its axis along the Z-direction of a cylindrical co-ordinate system while the direction of current flow is also the same. Then the applied electric field may be represented by

$$\vec{E} = \bar{a}_z E_z \quad (4.4)$$

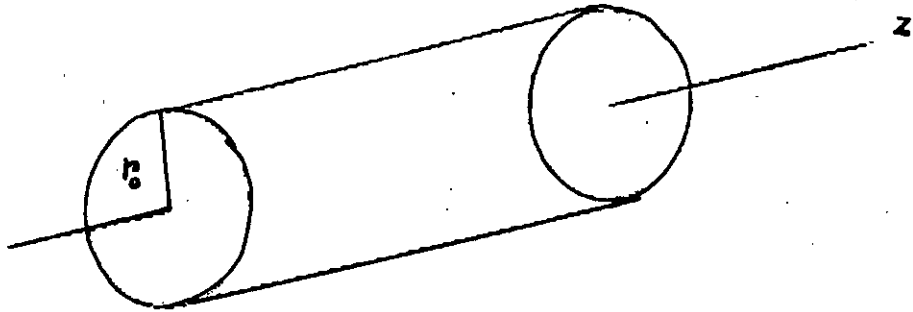


Fig. 4.1 A cylindrical conductor oriented along the z-axis.

To calculate the stress on the cross-section of the wire we let $\bar{n} = \bar{a}_z$ in equation(4.3), i.e. the normal to the surface under consideration is along the direction of electric field.

So according to equation(4.3) and (4.4), it is evident that the direction of the dielectric stress is such that it will produce compression on the conductor, where the magnitude of the total compression exerted by the electric field on the conductor is given by,

$$T_e = \oint_a \vec{t}^{(e)} \cdot d\vec{a}$$

$$= \frac{\epsilon}{2} \int_0^{r_0} E_z^2 (2\pi r) dr$$

Since $da = d(\pi r^2) = 2\pi r dr$

where r_0 the radius of the conductor and applying Ohm's law, $E = i/\sigma$, where i = the current density and σ the conductivity of the conductor, we get,

$$\begin{aligned}
 T_e &= \frac{\epsilon}{2} \int_0^{r_0} (i/\sigma)^2 (2\pi r) dr \\
 &= \frac{\epsilon\pi}{\sigma^2} \int_0^{r_0} i^2 r dr
 \end{aligned}
 \tag{4.5}$$

4.2.1 Stress under steady-state DC

For a direct current I , the current density is uniform throughout the conductor. Hence, the current density is given by,

$$i = \frac{I}{\pi r_0^2} \tag{4.6}$$

where, I = the total current flowing through the conductor area.

r_0 = the radius of the conductor.

Then, substituting the value of i from equation(4.6) in equation (4.5), we get

$$T_e = \frac{\epsilon I^2}{\pi r_0^2 \sigma^2} \int_0^{r_0} r dr = \frac{\epsilon I^2}{2\pi r_0^2 \sigma^2} \tag{4.7}$$

4.2.2 Stress under steady-state AC

In case of alternating current, the current density through-out the cross-section of the conductor is not Uniform. As the frequency of alternating current increases, the non-uniformity of distribution becomes more pronounced due to skin

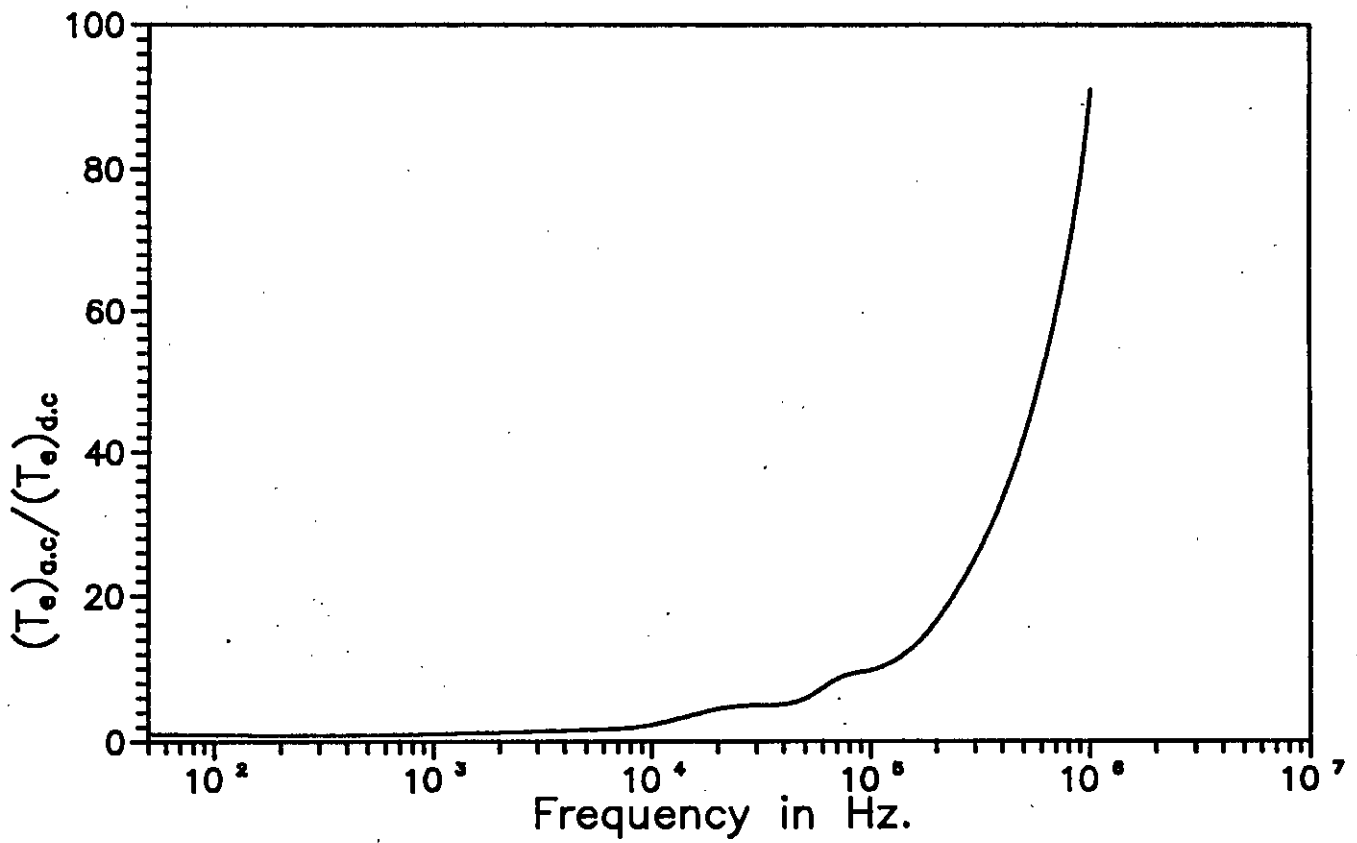


Fig. 4.2 Ratio of stress due to ac to that due to dc as a function of frequency.

effect [11]. In a circular cylindrical conductor the current density usually increases from the interior toward the surface.

Substituting the value of $i(r)$ from equation (3.38) in place of i in the integral of equation (4.5) we get,

$$T_e = \frac{\pi \epsilon i_0^2}{\sigma^2} \int_0^{r_0} \left(\frac{\text{Ber}(mr) + j\text{Bei}(mr)}{\text{Ber}(mr) + j\text{Bei}(mr)} \right)^2 r dr \quad (4.8)$$

Comparison of compression due to AC and DC

This comparison can be done by considering equal amounts of ac and dc currents flowing through the conductor. For I to be the total ac current with distribution given by equation (3.38),

$$I = \int_0^{r_0} 2\pi r i_0 \frac{\text{Ber}(mr) + j\text{Bei}(mr)}{\text{Ber}(mr) + j\text{Bei}(mr)} dr \quad (4.9)$$

Now dividing equation (4.8) by (4.7) and replacing I by equation

$$(4.9), \text{ we get the ratio, } \frac{T_{a.c}}{T_{d.c}} = \frac{r_0^2}{2} \frac{\int_0^{r_0} \left[\frac{\text{Ber}(mr) + j\text{Bei}(mr)}{\text{Ber}(mr) + j\text{Bei}(mr)} \right]^2 r dr}{\left[\int_0^{r_0} \frac{\text{Ber}(mr) + j\text{Bei}(mr)}{\text{Ber}(mr) + j\text{Bei}(mr)} r dr \right]^2}$$

A plot of this ratio as a function of frequency is made on a semilog paper in fig 4.2, where it is observed that the ratio increases from unity to as high as 90 at a frequency of 1 MHz. For lower range of frequencies the ratio rises slowly but a sharp rise is observed near 100 kHz.

4.3 Numerical Example:

Among mostly available conductors, silver (Ag) is the best conductor (Table 4.1) though it is not used in practice because of its high price. Copper(Cu) and aluminium(Al) conductors are used widely for practical purposes. Table 4.1 shows the conductivity of some practical conductors at about room temperature (20° C)[12].

TABLE 4.1 ELECTRICAL CONDUCTIVITY (σ) OF SOME PRACTICAL CONDUCTORS AT 20° C.:

<u>Name of the conductor</u>	<u>conductivity (σ) in $10^8 (\Omega\text{-m})^{-1}$</u>
Lithium (Li)	0.10
Silver (Ag)	0.625
Copper (Cu)	0.59
Aluminium (Al)	0.357
Iron (Fe)	0.10
Tungsten	
Nichrome	0.01

Stranded aluminium conductors are used for overhead power transmission and distribution lines and even in the underground cables copper is being replaced by aluminium. All aluminium conductors(AAC), aluminium conductor steel reinforced (ACSR) and all aluminium alloy conductors(AAAC) of different sizes are used

almost all over the world for power lines. In ACSR , one or more steel wires are kept as the core or central strand to strengthen the breaking capacity of the conductor against tensile stress.

Telephone lines are chiefly erected with copper wires, since the amount of conductor necessary is small and fair conductivity is also an important factor for such lines, as low voltage (only dc) is used for this purpose.

For the windings of electrical machines such as generators, motors and transformers, copper is used instead of aluminium, since the ohmic dissipation in aluminium is greater than that due to copper winding for the same amount of current to flow, hence greater cooling facilities is to be provided for Aluminium winding which becomes costly as well as the size of the machine becomes bulky . Moreover, rich conductivity is of great importance for such machines to reduce the copper loss of the machine i.e. to make the machine more efficient . Even then Aluminium is used for designing the rotor of squirrel cage induction motors.

Tungsten (An alloy steel, Fe:75-80%, Ni:20-14%, Cr:4-5%) filament is used in incandescent lamps for it emits light when heated. Nonlinearity is inherent in this conductor, which is an essential feature of its property. Similar is the case with Nichrome which is used in electric heaters, toasters and ovens and in irons also.

We deal here basically with power lines. i.e. overhead

transmission and distribution lines. Steady state conditions, fault current conditions and transient switching on conditions are studied separately with a view to evaluating the stress and resulting tensile/compressive force developed in conductors having different specifications, used for practical purposes.

4.3.1 Steady-state Condition:

The maximum continuous current rating (which may be considered as the maximum steady state operating current) of different conductors according to B.P.D.B.* specifications are given below in table 4.2 [13]. In article 4.2.2 we arrived at an expression given by equation (4.8) for the total compression acting on a conductor due to the electric field.

Table 4.2 Specification of some common conductors used for BPDB power lines.

A. Aluminium Conductor Still Reinforced (ACSR).

Code name used by BPDB	Overall dia(mm)	Stranding & wire dia(mm)		used for power lines	Continuous current carrying capacity(Amp)	Calculated breaking load(kN)
		Aluminium	steel			
GOPHER	7.08	6/2.36	1/2.36	11kV	140	9.61
RABBIT	10.05	6/3.35	1/3.35	11kV	205	18.35
DOG	14.15	6/4.72	7/1.57	11kV	300	32.70
WOLF	18.13	30/2.59	7/2.59	33kV	430	69.20
MERLIN	18.05	18/3.61	1/3.61	33kV	440	41.10
HAWK		6/2.36	1/2.36	33kV	560	
GROSBEAK		6/2.36	1/2.36	132kV	660	

*B.P.D.B: Bangladesh Power Development Board.

B.All Aluminium Conductor (AAC).

Code name used by BPDB	Overall dia(mm)	Stranding & wire dia(mm) ----- Aluminium wire.	used for power lines	Continuous current carrying capacity(Amp)	Calculated breaking load(kN)
GNAT	6.18	7/2.06	400V	140	3.99
ANT	9.30	7/3.10	400V	205	8.28
EARWIG	10.20	7/3.40	400V	310	9.90
WASP	13.17	7/4.39	400V	430	16.00

The total compression due to ac electric field is calculated and shown in table 4.4. To make a comparison with d.c, compression due to static field is also calculated handling with the same set of data and shown in table 4.3 . In fig. 3.2 it was shown that the current density is almost invariant (like d.c) throughout the cross-section of a thin wire at power frequencies (i.e. 50 or 60 cps), but in practical conductors used at high frequencies, current density may decrease to one millionth of its surface value in a distance of only a few thousands of a centimeter . So, the same set of calculations are repeated for different frequencies to be familiar with the frequency dependence of the stress distribution and compressive force.

Table 4.3 Compressive force on some common conductors used for BPDB power lines, for Direct Current(D.C).

Code	Overall dia(mm)	Current (Amp)	Compressive force due to elec. fld. in 10^{-19} N.
GNAT(400V)	6.18	140	48
ANT (400V)	9.30	200	44
EARWIG(400V)	10.20	260	61
WASP(400V)	13.17	310	52

Table 4.4 Compressive force on some common conductors used for BPDB power lines, for Alternating Current(A.C) at power frequency (50 Hz).

Code	Overall dia(mm)	Current (Amp)	Compressive force due to elec. fld. in 10^{-19} N.
GNAT(400V)	6.18	140	50
ANT (400V)	9.30	200	45
EARWIG(400V)	10.20	260	64
WASP(400V)	13.17	310	54

Assuming a steadystate current of 300A passing through a typical aluminium conductor of radius 4mm, the compressive force developed in Newton at different frequencies is shown in table 4.5.

Table 4.5 Compressive force on a specific conductor for ac at different frequencies.

Operating Freq.(Hz)	Compressive force due to elec. fld. in 10^{-18} N.
50.	6.7
5000.	9.8
10000.	14
50000.	37
100000.	63
500000.	270
1000000.	580

Again, the compressive stress distribution in N/m^2 (normalized) inside the same conductor at different frequencies is shown in table 4.6 .

Table 4.6 Compressive Stress distribution inside a conductor of circular cross-section for ac at different frequencies.

Operating Frequency	Radial Distance	Stress in N/m^2 (Normalized)
50	0.00	0.3470×10^{-26}
50	0.20	0.3470×10^{-26}
50	0.40	0.3470×10^{-26}
50	0.60	0.3470×10^{-26}
50	0.80	0.3471×10^{-26}
50	1.00	0.3473×10^{-26}
5000	0.00	0.3113×10^{-27}
5000	0.20	0.3151×10^{-27}
5000	0.40	0.3724×10^{-27}
5000	0.60	0.6309×10^{-27}
5000	0.80	0.1410×10^{-26}
5000	1.00	0.3473×10^{-26}
25000	0.00	0.7117×10^{-30}
25000	0.20	0.9310×10^{-30}
25000	0.40	0.4905×10^{-29}
25000	0.60	0.3974×10^{-28}
25000	0.80	0.3592×10^{-27}
25000	1.00	0.3473×10^{-26}
50000	0.00	0.3722×10^{-32}
50000	0.20	0.8484×10^{-32}
50000	0.40	0.1439×10^{-30}
50000	0.60	0.3242×10^{-29}
50000	0.80	0.8311×10^{-28}
50000	1.00	0.3473×10^{-26}
100000	0.00	0.2869×10^{-37}
100000	0.20	0.1977×10^{-36}
100000	0.40	0.1448×10^{-34}
100000	0.60	0.1456×10^{-32}
100000	0.80	0.4630×10^{-30}
100000	1.00	0.3473×10^{-26}

As the frequency is increased, no stress is developed at all inside the conductor even at a frequency of the range of 10^4 Hz, which is evident from fig. 4.4.

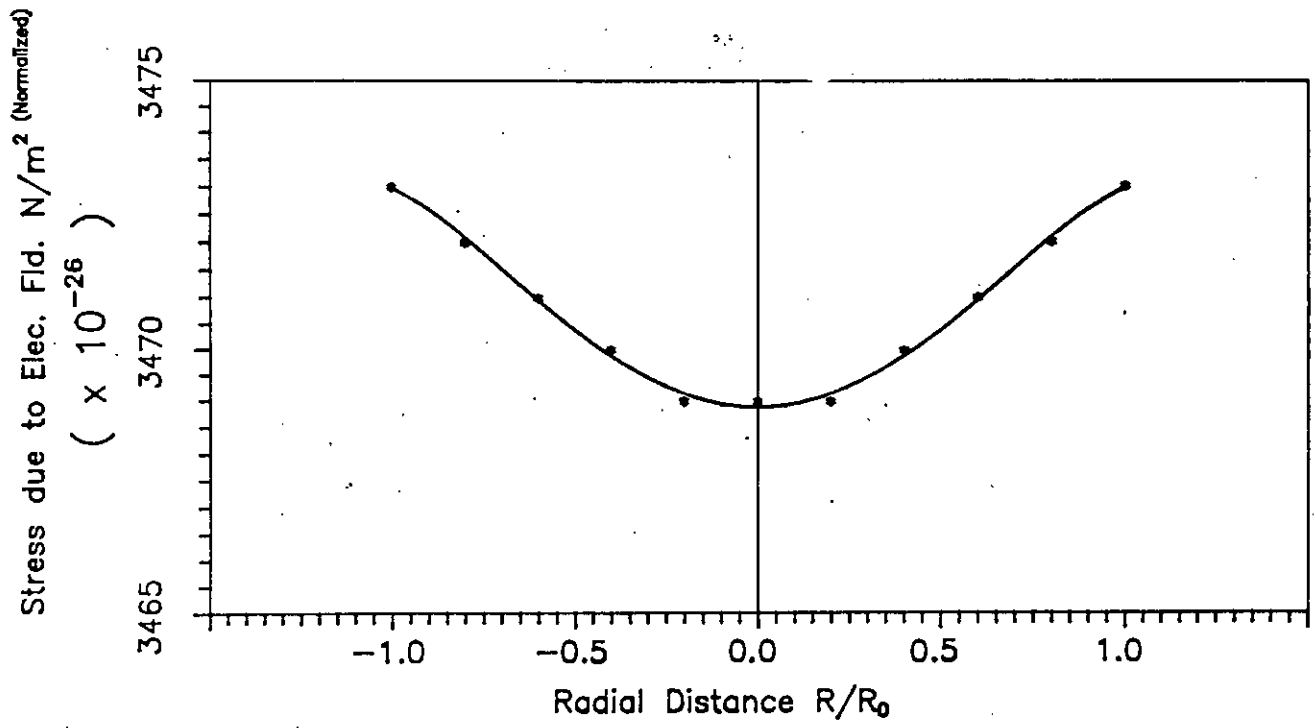


Fig.4.3 Radial distribution of stress due to electric field for AC 50Hz.

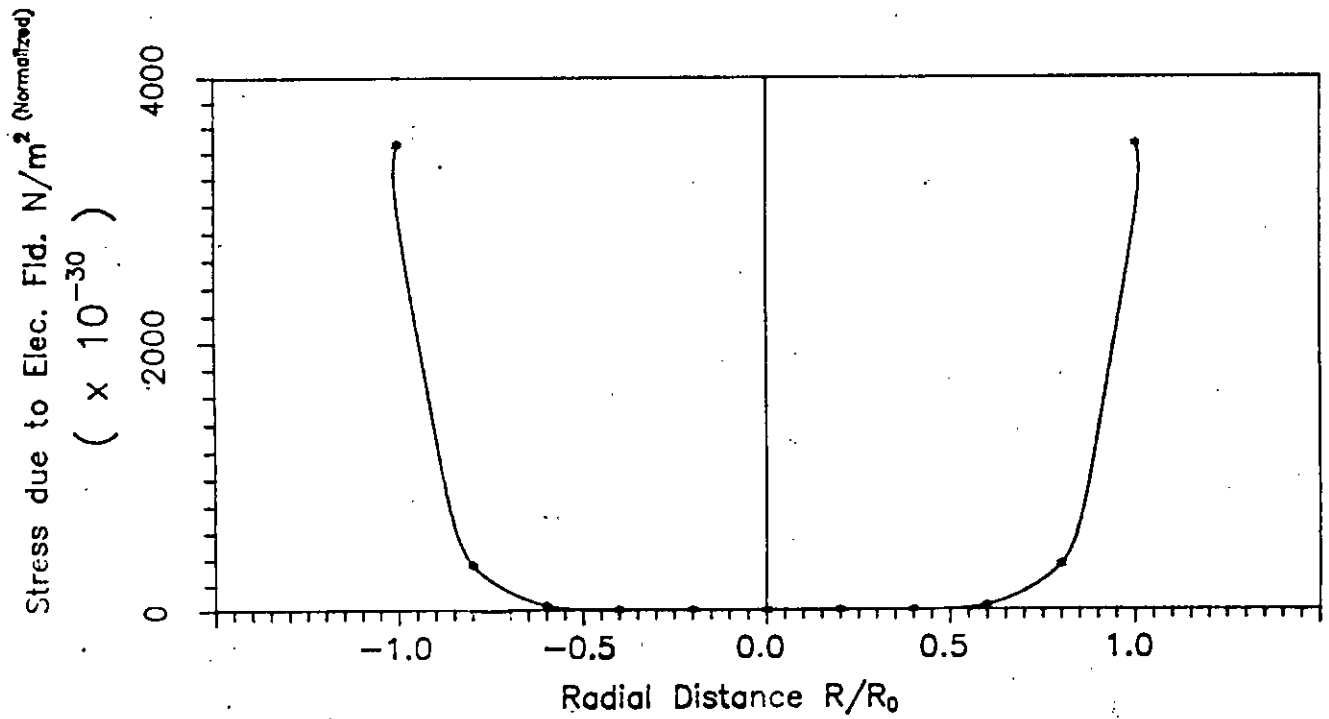


Fig.4.4 Radial distribution of stress due to electric field for AC 25kHz.

4.3.2 Fault Current Condition

Power lines are very often subjected to faults of different pattern, single line to ground fault, double line to ground fault, line to line fault and three phase symmetrical fault among which the last one is the severe one. Exact calculation of the r.m.s value of the fault current in a power system is exceedingly complicated. Approximate methods are more practical and usually sufficiently accurate. According to B.P.D.B. specifications, the maximum prospective three phase r.m.s symmetrical fault levels must not exceed the following values:-

- a) 33 KV system: 1,000 MVA(17.5 KA) r.m.s symmetrical.
- b) 11 KV system: 250 MVA(13.1 KA) r.m.s. symmetrical.
- c) 400/230 volt system: 29 MVA (41.9 KA) r.m.s symmetrical [14]

Table 4.8 Compressive force for a fault current(ac at power frequency) on conductors of BPDB power distribution lines.

Code	Overall dia(mm)	Fault current (kA)	Used for power lines of	Compressive force due to elec. fld. in 10^{-16} N.
GNAT	6.18	41.9	400v	4500
ANT	9.30	41.9	400v	2000
WASP	13.17	41.9	400v	980
GOPHER	7.08	13.1	11kV	190
RABBIT	10.05	13.1	11kV	94
DOG	14.15	13.1	11kV	50
MERLIN	18.05	17.5	33kV	64

4.3.3 Transient Switching on

Very often it is observed that different electrical appliances or fuses get damaged just after switching on so it is expected that the different forms of stresses become predominant at this instant. In article 3.3.2 effort has been made to establish an idea about the radial and time distribution of transient switching-on current both for static and time varying fields. Here we shall devote our attempt to give a picture of the stress distribution in a conductor. Assuming a typical aluminium conductor of radius 4mm, the compressive stress distribution in N/m^2 (normalized) inside the conductor at different frequencies with respect to time elapses after switching is shown in table 4.9

Table 4.9 dielectric stress distribution at different distances from the axis at 10⁻⁶-sec after switching on for ac at different frequencies.

Operating Frequency	Radial Distance	Stress in N/m^2 (Normalized)
50	0.00	0.1319×10^{-27}
50	0.20	0.1383×10^{-28}
50	0.40	0.1843×10^{-30}
50	0.60	0.8376×10^{-29}
50	0.80	0.7598×10^{-29}
50	1.00	0.3851×10^{-26}
20000	0.00	0.1377×10^{-27}
20000	0.20	0.1036×10^{-28}
20000	0.40	0.4784×10^{-30}
20000	0.60	0.5248×10^{-29}
20000	0.80	0.1180×10^{-28}
20000	1.00	0.3682×10^{-26}
50000	0.00	0.1309×10^{-27}
50000	0.20	0.1247×10^{-28}
50000	0.40	0.3205×10^{-30}
50000	0.60	0.1807×10^{-29}
50000	0.80	0.1032×10^{-28}
50000	1.00	0.3612×10^{-26}

Now in case of dc, the radial distribution of transient current just after switching is governed by a different expression as mentioned earlier in section 3.4. So for a similar aluminium conductor, the compressive stress distribution in N/m^2 (normalized) inside the conductor for a direct current passing through it after switching is shown in table 4.10 .

Table 4.10 Electric stress distribution at different distances from the axis of the conductor for dc (10 micro-sec after switching on).

Radial Distance	Stress in N/m^2 (Normalized)
0.00	0.1529×10^{-26}
0.20	0.5708×10^{-28}
0.40	0.1055×10^{-29}
0.60	0.4729×10^{-28}
0.80	0.8888×10^{-29}
1.00	0.3899×10^{-26}

In fig 4.5 the radial distribution of dielectric stress is shown for ac 50 Hz , at 10 micro-sec after switching . Assuming the surface current density to be unity, a normalized curve is plotted. A little amount of stress is developed near the axis of the conductor while almost the whole stress is found to concentrate near the surface. To get the actual value of the stress developed, the value shown in the figure should be multiplied by the square of the surface current density.

Fig 4.6 shows the stress distribution during dc switching. During switching instant (a few micro-sec after switching), in case of dc , the stress near the axis is found to be higher than that in the case of ac . With time the stress distribution changes and after several hundred micro-seconds it assumes the steady-state pattern (refer to Fig 4.3).

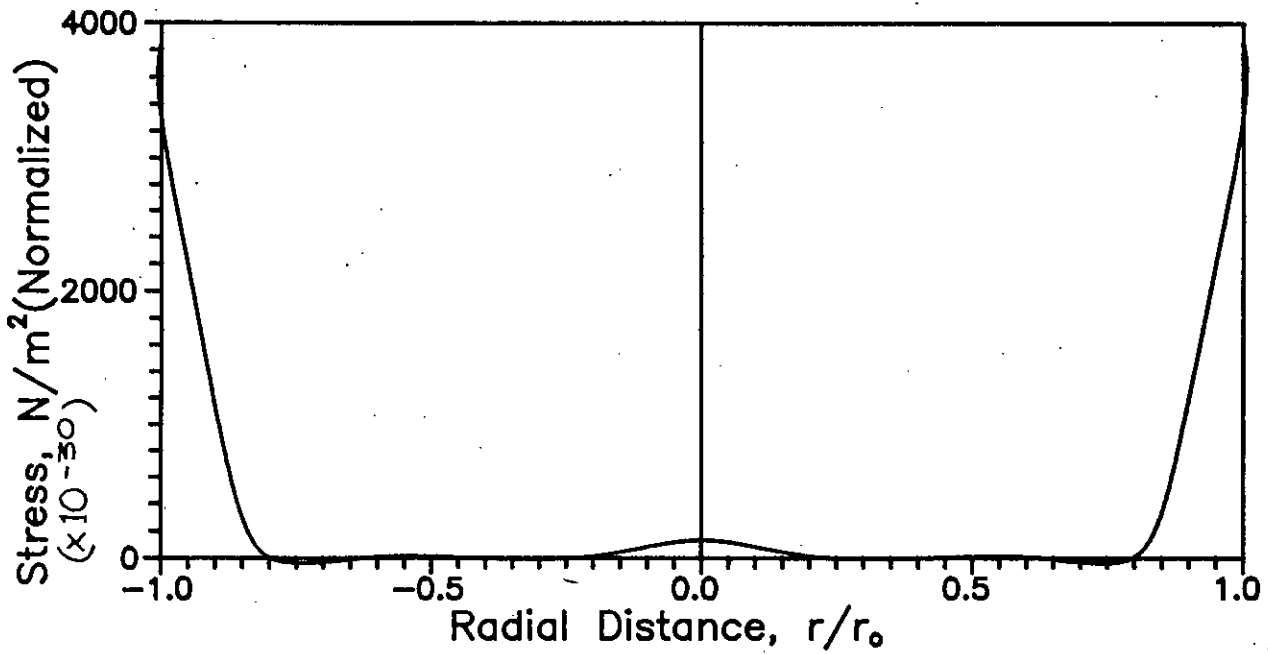


Fig. 4.5 Radial distribution of dielectric stress (ac 50 Hz) 10 micro-sec after switching.

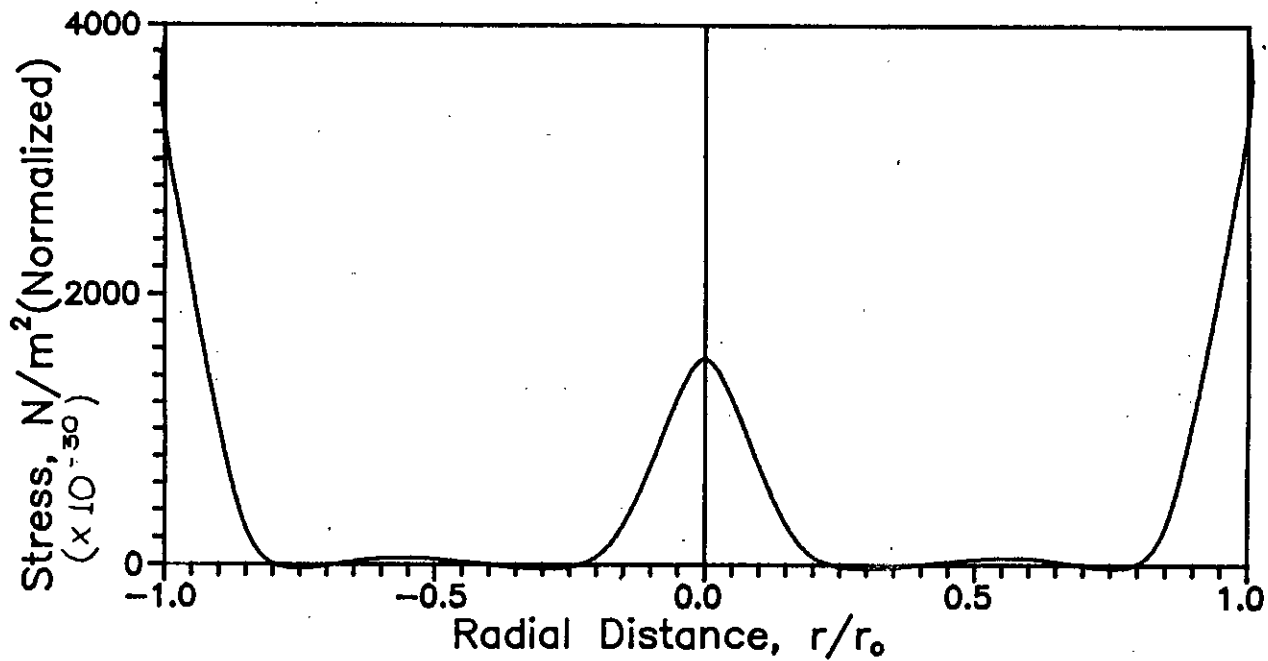


Fig. 4.6 Dielectric stress distribution (dc) 10 micro-sec after switching.

4.4 Discussion

We have outlined in this chapter the dielectric stress developed in the form of compression in conductors of different specifications. Particular emphasis is given on the transient conditions like fault current situation and transient switching on.

It is obvious that the tables through 4.3 to 4.10 give us a clear picture that the compressive force within the conductor resulting from energy stored in the electric field are negligibly small for conductors and it is of the order of 10^{-12} N.

76168

CHAPTER FIVE

CALCULATION OF MECHANICAL STRESS IN A
CONDUCTOR DUE TO MAGNETIC FIELD

5.1 Introduction

When current flows through a conductor magnetic field develops around it, the amount of which is given by Ampere's law. Inside the conductor a mechanical stress is produced by this magnetic field, which may be termed as magneto-mechanical stress. At first a mathematical model for magneto-mechanical stress calculation is established with the help of the stress tensor derived in chapter 2. Then stress and the resulting force are tabulated for conductors having different specifications in both the cases of ac and dc.

4.2 Stress Distribution in a Cylindrical Conductor:

The magneto-mechanical stress developed within a conductor due to the magnetic field can be calculated using relation (2.38),

$$\bar{t}^{(m)} = \hat{S}^{(m)} \cdot \bar{n} \quad (5.1)$$

where $\hat{S}^{(m)}$ = the stress tensor.

the components of $\hat{S}^{(m)}$ are given in table -2.2 of section 2.5, and the components of $\bar{t}^{(m)}$ can be written as,

$$t_j^{(m)} = \sum_{k=1}^3 S_{jk} \cdot n_k \quad (j = 1,2,3) \quad (5.2)$$

If in equation (4.2) the components of $\hat{S}^{(m)}$ are substituted from table-2.2, we get

$$\begin{aligned}
\vec{t}^{(m)} &= \bar{a}_x t_x + \bar{a}_y t_y + \bar{a}_z t_z \quad (4.1) \\
&= [\bar{a}_x \{ (B_x^2 - 1/2B^2)n_x + B_x B_y n_y + B_x B_z n_z \} \\
&\quad + \bar{a}_y \{ (B_y^2 - 1/2B^2)n_y + B_y B_x n_x + B_y B_z n_z \} \\
&\quad + \bar{a}_z \{ (B_z^2 - 1/2B^2)n_z + B_z B_y n_y + B_z B_x n_x \}] \\
&= [\bar{a}_x B_x (B_x n_x + B_y n_y + B_z n_z) \\
&\quad + \bar{a}_y B_y (B_x n_x + B_y n_y + B_z n_z) \\
&\quad + \bar{a}_z B_z (B_x n_x + B_y n_y + B_z n_z)] \\
&\quad - B^2 (\bar{a}_x n_x + \bar{a}_y n_y + \bar{a}_z n_z)
\end{aligned}$$

$$\vec{t}^{(m)} = \frac{1}{\mu} (\vec{B} \cdot \vec{n}) \vec{B} - \frac{1}{2\mu} B^2 \vec{n} \quad (5.3)$$

DC Case:-

Let us consider a cylindrical conductor, having circular cross-section, placed along the z-axis of a cylindrical co-ordinate system). The current is assumed to flow in the z-direction. Hence in cylindrical co-ordinates, the magnetic field developed at a distance r from the centre of the conductor due to the electric current will be given by

$$\begin{aligned}
\vec{H} &= \bar{a}_\phi H_\phi \\
&= \bar{a}_\phi \frac{I r}{2\pi r_0^2} \quad (\text{for } r < r_0) \quad (5.4)
\end{aligned}$$

where r_0 = the radius of the conductor.

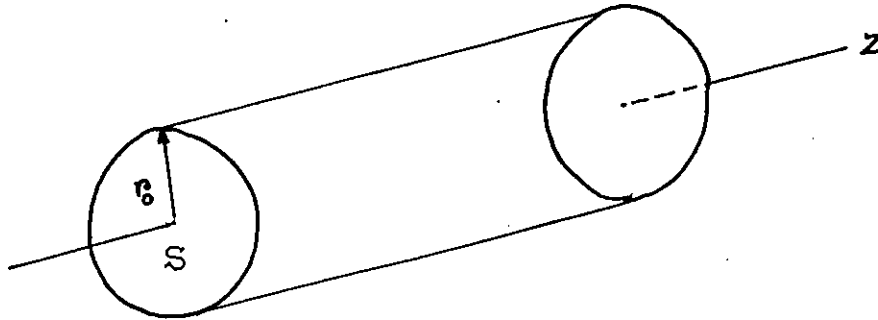


Fig. 5.1 A cylindrical conductor having circular cross-section, oriented in z-direction and carrying a current I.

Now for the surface under consideration (circular front face of the conductor shown in fig 5.1), the magneto-mechanical stress is given by equation (5.3), replacing \bar{B} by $\bar{a}_\phi B_\phi$ and \bar{n} by \bar{a}_z :

$$\begin{aligned} \bar{t}_m &= \frac{1}{\mu} (\bar{a}_\phi \cdot \bar{a}_z B_\phi) \bar{B} - \frac{1}{2\mu} B_\phi^2 \bar{a}_z \\ &= -\frac{\bar{a}_z \mu_0 \mu_r H_\phi^2}{2} \quad [B_\phi = \mu_0 \mu_r H_\phi] \end{aligned} \tag{5.5}$$

Exactly the same amount of stress will be experienced radially inward on the curved surface of the cylindrical conductor if we take the unit normal \bar{n} as \bar{a}_r . This stress will try to squeeze the conductor radially and this lateral strain will inturn manifests in the form of axial tension to produce longitudinal elongation. Thus we can say that axially the magneto-mechanical stress is acting in the form of tension.

For a direct current I , the magnitude of the net tension on the surface S of the conductor, shown in fig 5.1, is

$$\begin{aligned}
 T_m &= \int_a |\bar{t}_m| da \quad [a, \text{ the area of cross-section of the conductor}]. \\
 &= \frac{1}{2} \mu_0 \mu_r \int_0^{r_0} \left(\frac{I r}{2\pi r_0^2} \right)^2 d(\pi r^2) \\
 &= \frac{I^2}{4\pi} \mu_0 \mu_r \int_0^{r_0} \frac{r^3}{r_0^4} dr \\
 &= \frac{I^2}{16\pi} \mu_0 \mu_r \quad [I \text{ is taken out of the integration sign, since current is uniformly distributed throughout the cross-section of } S, \text{ in case of d.c.}]
 \end{aligned}$$

(5.6)

From equation(5.6), it is evident that the tension due to magnetic field is independent of the dimension of the conductor and directly proportional to the square of the current.

AC Case:

As the current distribution is not uniform throughout the cross-section of a conductor, current is also a variable depending on the distance from the centre of the conductor and the magnetic field developed inside the conductor at a distance r from its axis due to the electric current is given by

$$H_{\theta} = \int_0^{r_0} (x/r) i_x dx \quad (5.7)$$

Where, i_x = the current density at a distance x from the centre of the conductor.

r_0 = the radius of the conductor.

Thus the magnitude of the net tension on the surface x is given by,

$$\begin{aligned} T_m &= \left| \int_a \bar{t}_m da \right| \\ &= \frac{1}{2} \mu_0 \mu_r \int_0^{r_0} \left(\int_0^r (x/r) i_x dx \right)^2 d(\pi r^2) \\ &= \pi \mu_0 \mu_r \int_0^{r_0} \frac{r}{r^2} \left(\int_0^r x i_x dx \right)^2 dr \\ &= \pi \mu_0 \mu_r \int_0^{r_0} \frac{1}{r} \left(\int_0^r x i_x dx \right)^2 dr \end{aligned} \quad (5.8)$$

Comparison of magnetic tension due to AC and DC :

This comparison can be done in a similar fashion mentioned earlier in section 4.2.2 by considering equal amounts of ac and dc currents flowing through the conductor. Dividing equation (5.8) by equation (5.6) and putting the value of I from equation (4.8) and that of i_x from equation (3.39) we get the ratio as,

$$\frac{T_{ac}^{(m)}}{T_{dc}^{(m)}} = \frac{16 \pi^2 \int_0^{r_0} \frac{1}{r} \left(\int_0^r \frac{\text{Ber}(mx) + j \text{Bei}(mx)}{\text{Ber}(mr) + j \text{Bei}(mr)} x dx \right)^2 dr}{\left(\int_0^{r_0} r \frac{\text{Ber}(mr) + j \text{Bei}(mr)}{\text{Ber}(mr_0) + j \text{Bei}(mr_0)} dr \right)^2} \quad (5.10)$$

A plot of this ratio verses frequency is shown in fig 5.2 .

The ratio increases with the increase in frequency . A sharp upslope of the ratio is observed near 100 kHz.

5.3 Numerical Example.

As mentioned earlier in section 4.3, we shall assume conductors and their sizes which are used in practice. Particular emphasis is given on the study of magneto-mechanical stress and tensile force acting on power lines. Representative data for steady state conditions, short circuit(fault) conditions and switching transient situations have been used in determining the stress distribution and tension.

5.3.1 Steady state Condition

Tension on power lines due to the magnetic field is calculated using equation 5.8 . Tension due to d.c. field is also evaluated to make a comparison and to have an idea about the variation of magneto-mechanical tension with frequency, calculations are carried out for different frequencies also.

Table 5.1 Tensile force on some common conductors used for BPDB power lines, for dc .

Code	Overall dia(mm)	Amount of current(Amp)	Compressive force due to elec. fld. in 10^{-5} N.
GNAT(400V)	6.18	140	51
ANT (400V)	9.30	200	100
EARWIG(400V)	10.20	260	180
WASP (400V)	13.17	310	250

Table 5.2 Tensile force on some common conductors used for BPDB power lines, for ac at power frequency(50Hz.)

Code	Overall dia(mm)	Amount of current(Amp)	Compressive force due to elec. fld. in 10^{-5} N.
GNAT(400V)	6.18	140	56
ANT (400V)	9.30	200	110
EARWIG(400V)	10.20	260	190
WASP (400V)	13.17	310	270

Assuming a steadystate current of 300A passing through a typical aluminium conductor of radius 4mm, the tensile force developed in Newton at different frequencies is shown in table 5.3 to get an idea about the frequency dependence of the tensile force.

Table 5.3 Tensile force on a specific conductor for ac at different frequencies.

Operating Freq.(Hz)	Tension due to magnetic field 10^{-4} (N)
50.	25
5000.	65
10000.	97
50000.	270
100000.	460
500000.	2000
1000000.	4400

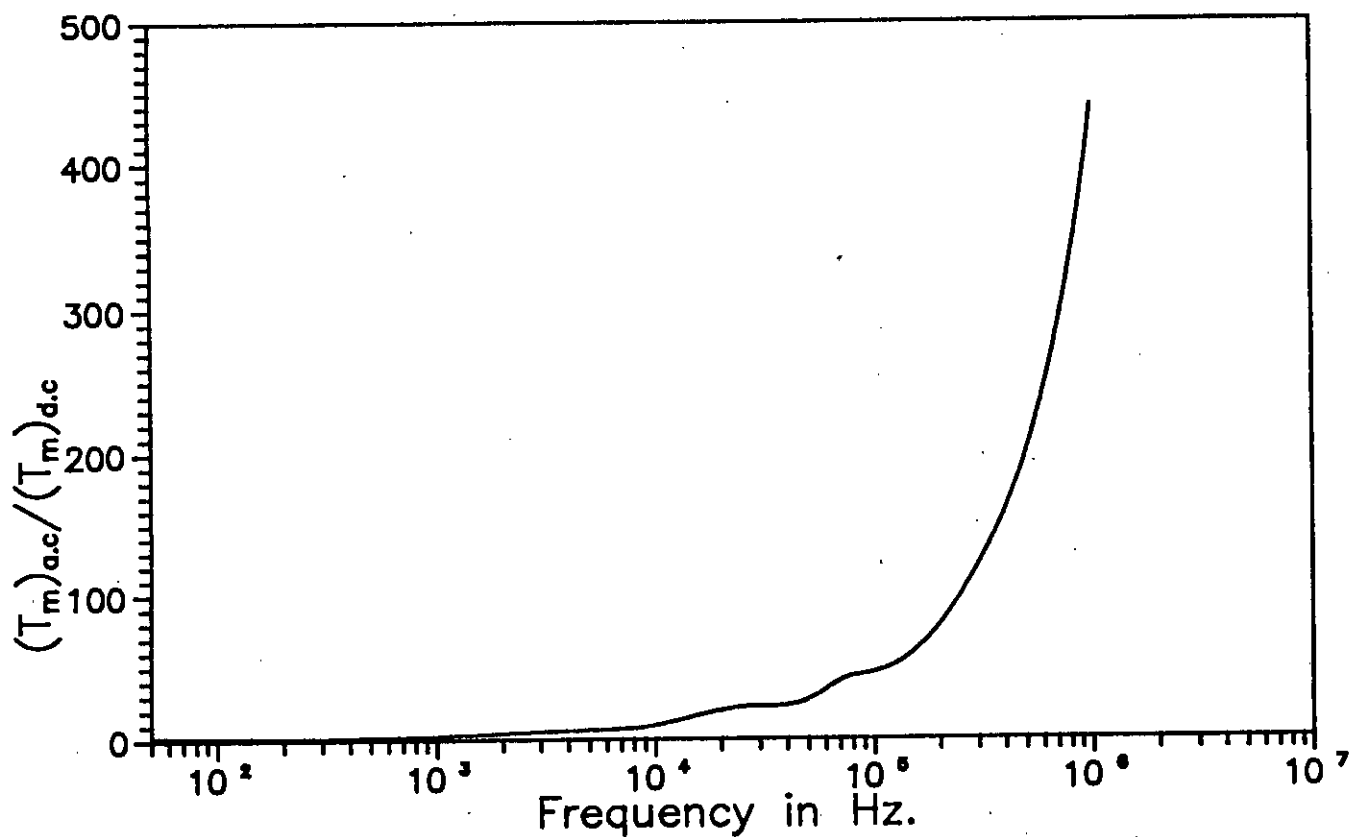


Fig. 5.2 Ratio of stress due to ac to that due to dc as a function of frequency.

To get an idea about the stress distribution inside a conductor due to steady-state ac , a typical aluminium conductor of radius 4mm is assumed for a current of 300A .The tensile stress distribution in N/m^2 (normalized) inside the conductor at different frequencies is shown in table 5.4

Table 5.4 Magneto-mechanical Stress distribution inside a conductor of circular cross-section for steady-state alternating currents at different frequencies.

Operating Frequency	Radial Distance	Stress in N/m^2 (Normalized)
50	0.00	0.0000×10^{-00}
50	0.20	0.1005×10^{-12}
50	0.40	0.4021×10^{-12}
50	0.60	0.9048×10^{-12}
50	0.80	0.1608×10^{-11}
50	1.00	0.2513×10^{-11}
10000	0.00	0.0000×10^{-00}
10000	0.20	0.1005×10^{-12}
10000	0.40	0.9048×10^{-12}
10000	0.60	0.1608×10^{-12}
10000	0.80	0.2513×10^{-11}
10000	1.00	0.3473×10^{-11}
50000	0.00	$0.0000 \times 10^{+00}$
50000	0.20	0.1300×10^{-18}
50000	0.40	0.2318×10^{-17}
50000	0.60	0.5459×10^{-16}
50000	0.80	0.1407×10^{-14}
50000	1.00	0.4974×10^{-13}
5000000	0.00	$0.0000 \times 10^{+00}$
5000000	0.20	0.7586×10^{-43}
5000000	0.40	0.4509×10^{-30}
5000000	0.60	0.1139×10^{-22}
5000000	0.80	0.2019×10^{-17}
5000000	1.00	0.2375×10^{-13}

A parabolic stress distribution is observed for steady-state AC at power frequency (refer to fig. 5.3), and it is found that no stress is developed at the axis of the conductor due to magnetic field but the stress is maximum at the surface , since

the current enclosed increases from zero to maximum from the axis towards the surface. The stress distribution for a frequency of 50 kHz is shown in fig 5.4 . The stress is almost zero from the axis up to very near the surface, where it rises very sharply. This is because at this high frequency the current density inside the conductor is almost zero and current exists only near the surface.

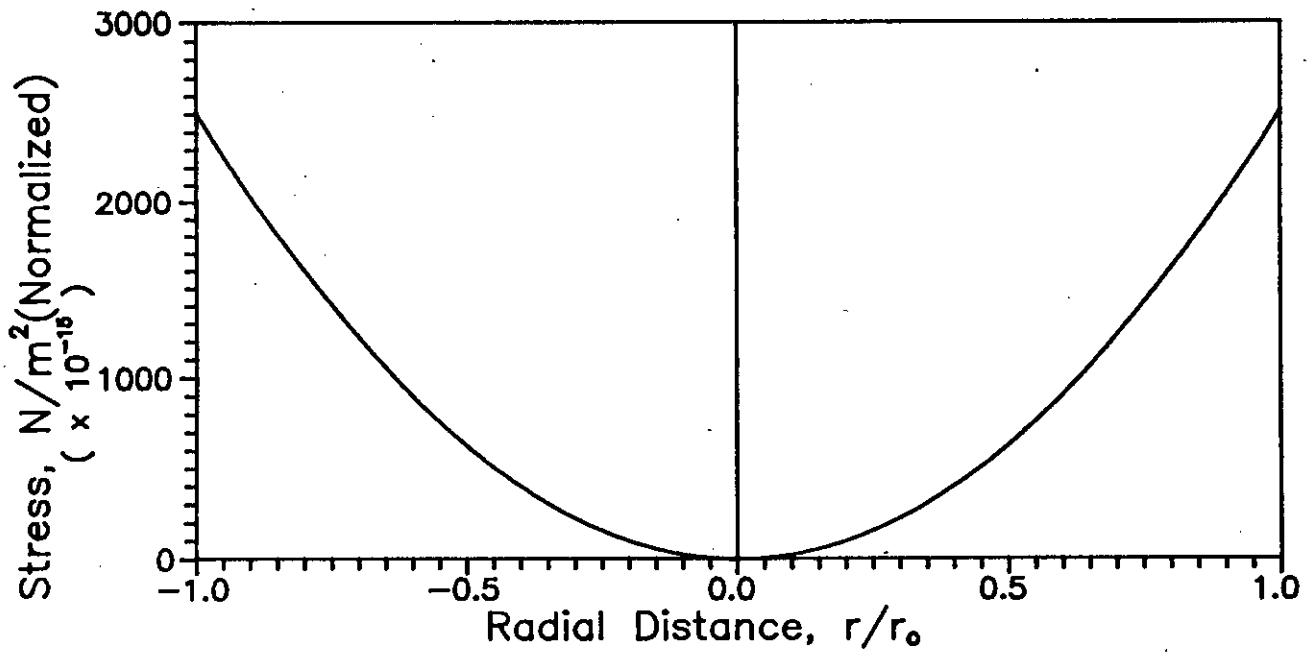


Fig. 5.3 Radial distribution of stress due to magnetic field. Steady-state ac 50 Hz.

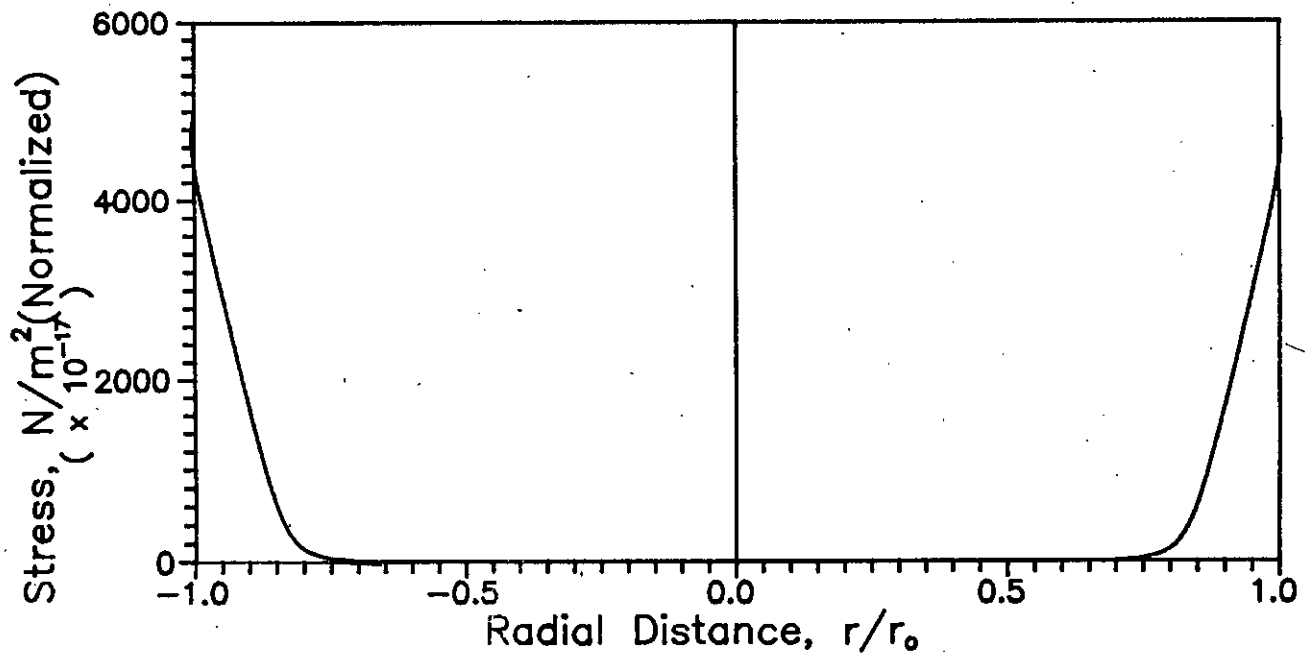


Fig. 5.4 Radial distribution of stress due to magnetic field. Steady-state ac 50 kHz.

5.3.2 Fault Current Study

Using the set of conductor specifications mentioned in section 4.3.2, the magneto-mechanical stress and the resulting tension are calculated and shown in table 5.5.

Table 5.5 Magneto-mechanical tension developed for a fault current (ac at power frequency) on conductors of BPDB power distribution lines.

Code	Overall dia(mm)	Fault current (kA)	Used for power lines of	Tensions due to Magnetic field in Newton.
GNAT	6.18	41.9	400v	49.00
ANT	9.30	41.9	400v	49.00
WASP	13.17	41.9	400v	49.00
GOPHER	7.08	13.1	11kV	1.20
RABBIT	10.05	13.1	11kV	1.20
DOG	14.15	13.1	11kV	1.10
MERLIN	18.05	17.5	33kV	3.20

5.3.3 Transient Switching on Cndition

Substituting equation (3.60) in to (5.8) and integrating numerically the magneto-mechanical tensile stress distribution with respect to the distance from the axis of the conductor is calculated for ac of different frequencies. A typical aluminium conductor of radius 4mm is considered for this purpose, and the time considered is 10 sec after switching. The result is shown in table 5.6 and the variation is plotted in fig. 5.5. Inside the conductor the stress increases very slowly but it rises very sharply near the surface.

Table 5.6 Magnetic stress distribution inside the conductor for ac of different frequencies at 10 μ -sec after switching.

Operating Frequency	Radial Distance	Stress in N/m ² (Normalized)
50	0.00	0.0000x10 ⁻⁰⁰
50	0.20	0.7058x10 ⁻¹⁵
50	0.40	0.1693x10 ⁻¹⁴
50	0.60	0.3122x10 ⁻¹⁴
50	0.80	0.5258x10 ⁻¹⁴
50	1.00	0.4604x10 ⁻¹³
20000	0.00	0.0000x10 ⁻⁰⁰
20000	0.20	0.6249x10 ⁻¹⁵
20000	0.40	0.1585x10 ⁻¹⁴
20000	0.60	0.3373x10 ⁻¹⁴
20000	0.80	0.5607x10 ⁻¹⁴
20000	1.00	0.4868x10 ⁻¹³
50000	0.00	0.0000x10 ⁻⁰⁰
50000	0.20	0.6486x10 ⁻¹⁵
50000	0.40	0.1520x10 ⁻¹⁴
50000	0.60	0.3350x10 ⁻¹⁴
50000	0.80	0.6623x10 ⁻¹⁴
50000	1.00	0.5954x10 ⁻¹³
5000000	0.00	0.1318x10 ⁻¹⁷
5000000	0.20	0.3005x10 ⁻¹⁷
5000000	0.40	0.3005x10 ⁻¹⁷
5000000	0.60	0.6918x10 ⁻¹⁷
5000000	0.80	0.1756x10 ⁻¹⁶
5000000	1.00	0.2436x10 ⁻¹³

Now in case of DC, the radial distribution of transient current just after switching is governed by equation (3.6~~5~~) as mentioned earlier in section 3.4. So at 10 μ -sec after switching, the compressive stress distribution in N/m^2 (normalized) inside a similar aluminium conductor as above for a direct current passing through it is calculated and shown in table 5.7.

Table 5.7 Magnetic stress distribution inside the the conductor at 10 μ -sec after switching on for dc.

Radial Distance	Stress in N/m^2 (Normalized)
0.00	$0.0000 \times 10^{+00}$
0.20	0.1421×10^{-15}
0.40	0.5245×10^{-16}
0.60	0.5371×10^{-16}
0.80	0.7377×10^{-17}
1.00	0.4766×10^{-14}

In fig 5.6 the stress distribution for DC switching on is shown, where it is found that except a few oscillations, the stress inside the conductor is almost zero, and increases sharply near the surface.

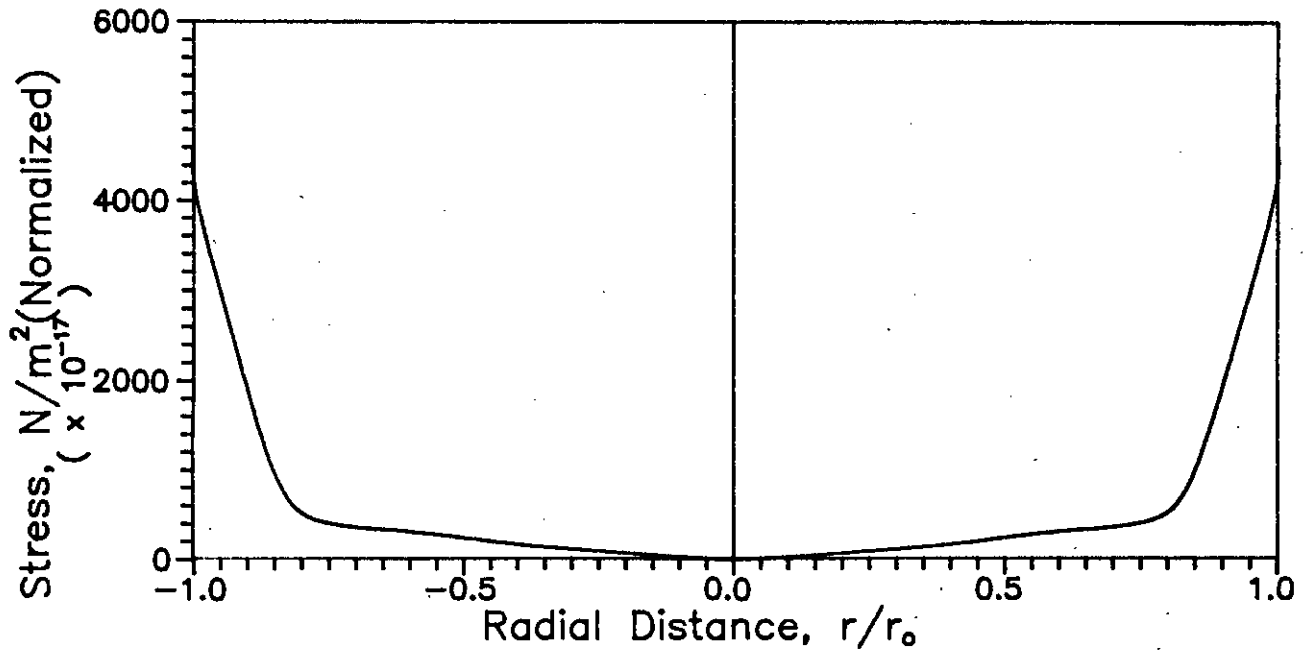


Fig. 5.5 Radial distribution of stress due to magnetic field. 10 micro-sec after switching (ac 50 Hz).

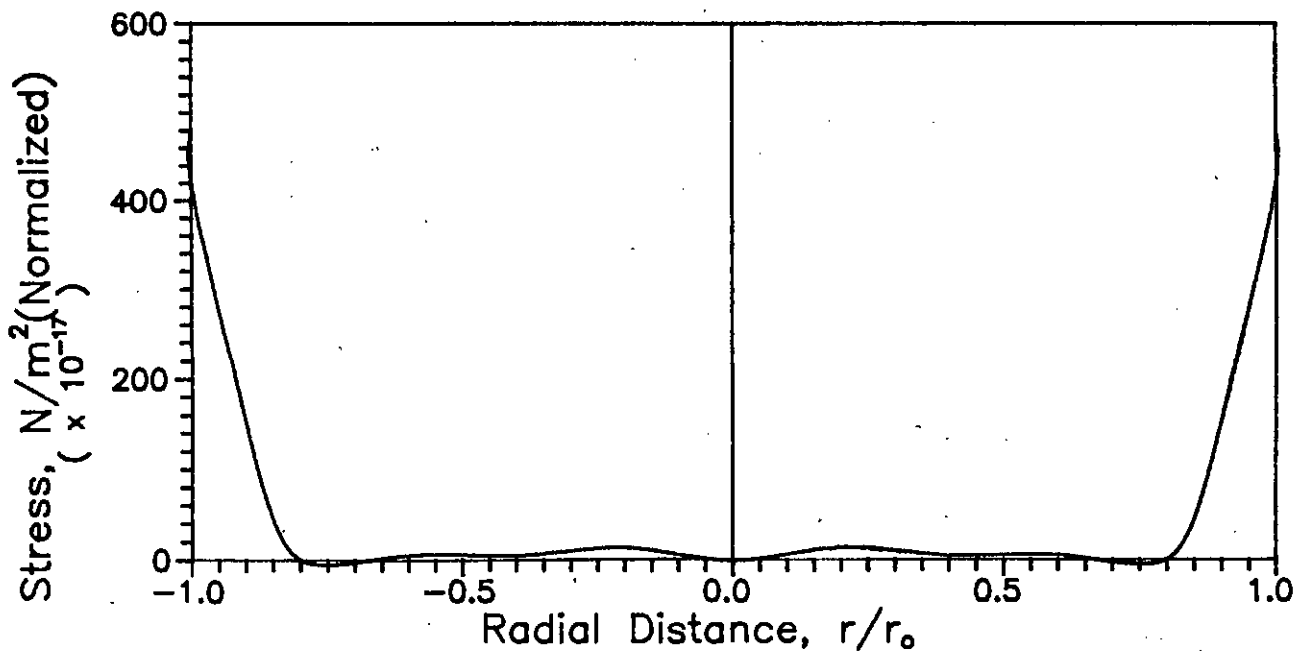


Fig. 5.6 Radial distribution of stress due to magnetic field. 10 micro-sec after switching (dc).

5.4 Discussion

The above chapter has been devoted to study the magnetic stress distribution and total tensile force which is developed as a result of this stress in a cylindrical conductor .

In chapter -4, we have observed that the dielectric stress is compressive in nature. Here we have seen that the magnetic stress has a tensile property i.e. a property of opposing the dielectric stress. Although the magnitude of the resulting tension was not of considerable extent during steady state operations during transient overcurrent situations (fault conditions) it may reach as high as several tenths of Newton in most conductors of practical utility. It is also notable to state that the amount of this tension (tensile stress) increases with frequency as shown in fig. 5.2 .

CHAPTER SIX

**CALCULATION OF STRESS DUE TO
JOULE-HEATING**

6.1 Introduction

It is a regular phenomenon that when current passes through a conductor I^2R loss or Ohmic^{mic} dissipation occurs within the conductor in the form of heat due to the resistance of the conductor. This heat in turn increases the temperature of the conductor up to a certain limit, which puts the conductor into a state of Joule-heating or thermally stressed condition. In chapter-2, separate expression for stress due to Joule-heating developed in a conductor has been derived. On the basis of that expression numerical calculations of thermal stress and the associated forces in cylindrical conductors are discussed in this chapter.

5.2 Stress Distribution in a Cylindrical Conductor

Electro-thermal stress was found to be :

$$\bar{t}^{(th)} = \hat{S}^{(th)} \cdot \bar{n} \quad (6.1)$$

in section 2.5 of chapter 2.

where $\hat{S}^{(th)}$ = the stress tensor.

the components of $\hat{S}^{(th)}$ are given in table -2.3 of section 2.5, and the components of $\bar{t}^{(th)}$ can be written as,

$$t_j^{(th)} = \sum_{k=1}^3 S_{jk} \cdot n_k \quad (j = 1, 2, 3) \quad (6.2)$$

If in equation (6.2) the components of $\hat{S}^{(th)}$ are substituted from table-2.3

$$\begin{aligned}
\bar{t}^{(th)} &= \bar{a}_x t_x + \bar{a}_y t_y + \bar{a}_z t_z \\
&= 2\sigma t \{ \bar{a}_x \{ (E_x^2 - 1/2E^2)n_x + E_x E_y n_y + E_x E_z n_z \} \\
&\quad + \bar{a}_y \{ (E_y^2 - 1/2E^2)n_y + E_y E_x n_x + E_y E_z n_z \} \\
&\quad + \bar{a}_z \{ (E_z^2 - 1/2E^2)n_z + E_z E_y n_y + E_x E_z n_x \} \} \\
&= 2\sigma t \{ \bar{a}_x E_x (E_x n_x + E_y n_y + E_z n_z) \\
&\quad + \bar{a}_y E_y (E_x n_x + E_y n_y + E_z n_z) \\
&\quad + \bar{a}_z E_z (E_x n_x + E_y n_y + E_z n_z) \} \\
&\quad - \sigma t E^2 (\bar{a}_x n_x + \bar{a}_y n_y + \bar{a}_z n_z)
\end{aligned}$$

$$\bar{t}^{(th)} = 2\sigma t (\bar{E} \cdot \bar{n}) \bar{E} - \sigma t E^2 \bar{n} \quad (6.3)$$

Now Let us consider a cylindrical conductor with its axis along the z-direction of a cylindrical co-ordinate system. If the current flows along the z-direction, the applied electric field will be given by

$$\bar{E} = \bar{a}_z E_z \quad (6.4)$$

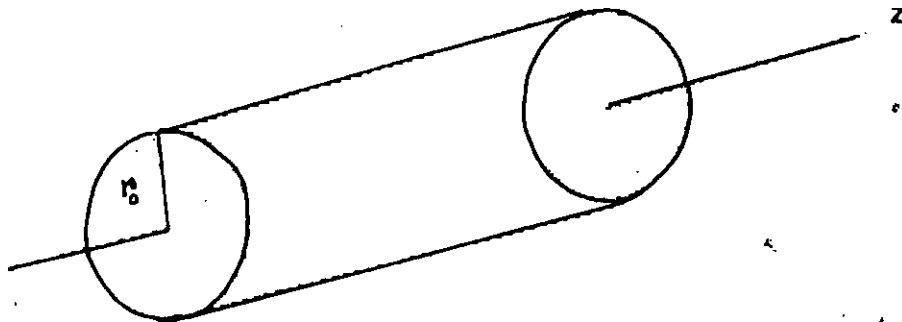


Fig. 6.1 Cylindrical conductor whose axis is along the z-direction

Let us calculate the stress on the cross-section of the wire . The normal to the surface (Surface S in fig.6.1) under consideration must be along the direction of electron motion , because the heat transfer is associated with the motion of the electron . Hence for stress due to Joule-heating , $\bar{n} = -\bar{a}_z$, and from equation (2.28), it can be said that this stress acts in the form of tension on the conductor . The magnitude of total tension resulting from the stress due to Joule-heating is given by ,

$$\begin{aligned}
 T^{(th)} &= \left| \int_S \bar{t}^{(th)} ds \right| \\
 &= \sigma t \int E_z^2 d(\pi r^2) \quad [\text{since } ds = d(\pi r^2)] \\
 &= \sigma t \int_0^{r_0} E_z^2 \cdot 2\pi r dr \\
 &= \sigma t \int_0^{r_0} (i/\sigma)^2 \cdot 2\pi r dr \\
 &= \frac{2\pi t}{\sigma} \int_0^{r_0} r i^2 dr \quad (6.5)
 \end{aligned}$$

DC Case:-

For DC, current distribution is uniform throughout the cross-section . So if I be the total current , then

$$i = I/\pi r_0^2 \quad (6.6)$$

putting this value of i in equation (6.5),

$$\begin{aligned}
 T^{(th)} &= \frac{2I^2 t}{\pi \sigma r_0^4} (r_0^2/2) \\
 &= \frac{I^2 t}{\pi \sigma r_0^2} \quad (6.7)
 \end{aligned}$$

Where, t = the time in second required for the conductor to reach its ultimate steady state temperature.

The ultimate steady state temperature being constant for a particular conductor but the time required to reach the

temperatur varies with the amount of current and the ambient condition.

AC Case:-.

For AC the current density is also a function of the distance from the axis 'r' , and is given by equation (3.38), thus

$$T^{(th)} = 2 \frac{\pi t i_o^2}{\sigma} \int_0^R \left[\frac{\text{Ber}(mr) + j\text{Bei}(mr)}{\text{Ber}(mr_o) + j\text{Bei}(mr_o)} \right]^2 r dr \tag{6.8}$$

Comparison of the thermal tension due to AC to that due to DC:

Considering the same amount of AC and DC current , and similar conductor specifications, and replacing I of equation (6.7), by equation (4.8),we get,

$$\frac{T_{a.c}^{(th)}}{T_{d.c}^{(th)}} = \frac{r_o^2}{2} \frac{\int_0^R \left[\frac{\text{Ber}(mr) + j\text{Bei}(mr)}{\text{Ber}(mr_o) + j\text{Bei}(mr_o)} \right]^2 r dr}{\left[\int_0^R \frac{\text{Ber}(mr) + j\text{Bei}(mr)}{\text{Ber}(mr_o) + j\text{Bei}(mr_o)} r dr \right]^2} \tag{6.9}$$

This ratio is the same as that derived for stress due to electric field discussed in chapter 4 and fig 4.2 represents the plot of this ratio as a function of frequency.

6.3 Numerical Example:

Maximum ambient air temperature , ground temperature at one meter, ground thermal resistivity and maxium conductor temperatures etc are the essential features or design parameters for errection of power lines, because very often power conductors

are subject to thermally stressed condition due to continuous operation or overcurrent situations arising from short circuit or from any other abnormal operating conditions.

In chapter -2 we have formulated expressions for evaluating the mechanical stress developed in a conductor due to Joule-heating (I^2R loss). There we have shown that it is a time dependent quantity. A characteristic curve to denote the time constant for Linnet conductor(ACSR) has also been shown. From fig. 2.2 ,it is observed that the time required for Linnet conductor to reach its ultimate steady-state temperature rise when subject to change in current is approximately 30 minutes for a particular ambient condition (refer to fig. 2.2) .

Almost in every substations and with transformers , switchgear and circuit breakers i.e. protective devices are provided to prevent the fault currents from damaging the conductor and other valuable electrical appliances, there are different types of circuit breakers depending on the speed of the breaker [15].

<u>Type of Breaker</u>	<u>The ckt has to withstand the fault current up to</u>
1) 8 cycle breakers	: 8 x 1/f sec.
2) 5 cycle breakers	: 5 x 1/f sec.
3) 3 cycle breakers	: 3 x 1/f sec.
4) 2 cycle breakers	: 2 x 1/f sec.

Where f is the frequency of operation (supply frequency). So the duration of the fault current should be considered according to the speed of the breaker. 8 cycle breaker

assumptions will be made for calculating the stress during fault current condition.

6.3.1 Steady-state Condition:

The total tension resulting from thermal stress is expressed in equation (6.8), where utilizing the set of data from table 4.2 and assuming a time of 30 minutes, table 6.2 is prepared. Tension due to d.c case is also tabulated (table 6.1) to make a comparison.

Table 6.1 Mechanical tension developed on some common conductors used for BPDB power lines due to Joule-heating for Direct Current(D.C).
(Assuming a saturation time of 30 minutes.)

Code	Overall dia(mm)	Current (Amp)	Tension due to Joule-heating in Newton.
GNAT(400V)	6.18	140	211
ANT (400V)	9.30	200	390
EARWIG(400V)	10.20	260	580
WASP (400V)	13.17	310	741

Table 6.2 Mechanical tension developed on some common conductors used for BPDB power lines due to Joule-heating for ac at power frequency(50 Hz.) and assuming a saturation time of 30 minutes.

Code	Overall dia(mm)	Current (Amp)	Tension due to Joule-heating in Newton
GNAT(400V)	6.18	140	215
ANT (400V)	9.30	200	395
EARWIG(400V)	10.20	260	581
WASP (400V)	13.17	310	745

Assuming a steadystate current of 300A passing through a typical aluminium conductor of radius 4mm, the tensile force developed in Newton at different frequencies is tabulated below (table 6.3) to get an idea about the frequency dependence of the tensile force developed in a conductor due to Joule-heating.

Table 6.3 Tensile force on a specific conductor for alternating currents at different frequencies.

Operating Freq.(Hz)	Tension due to Joule-heating in N.
50.	716
5000.	1074
10000.	1566
50000.	4072
100000.	6712
500000.	29535
1000000.	62650

The tensile stress distribution in N/m^2 (normalized) inside the same conductor at different frequencies is shown in table 6.4.

Table 6.4 Tensile Stress distribution inside a conductor of circular cross-section for steady-state ac at different frequencies. (aluminium wire of radius, 4mm).

Operating Frequency	Radial Distance	Stress in N/m ² (Normalized)
50	0.00	00x10 ⁺⁰⁰
50	0.20	13x10 ⁻⁰⁹
50	0.40	27x10 ⁻⁰⁹
50	0.60	40x10 ⁻⁰⁹
50	0.80	54x10 ⁻⁰⁹
50	1.00	67x10 ⁻⁰⁹
10000	0.00	00x10 ⁺⁰⁰
10000	0.20	42x10 ⁻¹²
10000	0.40	11x10 ⁻¹¹
10000	0.60	37x10 ⁻¹¹
10000	0.80	16x10 ⁻¹⁰
10000	1.00	81x10 ⁻¹⁰
25000	0.00	00x10 ⁺⁰⁰
25000	0.20	29x10 ⁻¹⁴
25000	0.40	18x10 ⁻¹³
25000	0.60	21x10 ⁻¹²
25000	0.80	30x10 ⁻¹¹
25000	1.00	48x10 ⁻¹⁰
50000	0.00	00x10 ⁺⁰⁰
50000	0.20	21x10 ⁻¹⁷
50000	0.40	50x10 ⁻¹⁶
50000	0.60	22x10 ⁻¹⁴
50000	0.80	13x10 ⁻¹²
50000	1.00	28x10 ⁻¹⁰
100000	0.00	00x10 ⁺⁰⁰
100000	0.20	13x10 ⁻²³
100000	0.40	21x10 ⁻²¹
100000	0.60	80x10 ⁻¹⁹
100000	0.80	10x10 ⁻¹⁴
100000	1.00	23x10 ⁻¹⁰

The stress distribution due to Joule-heating for AC 50 Hz steady-state is shown in fig 6.2. The stress is zero at the axis but it increases almost linearly from the axis towards the surface where it becomes maximum. At a high frequency (25 kHz) as in fig 6.3, the stress remains zero from the axis up to the middle of the conductor and rises very sharply near the surface which resembles the pattern of current distribution.

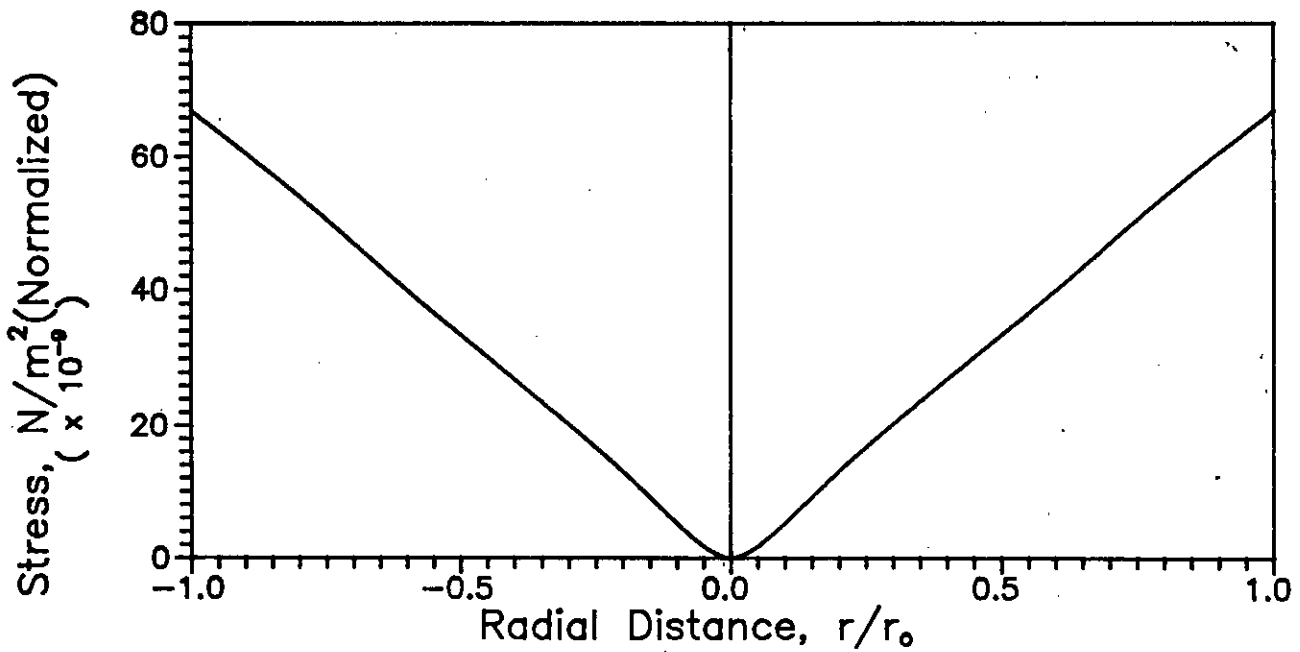


Fig. 6.2 Radial distribution of stress due to Joule-heating. Steady-state ac 50 Hz.

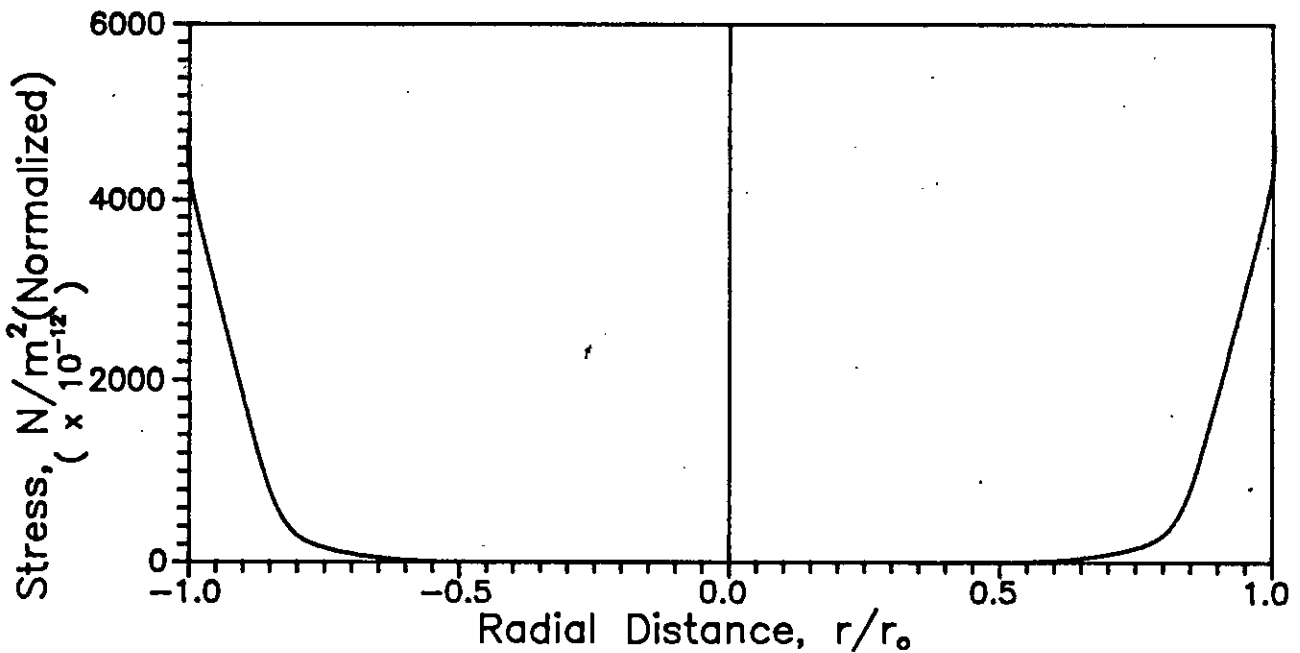


Fig. 6.3 Radial distribution of stress due to Joule-heating. Steady-state ac 25 kHz.

6.3.2 Fault Current Study

Power lines' specification, mentioned in table 4.2 and fault current conditions specified in art. 4.3.2 are put in equation(6.8) and with an assumption of 8 cycle breaker the tension due to Joule-heating are evaluated and shown in table 6.5

Table 6.5 Thermo-electric tension developed for a fault current (ac at power frequency) on conductors of BPDB power distribution lines.(due to Joule heating).

Code	Overall dia(mm)	Fault current (kA)	Used for power lines of	Tension due to Jule-heating in kN.
DOG	14.15	17.5	33kV	1.40
MERLIN	18.05	17.5	33kV	1.80

6.3.3 Switching Condition

With the help of equation (3.60) and equation (6.5) thermo-electric stress distribution and the resulting tension is calculated for a typical aluminium conductor . In chapter-3, we have seen in fig 3.3 that the transient switching current does not exist more than a few milli secs, so time integration is made for a duration of dying out of the transient current.

Table 6.6 Thermo-electric stress distribution at different distances from the axis after switching on for ac (at power freq. i.e.50Hz.) up to dying out of the transient current.

Radial Distance	Stress in N/m ² (Normalized)
0.00	0.1058x10 ⁻¹¹
0.20	0.1110x10 ⁻¹²
0.40	0.1510x10 ⁻¹⁴
0.60	0.6744x10 ⁻¹³
0.80	0.6094x10 ⁻¹³
1.00	0.3104x10 ⁻¹⁰

Table 6.7 Thermo-electric stress distribution at different distances from the axis after switching on for dc, up to dying out of the transient current.

Radial Distance	Stress in N/m ² (Normalized)
0.00	0.1319x10 ⁻²⁷
0.20	0.1383x10 ⁻²⁸
0.40	0.1510x10 ⁻¹⁴
0.60	0.6744x10 ⁻¹³
0.80	0.6094x10 ⁻¹³
1.00	0.3104x10 ⁻¹⁰

During the switching instant for AC 50 Hz , it is observed (fig 6.4) , that though a small amount of stress is sensed at the conductor axis , the conductor experiences almost no stress up to 80% of its cross-section from the axis .The stress increases very sharply and linearly from very close to the surface . This is because there exists a very little current inside the conductor during switching period.

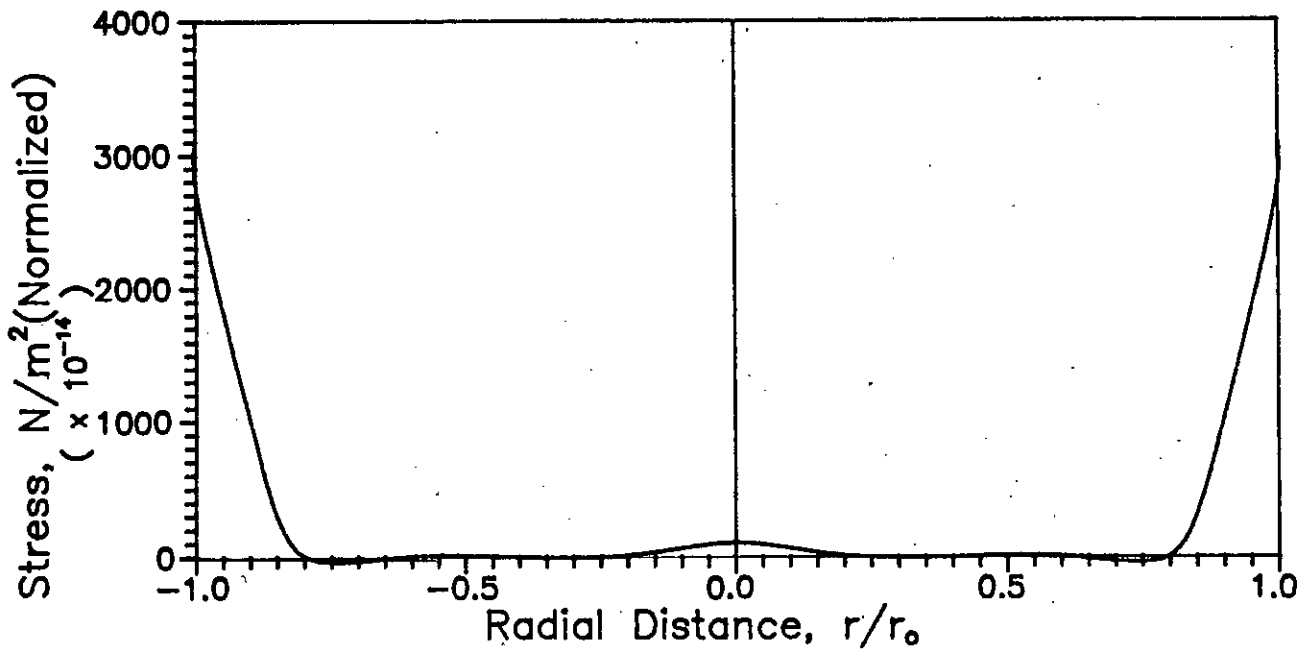


Fig. 6.4 Radial distribution of stress due to Joule-heating. Switching instant (ac 50 Hz).

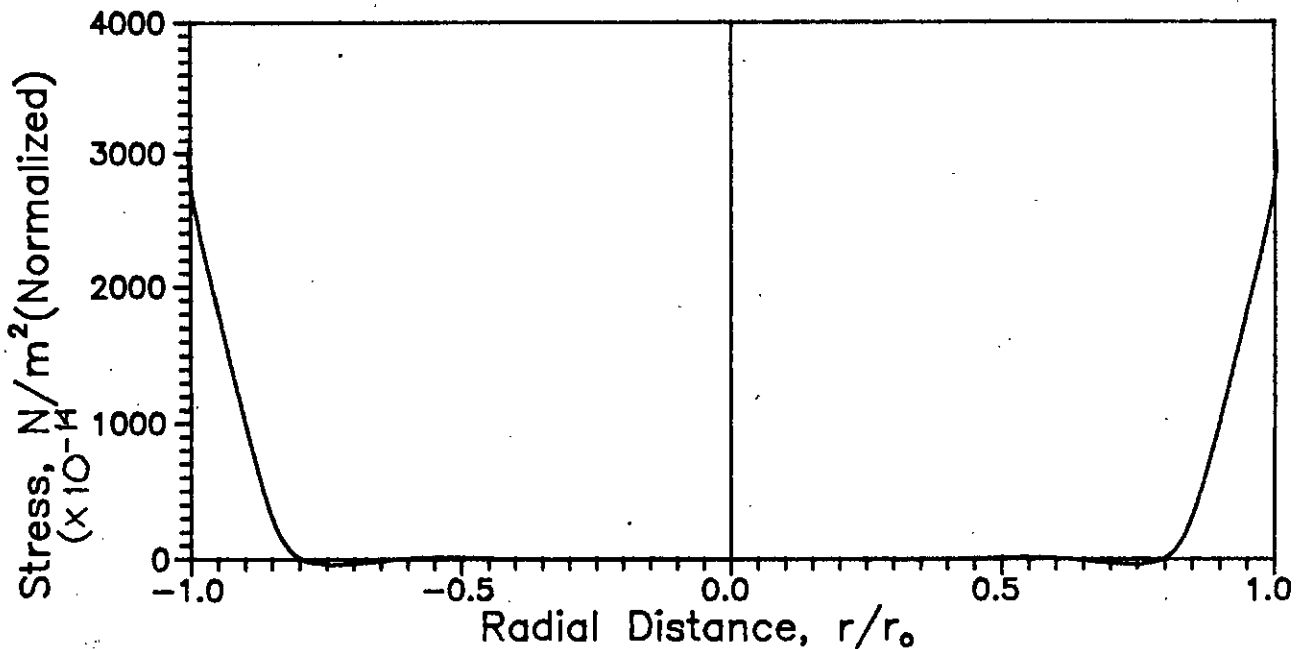


Fig. 6.5 Radial distribution of stress due to Joule-heating. Switching instant (dc).

6.4 Discussion

It is observed that even for steady state operation of a conductor the mechanical tension due to the stress resulting from Joule-heating is as high as several hundred N on conductors used for 400 volt overhead lines. During fault current condition it is found to be of similar magnitude, whereas the calculated breaking load of the same conductor is about 10-40 KN (table 4.2) . So the conductor will be highly stressed due to a continuous operation at its maximum continuous current carrying capacity or it may be damaged if a fault is not cleared by a fast breaker.

CHAPTER SEVEN

COMPARATIVE STUDY OF THE THREE
TYPES OF ELECTRO-MECHANICAL
FORCES IN A CONDUCTOR

7.1 Introduction

After getting a set of results about the mechanical stress due to electric field, magnetic field and Joule-heating individually in the previous three chapters, we turn our attention in the current chapter to depict a comparative picture of these three types of forces in a cylindrical conductor. The chapter will be occupied with set of tables of comparison followed by graphical representations with probable reasons of variations.

7.2 Variation of Forces with Current

Let us first study the amount of three different forces on a given conductor for power frequency (50 Hz) a.c. Table 7.1 represents the three different types of forces developed in an aluminium conductor of 8 mm diameter. The results are plotted in fig 7.1.

Table 7.1 Forces for different amount of current.

(Ambient temperature 27°C).

Current I Amp	Compressive / Tensile force			Ultimate temperature. rise °C
	Due to dielectric stress. T_e in 10^{-18} N	Due to Magnetic field. T_m in 10^{-4} N	Due to Joule- heating T_{th} in N	
50	.38	.71	30.2	4.3
100	1.50	2.80	118.7	16.87
150	3.50	6.40	244.3	34.7
200	6.10	11.0	392.8	55.8
250	9.60	18.0	551.3	78.3
300	14.00	25.0	713.2	101.3

It is observed from fig.7.1 that all the three forms of stresses increase in the form of a two degree parabola with the increase in currents. Actually stress distribution of power frequency a.c. is almost similar to that for d.c. field and is proportional to the square of the current as mentioned in sections 4.2 ,5.2 ,6.2 . It can be noted that the three forces at power frequency are such that $T_{th} > T_m > T_e$. Electric polarizability and the magnetic susceptibility are negligibly small in case of good conductors ,compared to its conductivity. So energy stored in the electric and magnetic fields are negligible in comparision to that dissipated in the form of Joule-heating.

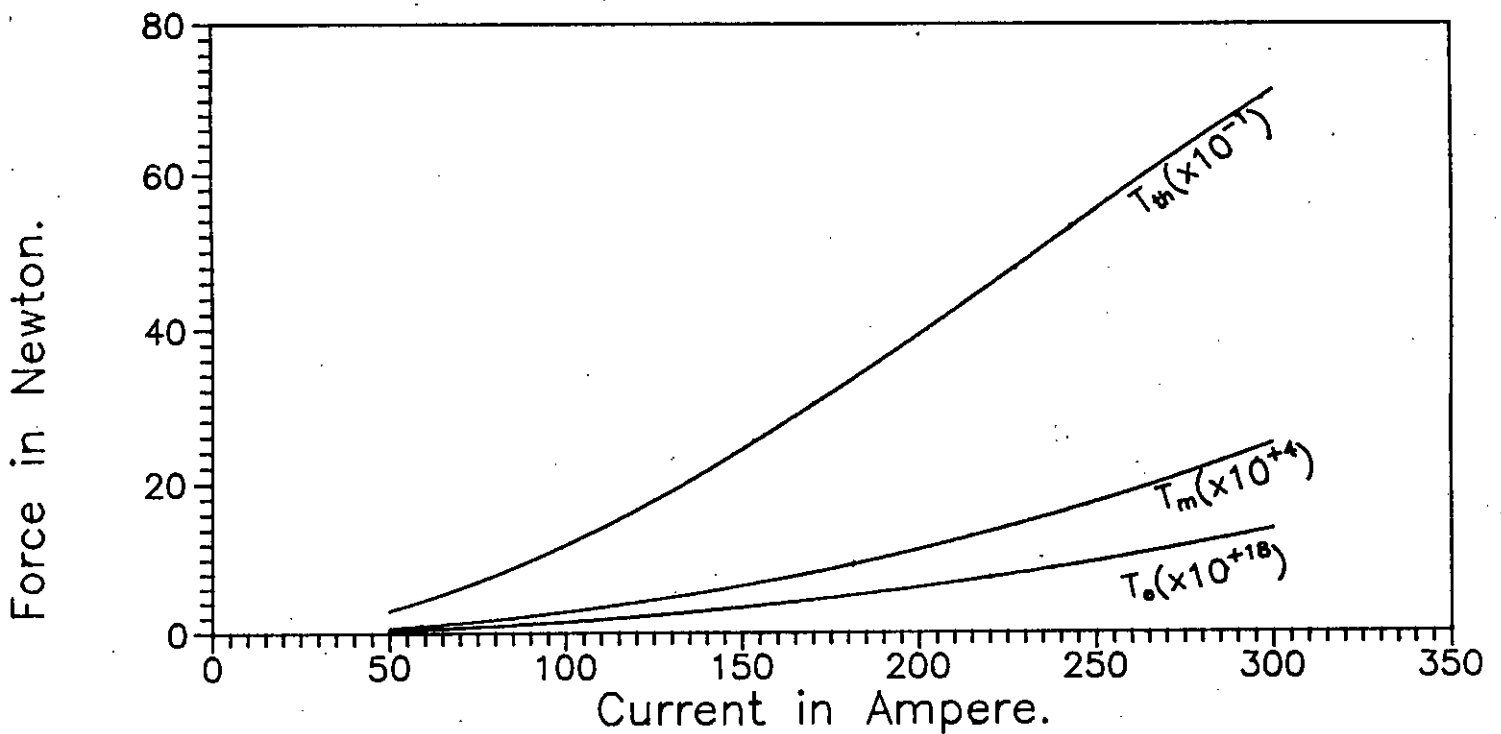


Fig. 7.1 Three types of forces as functions of currents.

7.3 Variation of the Forces with Conductor Specifications

Dependence of the forces on conductor specifications are different for the three forms of stresses. The major specifications of the conductor are its diameter and resistivity.

7.3.1 Variation with the diameter of the conductor

Forces on aluminium conductor of different radii for an alternating current of 300A at 50 Hz is shown in table 7.2 and plotted in fig 7.2.

Table 7.2 Forces on aluminium conductors of different diameter.

Conductor size diameter in mm.	Compressive / Tensile force		
	Due to dielectric stress. T_e in 10^{-18} N	Due to Magnetic field. T_m in 10^{-4} N	Due to Joule-heating T_{th} in N
8	31.0	25	735.0
12	14.0	26	316.0
16	7.8	26	178.8
20	5.0	26	115.6
24	3.5	26	73.9
30	2.5	26	52.4

The forces due to dielectric stress and that resulting from Joule-heating decrease in a hyperbolic form with the increase in conductor size (diameter) . This is because at power frequency those two forms of tension have inverse relationship with the square of the conductor diameter ,while the force due to magnetic field is independent of the conductor size as mentioned in sections 4.2, 5.2, 6.2 .

7.3.2 Variation with the resistivity of the conductor

Table 7.3 and fig 7.3 illustrate this variation for 8 mm dia conductors having different resistivities. A current of 300A is assumed.

Table 7.3 Forces on conductors having different resistivities.

Resistivity: ρ in $10^{-8} \Omega\text{-m}$	Compressive / Tensile force		
	Due to dielectric stress. T_e in 10^{-18}N	Due to Magnetic field. T_m in 10^{-4}N	Due to Joule-heating T_{th} in N
1.6	10	25	421
1.7	12	25	424
2.8	18	25	731
10.0	86	25	2559
30.0	780	25	8180

With the increase in resistivity that is for poorer conductors stress due to Joule-heating increases almost linearly (fig 7.4) while the dielectric stress increases in a parabolic pattern but stress due to magnetic field remains unchanged as it does not depend on this property of the conductor (equation 5.7).

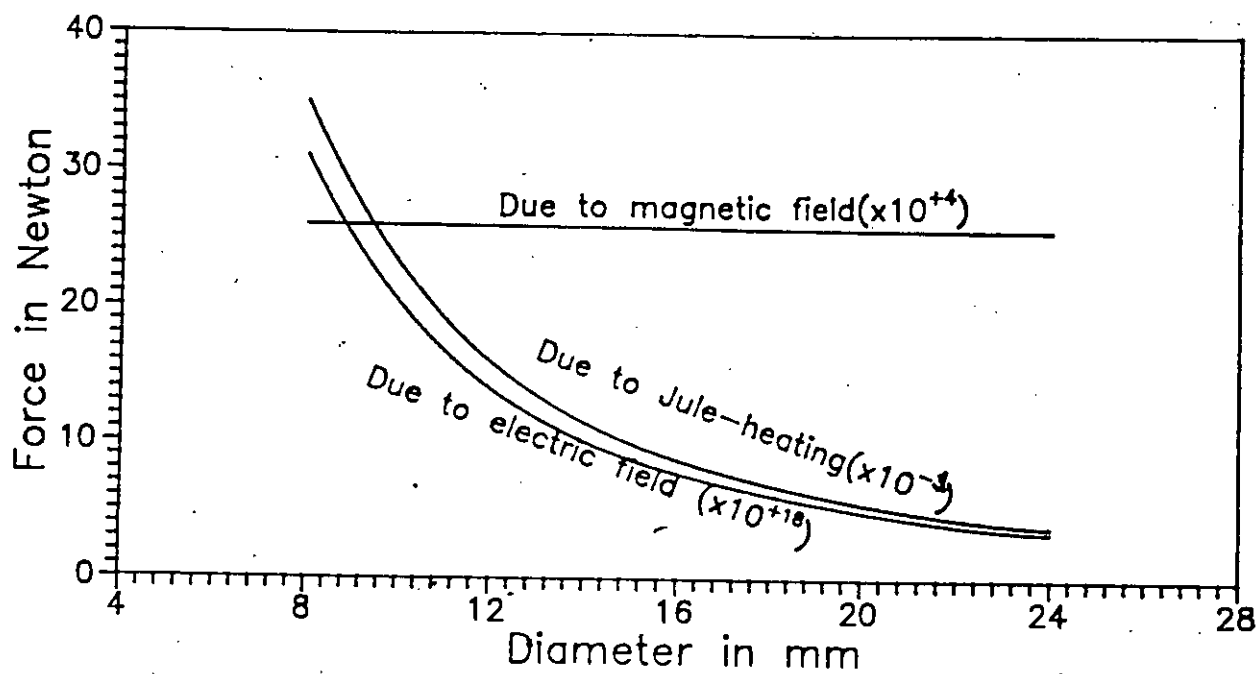


Fig. 7.2 Dependence of forces on conductor size (diameter).

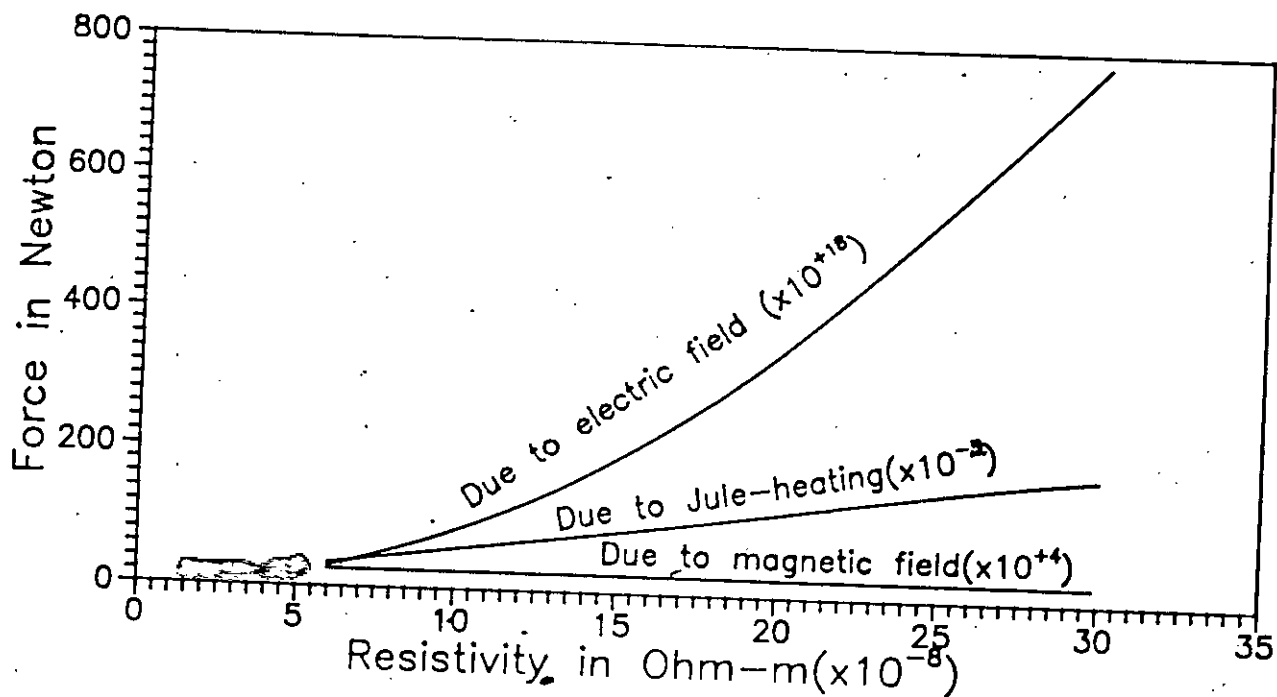


Fig. 7.3 Variations of forces with resistivity of the conductor.

7.4 Variation of forces with frequency

Now we shall investigate the relative frequency dependence of the electro-mechanical stresses on a specific conductor, for a wide range of frequencies. Forces on an aluminium conductor having a radius of 4 mm with a current flow of 300A are listed in table 7.4 with graphical plot in fig 7.4.

Table 7.4 Forces on an aluminium conductor for ac at different frequencies.

Operating frequency in Hz. f	Compressive / Tensile force		
	Due to Electric fld. T_e in 10^{-18} N	Due to Magnetic fld. T_m in (10^{-4}) N	Due to Joule-heating T_{th} in N
50	6.7	25	716
5000	9.8	65	1074
10000	14.0	97	1566
50000	37.0	270	4072
100000	63.0	460	6712
500000	270.0	2000	29535
1000000	580.00	4400	62650

All the three forces increase with the increase in frequency. For lower range of frequencies, they increase slowly but a sharp rise of them is observed near 100 kHz.

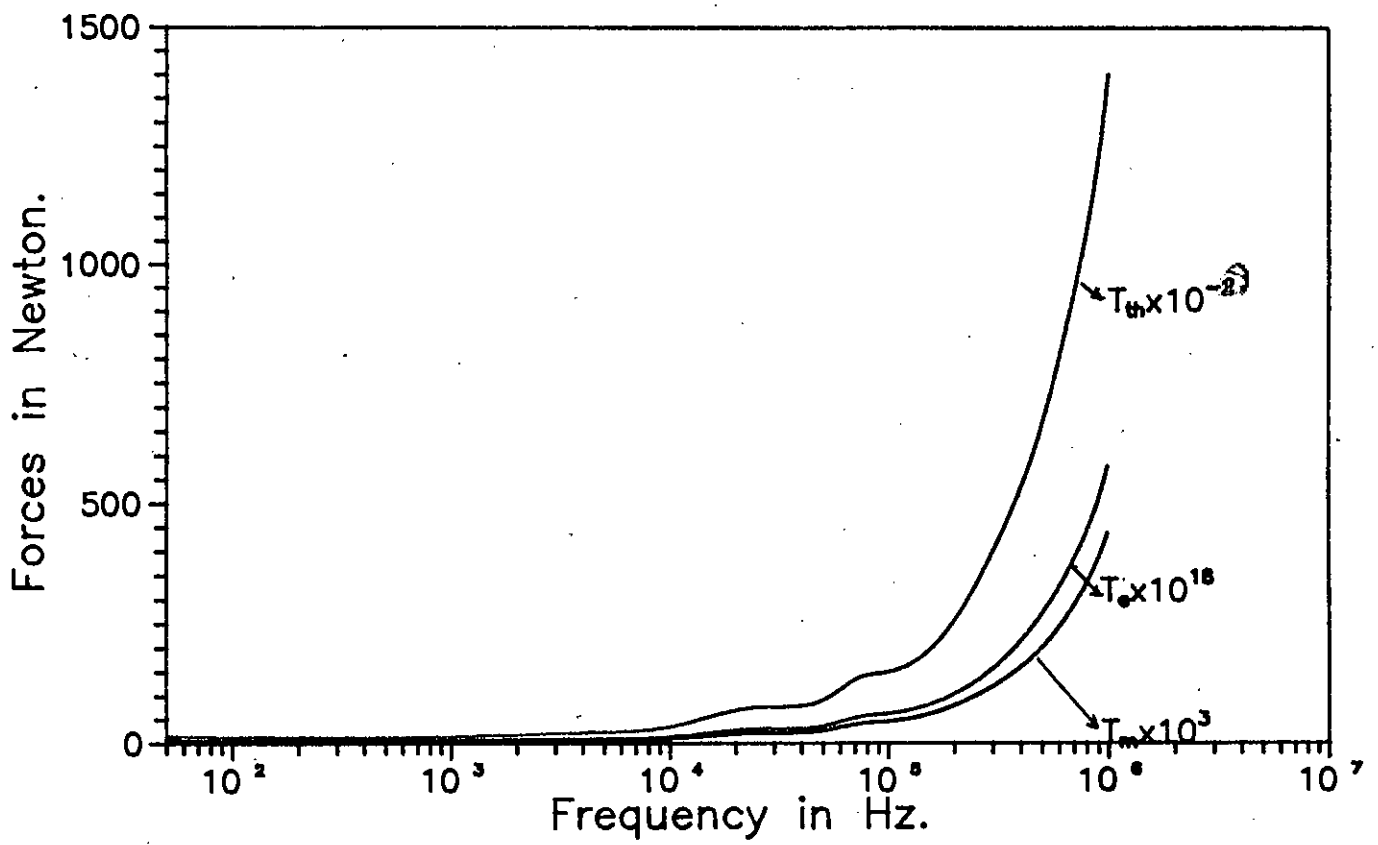


Fig. 7.4 Three forms of forces as functions of frequency.

7.5 Discussion

In course of the comparative study of the electro-mechanical forces on a current carrying conductor some important features are observed ,which are, 1) eletro-mechanical forces are directly proportional to the square of the current flowing through the conductor at power frequency a.c . 2) forces due to electric field and that due to Joule-heating are inversely proportional to the square of the conductor diameter while the force due to magnetic field is independent of the diameter of the conductor . 3) forces arising from electric field are smaller for good conductors and increases parabollically with resistivity of the conductor . ~~But~~ for Joule-heating ,force increases linearly with the increase in resistivity and magneto-mechanical force remains unchanged with respect to the resistivity of the conductor. 4) frequency response of the forces are such that they increase with the increase in frequency and a very rapid increament is observed above 100 kHz .In the above study ~~only~~ the steady-state forces are considered.


CHAPTER EIGHT

GENERAL DISCUSSION AND CONCLUSION

A current carrying conductor is usually exposed to different forms of stresses, some of them are caused externally viz, by ambient conditions, wind thrust, solar irradiation, ice loading (in cold countries) and some of them due to its own mechanical and electrical causes, In case of overhead conductors it is stressed owing to its self load also. But electrically on the course of carrying current in any condition it has to undergo three forms of electro-mechanical stresses.

Our observation says that, the dielectric stress , though plays a vital role in causing damage to an insulator, is negligible in case of conductors and of the order of 10^{-12} N/m , when subjected to a fault current of 17.1 kA at 33kV .

The tension due to magnetic field is found to be considerably high of the order of a few newton , yet it is very small to cause any severe damage to the conductor, even when a fault current of several KA range is allowed to pass through the conductor, because the breaking strength of the specimen conductor for which the stress was calculated was of the range of kN.

The mechanical tension on practical overhead conductors resulting from Joule-heating is high enough even for steady state current. It is of the order of kN which may cause increase in the sag of overhead conductors and may result hazardous ground clearance of them. Stress of this form due to fault current is high enough if the breaker tripping were not sufficiently fast, i.e,if the breaker failed to clear the fault current rapidly it may cause permanent deformations to them,  vivid example of which was the cause of the

black out of the whole New York city for a long duration of 23 hours, on July 13, 1977. Later it was investigated out that after two consecutive lightning strokes, three 345-kV lines were crippled pushing the remaining lines above their thermal limits, and due to thermal expansion the conductors of another 345-KV line sagged deep enough to cause short circuit via small tree. The line tripped causing further overload of the few remaining ties [16].

In course of our study we have seen that the stress due to magnetic field is directly proportional to the relative permeability of the material which was assumed to be unity for conductors like copper and aluminium, but material like silicon steel, which is used for the construction of the core of different electrical machines like, generators, motors and transformers, are blessed with a large value of relative permeability $\mu_r = 7000$ at room temperature [17]. Almost in all applications eddy current flows through a magnetic core though its amount is limited to a low value by slicing them in thin laminations, yet owing to their large permeability, they will have to withstand a considerable stress resulting from the magnetic field produced by the eddy current. Moreover, a core is also exposed to a huge amount of magnetic field, while the electrical machine is running. Hence obviously it is of practical importance to measure the amount by which such a typical core is stressed due to magnetic field. This may be a future research project.

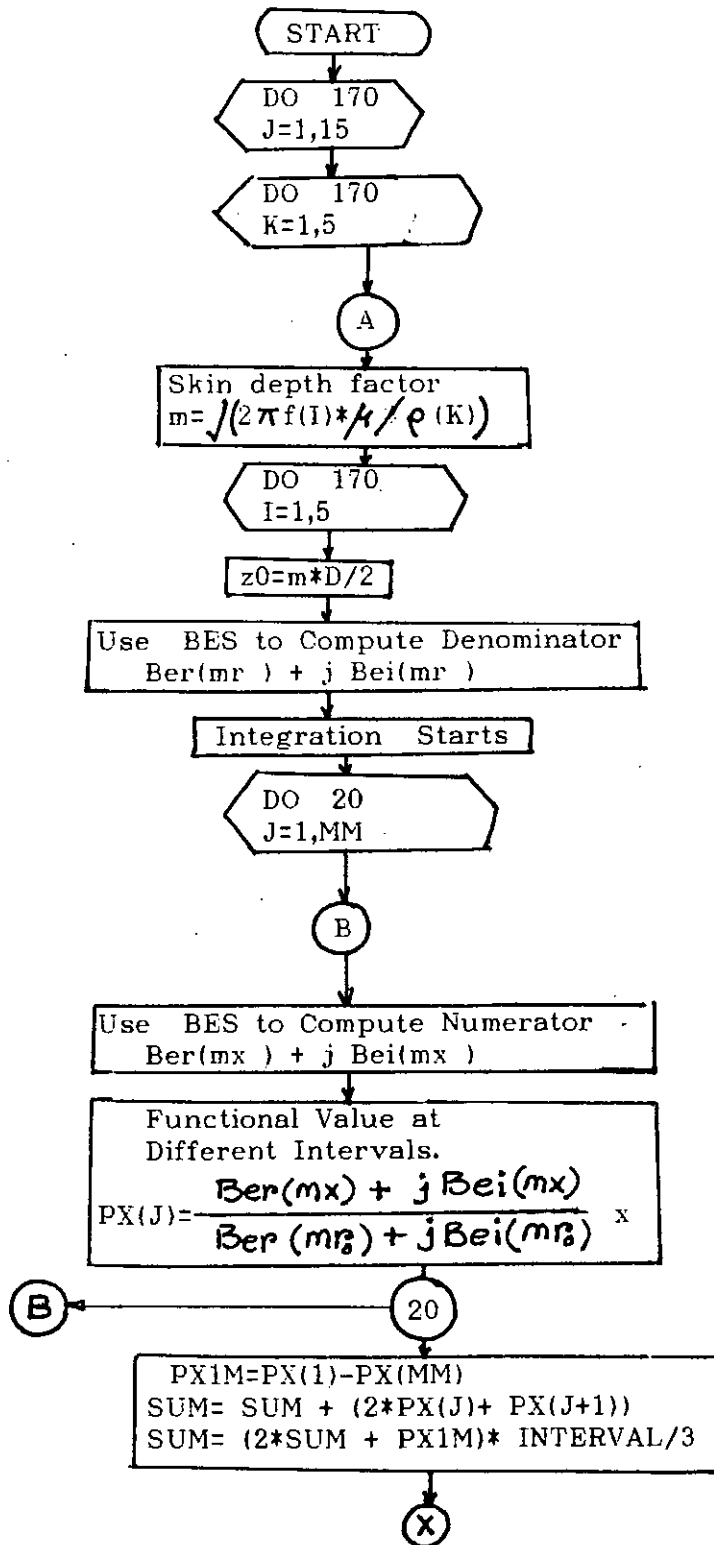
It may be further noted that while calculating the stress due to Joule-heating during steady state operation of overhead power lines we have to assume the time constants and saturation time of the Linnet conductor specimen as the standard one, on which experiment was carried out by Black[4]. It was mentioned earlier in section 3.4 that the time constant and saturation time of a conductor is a function of various parameters, such as ambient condition, wind velocity, solar irradiation and absorbtivity of the conductor, heat conduction and convection co-efficients of the conductor etc. So it has got considerable practical importance to determine the time constants and saturation time of typical conductors used for overhead power lines .

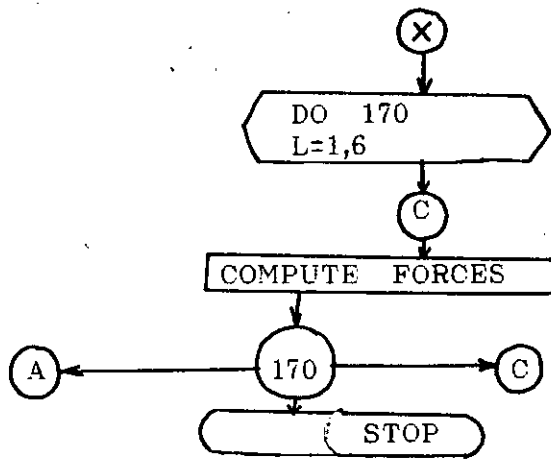
Finally we would like to propose that the nature and effect of stresses developed in overhead power conductors due to lightning stroke may be a valuable query for power engineers. There are three ways in which lightning can generate over-voltages on an overhead line. Among these the surge (induced in the conductor due to the electrostatic and electromagnetic coupling from a nearby lightning strike to ground) that travel along the conductor in opposite directions away from the point of impact rises up to 100 KV in distribution system [18,19] causing a current of million ampere range for micro-sec duration . Since the duration of this current is negligibly small, stress resulting from magnetic field may be higher than that resulting from Joule heating.

APPENDIX

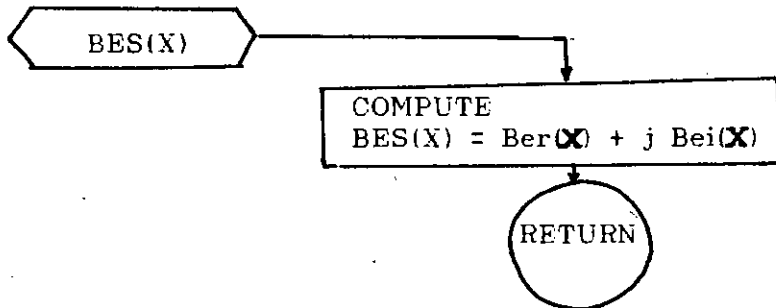
FLOW CHART FOR CALCULATION OF THE FORCES

MAIN PROGRAM





SUBROUTINE



```

C      COMPUTER PROGRAM FOR CALCULATING THE FORCES DUE TO
C      DIELECTRIC STRESS, MAGNETO-MECHANICAL STRESS AND STRESS DUE
C      TO JOULE-HEATING DEVELOPED IN A CURRENT CARRYING
C      CONDUCTOR.
C      -----
C      VARIABLES ARE FREQUENCY OF THE APPLIED FIELD, CURRENT,
C      DIAMETER AND RESISTIVITY OF THE CONDUCTOR.
C      -----
C      DIMENSION PX(800),PY(800),PM(800),D(10),RE(10),F(10),PO(10),
*PYY(800)
      INTEGER F
      REAL M,MU,J0,OMEGA
      COMPLEX SUM,CEXP,BES,BEMR,BEMX,BEMY,SUMY,PY,PY1M,PX,PX1M,PM,PM1M
      COMPLEX CMLX
      COMPLEX SUMM
      OPEN(UNIT=5,STATUS='OLD',FILE='INPUT')
      OPEN(UNIT=3,STATUS='NEW',FILE='OUTPUT')
      A=0.0
C      A=1.805/1000 FOR ACSR, THE STEEL STRAND IS TO BE NEGLECTED.
      PAI=22/7
      EPSI=8.852E-12
      N=100
      PRINT *,1
      READ(5,*)(PO(I),I=1,6)
      READ(5,*)(F(I),I=1,15)
      READ(5,*)(D(I),I=1,5)
      READ(5,*)(RE(I),I=1,5)
      DATA MU/0.000001256
      PRINT *,2
      WRITE(3,8)
8  FORMAT(4X,'I',5X,'FREQUENCY',6X,'TEAC',5X,'TEDC',5X,
* 'TE(AC)/TE(DC)',5X,'TMAC',5X,'TMDC',5X,'TM(AC)/TM(DC)',5X,
* 'TTHAC',4X,'TTHDC',4X,'TH(AC)/TH(DC)'/)
C      ITERATION FOR DIFFERENT CURRENTS STARTS
      DO 170 L=1,6
C      ITERATION FOR DIFFERENT DIAMETERS STARTS
      DO 170 I=1,5
C      ITERATION FOR DIFFERENT FREQUENCIES STARTS
      DO 170 J=1,15
C      ITERATION FOR DIFFERENT RESISTIVITIES STARTS
      DO 170 K=1,5
21  R0=D(I)/2000.
      DATA MU/0.000001256
      RO=RE(L)
      OMEGA=2*PAI*F
14  M=SQRT(OMEGA*MU/RO)
C      A SATURATION TIME OF THIRTY MINUTES IS ASSUMED FOR
C      CALCULATING THE STRESS DUE TO JOULE-HEATING.
      TIME=1800
      Z0=M*RO
      PRINT *,3
      BEMR=BES(Z0)*BES(Z0)
C      INTEGRATION STARTS
C      -----
      H=(R0-A)/N
11  X=H
      MM=N+1
      Z=M*X
C      ITERATION FOR EVALUATING THE FUNCTION STARTS

```



```

C      INTEGRATION STARTS
C      -----
      H=(R0-A)/N
11     X=H
      MM=N+1
      Z=M*X
C      ITERATION FOR EVALUATING THE FUNCTION STARTS
      DO 20 J=1,MM
65     BEMX=BES(Z)*BES(Z)
      PX(J)=(BEMX/BEMR)*X
C      NESTED INTEGRATION FOR MAGNETO-MECHANICAL STRESS STARTS
16     Y=A
      NN=20
      HH=(X-A)/NN
      MY=N+1
      ZZ=M*Y
C      ITERATION FOR NESTED INTEGRATION STARTS
      DO 25 K=1,MY
55     PY(K)=(BES(MZ)/BES(Z))*Y
      Y=Y+HH
      ZZ=M*Y
25     CONTINUE
      PY1M=PY(1)-PY(MY)
      SUMY=0.0
      DO 35 K=2,NN,2
35     SUMY=SUMY+(2.0*PY(K)+PY(K+1))
      SUMY=(2.0*SUMY+PY1M)*HH/3.
      PM(J)=(SUMY**2)/X
      X=X+H
20     Z=M*X
      PM1M=PM(1)-PM(MM)
      SUMM=0.0
      DO 30 K=2,N,2
30     SUMM=SUMM+(2.0*PM(K)+PM(K+1))
      SUMM=(2.0*SUMM+PM1M)*H/3.
      PX1M=PX(1)-PX(MM)
      SUM=0.0
      DO 33 K=2,N,2
33     SUM=SUM+(2.0*PX(K)+PX(K+1))
      SUM=(2.0*SUM+PX1M)*H/3.
C      CALCULATION OF SURFACE CURRENT DENSITY STARTS
C      -----
      Y=A
      HH=(R-A)/N
      MM=N+1
      ZZ=M*Y
      DO 26 K=1,MM
      PY(K)=(BES(ZZ)/BES(Z0))*Y
      Y=Y+HH
      ZZ=M*Y
26     CONTINUE
      PY1M=PY(1)-PY(101)
      SUMY=0.0
      DO 36 K=2,100,2

```

```

36 SUMY=SUMY+(2.0*PY(K)+PY(K+1))
SUMY=(2.0*SUMY+PY1M)*HH/3.
JO=P0/(2*PAI*SUMY)
C CALCULATION OF SURFACE CURRENT DENSITY COMPLETED
C CALCULATION OF THE FORCES STARTS
C -----
C FORCES DUE TO DIELETRIC STRESS
TEAC=PAI*EPSI*(RO*RO)*(JO*JO)*SUM
TEDC=EPSI*(P0*P0)*(RO*RO)/(2*PAI*R*R)
RAT1=TEAC/TEDC
C FORCES DUE TO MAGNETO-MECHANICAL STRESS
TMDC=(P0*P0*MU)/(16*PAI)
TMAC=PAI*MU*SUMM*(JO*JO)
RAT2=TMAC/TMDC
C FORCES OWING TO THE STRESS DUE TO JOULE-HEATING
TTHAC=PAI*RO*(JO*JO)*SUM*TIME
TTHDC=TIME*(P0*P0)*RO/(PAI*R*R)
RAT3=TTHAC/TTHDC
PRINT *,5
WRITE(3,110) RE(L),D(I),TEAC,TEDC,RAT1,TMAC,TMDC,RAT2,TTHAC,
*TTHDC,RAT3
110 FORMAT(/1X,E7.2,3X,F5.4,4X,E8.2,3X,E8.2,3X,E7.2,3X,E8.2,3X,E8.2,
*4X,E7.2,4X,E8.2,4X,E8.2,4X,E7.2/)
170 CONTINUE
180 STOP
END
C END OF MAIN PROGRAM,SUBROUTINE STARTS
C FUNCTION SUBPROGRAM BES(X) FOR CALCULATING THE BESSEL REAL
C AND BESSEL IMAGINARY .
C -----
C COMPLEX FUNCTION BES(X)
C -----
IF(Z.LE.1) GO TO 40
IF(Z.GT.1.AND.Z.LE.8) GO TO 60
IF(Z.GT.1) GO TO 70
C FIRST SLAB STARTS
40 BER=1.
BEI=0.
INF=6
DO 50 K=1,INF,1
FAC=1.
K2=2*K
DO 24 I=1,K2
24 FAC=FAC*I
FAK2=FAC
BER=BER+((-1)**K)*((Z*Z*.25)**K2)/(FAK2**2)
FACI=1.
KD=2*K-1
DO 26 I=1,KD
26 FACI=FACI*I
FACIT=FACI
BEI=BEI+((-1)**(K-1))*((Z*Z*.25)**KD)/(FACIT**2)
50 CONTINUE
BES=CMPLX(BER,BEI)

```

```

RETURN
SECOND SLAB STARTS
60 BER=1-64*(Z/8)**4+113.77777774*(Z/8)**8-32.3634565*(Z/8)**12
++2.641913976*(Z/8)**16-.08346906*(Z/8)**20+.00122552*(Z/8)**24
+-.00000901*(Z/8)**28
BEI=16*(Z/8)**2-113.77777774*(Z/8)**6+72.8177775*(Z/8)**10
+-10.56765779*(Z/8)**14+.52185615*(Z/8)**18-.01103667*(Z/8)**22
++0.00011346*(Z/8)**26
BES=CMPLX(BER,BEI)
RETURN
C THIRD SLAB STARTS
70 PAI=22/7
EPSI1=1.E-7
EPSI2=3.E-7
FK=SQRT(PAI/(2*X))
GK=1/SQRT(2*PAI*X)
FARG=-CMPLX(.707,.707)*X+THETA(-X)
FRA=REAL(FARG)
FIA=AIMAG(FARG)
N=FIA/(2*PAI)
FIA=FIA-N*2*PAI
FX=FK*EXP(FRA)*CMPLX(COS(FIA),SIN(FIA))
FR=REAL(FX)/PAI
FI=AIMAG(FX)/PAI
GARG=CMPLX(.707,.707)*X+THETA(X)
GRA=REAL(GARG)
GIA=AIMAG(GARG)
M=GIA/(2*PAI)
GIA=GIA-M*2*PAI
GX=GK*EXP(GRA)*CMPLX(COS(GIA),SIN(GIA))
BES=GX*(1+EPSI2)+CMPLX(-FI,FR)*(1+EPSI1)
RETURN
END
C FUNCTION SUBPROGRAM 2
COMPLEX FUNCTION THETA(X)
COMPLEX CMPLX
43 TREAL=.0110486*(8/X)-.0000906*(8/X)**3-.0000252*(8/X)**4-.0000035
+(8/X)**5+.0000006*(8/X)**6
TIMAG=-.3926994-.0110485*(8/X)-.0009765*(8/X)**2-.0000901*
+(8/X)**3-.00000009*(8/X)**4+.0000051*(8/X)**5+.0000019*(8/X)**6
THETA=CMPLX(TREAL,TIMAG)
111 RETURN
END

```

```

C      COMPUTER PROGRAM FOR THE DETERMINATION OF THE ROOTS OF THE
      BESSEL EQUATION , JO(V)=0.
C      -----
C      PRECISION IS UP TO TWO DECIMAL PLACES.
C      -----
      OPEN(UNIT=1,STATUS='OLD',FILE='INPUT')
      OPEN(UNIT=3,STATUS='NEW',FILE='OUTPUT')
      WRITE(3,*) 'ROOTS OF THE BESSEL EQUATION ARE ..... '
5     FORMAT(3X,'APPX. ROOT',4X,'FUNCTIONAL VALUE'/)
      RNU=0
      DO 30 RKA=2,50,.01
10    FV=BESJP(RKA,RNU)
      IF (RKA.LE.1.0E-6) THEN
      WRITE(3,*) RKA,FV
      ELSE
      GO TO 10
      ENDIF
30    CONTINUE
      STOP
      END

C      FUNCTION SUBPROGRAM 1
      DOUBLE PRECISION FUNCTION BESJP(X,P)
C      SUBROUTINE BESSEL(BESJP,X,P)
C      COMPUTATION OF BESSEL FUNCTIONJ(X,J) OF THE ORDER OF P
C      LIMITATION X.GE.0.AND.P.GT.(-1)
C      RETURNS THE VALUE ZERO IF X.LT.0.OR.P.LT.(-1).OR.IF(X.EQ.0.
C      AND P.LT.0).OR.WHEN THE VALUE OF THE BESSEL FUNCTION WOULD CAUSE
C      AN UNDER FLOW.

      DOUBLE PRECISION A,A1 AK,AL,ALOGUF,BL,Y2,DABS,DCOS,DEXP,DLOG,
+DSIN,DSQRT,EMPACH,FF,FI,P,PP,PN,QN,S,SIGN,U,UB,UU,U1,V,X,XB,
+XX,Y,Y1,PI
      INTEGER I,K,L,NP,NU,NUB,NUM
C      THE CONSTANTS DEFINED IN THE FOLLOWING DATA STATEMENT ARE MACHINE
C      DEPENDENT
C      ALOGUF IS THE NATURAL LOGARITHM OF THE LAGEST MACHINE NUMBER.
C      EMPACH IS THE SMALLEST POSITIVE NUMBER SO THAT (1+EPMACH) > 1.
      DATA ALOGUF/1.70D+02/
      DATA EMPACH/1.0D-16/
      DATA PI/3.14159265358979323846264338327950288D+00/
42    BESJP=0.0D+00
      IF(X.EQ.0.0D+00.AND.P.EQ.0.0D+00)BESJP=1.0D+00
      IF(X.LE.0.0D+00.OR.P.LE.(-1.0D+00))GO TO 110
      XB=(-15.0D-01)*(DLOG(EMPACH))
      IF(X.GE.XB.AND.P.LT.X)GO TO 60
      NP=X-P
      PP=NP
      IF(NP.GT.0)U=P+PP+1.0D+00
      IF(NP.LE.0)U=P
C      COMPUTATION OF THE LOGARITHM OF THE GAMMA FUNCTION
      UU=U
      AL=0.0D+00
      NUB=10
      IF(EMPACH.LT.1.0D-17)NUB=50

```

```

UB=NUB
IF(U.GE.UB)GO TO 20
NU=U
L=NUB-NU
BL=L
UU=U+BL
S=1.0D+00
DO 10 K=1,L
AK=K
S=S*(U+AK)
10 CONTINUE
AL=DLOG(S)
20 A=2.5D-01*X*X/(U+1.0D+00)
XX=1.0D+00/(UU+1.0D+00)**2
F1=(((X/1.56D+02-6.91D+02/3.60360D+05)*XX+1.0D+00/1.188D+03)
+*XX-1.0D+00/1.680D+03)*XX+1.0D+00/1.260D+03)*XX-1.0D+00/3.6D+02)
+*XX+1.0D+00/1.2D+01)/(UU+1.0D+00)-AL
FF=-F1-A+U*DLOG(5.0D-01*X)+UU*(1.0D+00-DLOG(UU+1.0D+00))+1.0D+00
+-5.0D-01*DLOG(2.0D+00*PI*(UU+1.0D+00))
IF(-FF.GT.(ALOGUF-1.0D+01))GO TO 110
FF=DEXP(FF)
C EVALUATION OF SERIES EXPANSION
V=1.0D+00
Y1=0.0D+00
BESJP=1.0D+00
S=U-A
DO 30 I=2,200
AI=I
Y2=A*(Y1*(AI+AI-2.0D+00)-V*A)/(AI*(AI+U))
BESJP=BESJP+Y2
S=S+(U-A+AI)*Y2
IF(X.LT.1.0D-01.AND.DABS(Y2).LT.(1.0D-02*EMPACH))GO TO 40
IF((1.0D+01/EMPACH)*(U-A+AI)*(DABS(Y1)+DABS(Y2)).LT.DABS(S))GO TO
+40
V=Y1
Y1=Y2
30 CONTINUE
40 BESJP=BESJP*FF
IF(NP.LE.0)GO TO 110
C START OF BACKWARD RECURSION(WHEN X.LT.XB.AND.P.LT.X)
XX=2.0D+00/X
V=S*XX*FF
DO 50 K=1,NP
AK=K
Y=XX*(U-AK)*V-BESJP
BESJP=Y
V=Y
50 CONTINUE
BESJP=V
GO TO 110
C COMPUTATION WHEN X.GE.XB.AND.P.LT.X
60 NUM=1
IF(P.GT.2.0D+00)NUM=2
NP=P

```

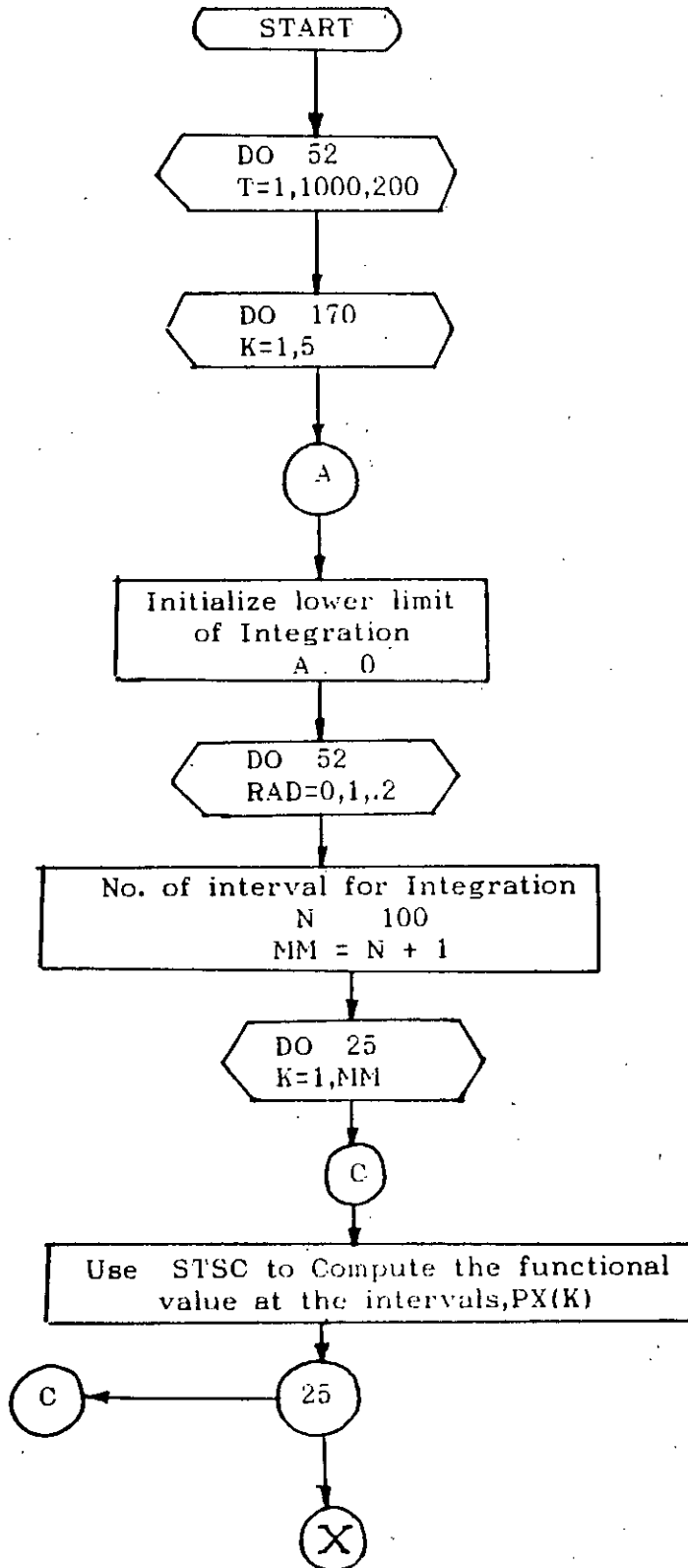
```

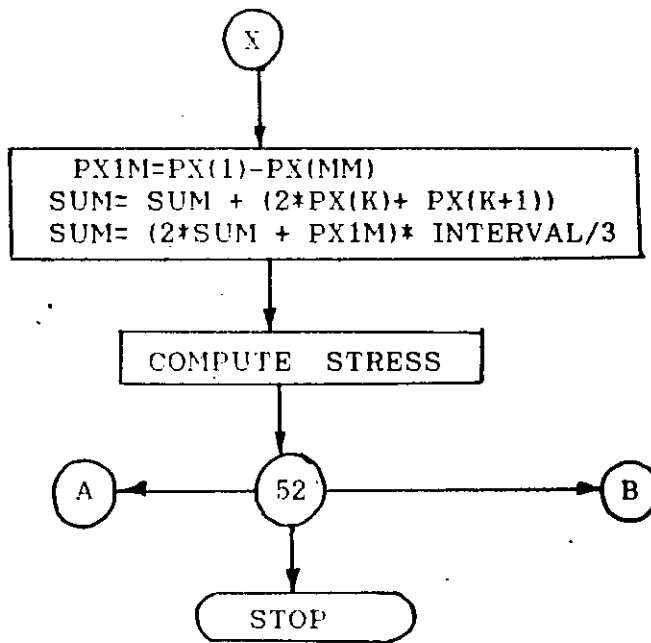
PP=NP
UU=P-PP+1.0D+00
IF(NUM.EQ.1)UU=P
DO 90 K=1,NUM
AK=K
U=UU+1.0D+00-AK
C HANKEL'S ASYMPTOTIC EXPANSION OF BESSEL FUNCTION
V=1.0D+00
U1=4.0D+00*U*U
XX=8.0D+00*X
PN=1.0D+00
QN=0.0D+00
SIGN=1.0D+00
AI=-1.0D+00
DO 70 I=1,100
AI=AI+2.0D+00
V=V*(U1-AK*AK)/(AI*XX)
IF(DABS(V).LT.EMPACH)GO TO 80
SIGN=-SIGN
70 CONTINUE
80 FI=X-(5.0D-01*U+2.5D-01)*PI
Y1=DSQRT(2.0D+00/(PI*X))*(PN*X)*(PN*DCOS(FI)-QN*DSIN(FI))
IF(NUM.EQ.1)Y2=Y1
90 CONTINUE
BESJP=Y2
IF(NUM.EQ.1)GO TO 110
C START OF FORWARD RECURSION(WHEN X.GT.2.AND.P.LT.X)
XX=2.0D+00/X
DO 100 K=2,NP
BESJP=XX*UU*Y2-Y1
UU=UU+1.0D+00
Y1=Y2
Y2=BESJP
100 CONTINUE
110 RETURN
END

```

FLOW CHART FOR CALCULATION OF STRESS DISTRIBUTION

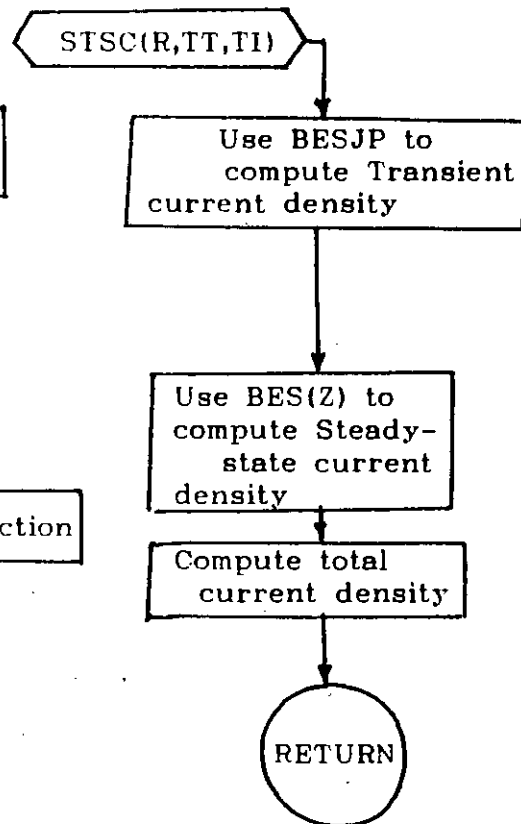
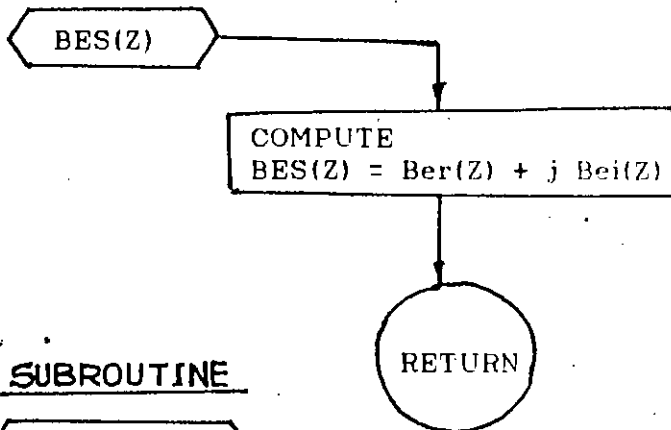
MAIN PROGRAM



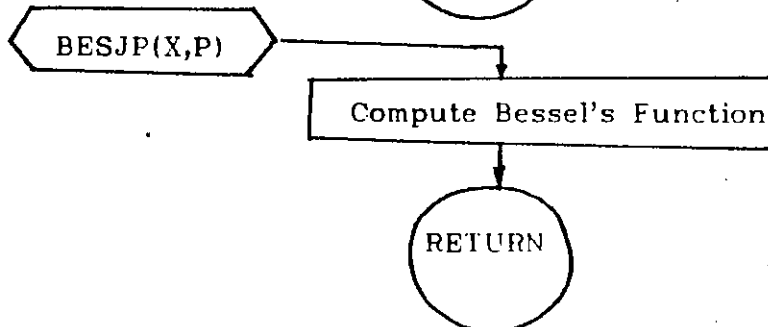


SUBROUTINE

SUBROUTINE



SUBROUTINE




```

C      COMPUTER PROGRAM FOR THE DETERMINATION OF RADIAL AND TIME
      DISTRIBUTION OF TOTAL CURRENT, TRANSIENT CURRENT AND
      STEADY-STATE CURRENT
C      -----
C      VARIABLES ARE RADIAL DISTANCE, TIME IN MICRO-SEC AND
      FREQUENCY IN HZ.
C      -----
      DIMENSION PM(50)
      COMPLEX PMR,SUM,TR,DEN,SSI,TI
      COMPLEX CMLX
      REAL MUS,M,MU
      OPEN(UNIT=1,STATUS='OLD',FILE='INPUT')
      OPEN(UNIT=3,STATUS='NEW',FILE='OUTPUT')
      INTEGER F
      READ(1,*) (PM(I),I=1,21)
      READ(1,*) (F(I),I=1,15)
      DATA PI/3.141592653
      DATA MU/0.00001256
      DATA TT/1200
      DATA SIGMA/3.58E+08
      MUS=MU*SIGMA
11  R0=.004
      WRITE(3,5)
5   FORMAT(3X,'FREQ.',3X,'TIME',4X,'R/R0',5X,'TRAN.CUR',5X,'PH.TC',
+6X,'SS.CUR',8X,'PH.SSC',8X,'TOT.CUR',6X,'PH.TTC'/)
C      DETERMINATION OF STEADY-STATE CURRENT DENSITY
      DO I=1,15
      AF=2*PI*F(I)
      M=SQRT(AF*MUS)
      ROM=R0*M
      DO 30 T=10,TT,50
      TIM=T*1.0E-6.
      AM=AF*TIM
      K=AM/(2*PI)
      AM=AM-K*2*PI
      DO 30 RAD=0,1.0,0.2
      R=RAD*R0
      RM=M*R
      SSI=(BES(RM)/BES(ROM))CEXP(AM)
C      DETERMINATION OF TRANSIENT CURRENT DISTRIBUTION
      SUM=CMPLX(0.0,0.0)
      DO 14 J=1,8
      PMS=PM(J)*PM(J)
      PRG=M*R0*R0
      PMR=CMPLX(PMS,PRG)
      XE=((-(PM(J)/R0)**2)*(TIM/MUS))
      IF (XE.LE.-170) THEN
      EXE=0
      ELSE
      EXE=EXP(XE)
      ENDIF
      RKA=RAD*PM(J)
      RNU=0
      IF (RKA.EQ.0.)THEN

```

```

UME=EXE
ELSE
UME=BESJP(RKA,RNU)*EXE
ENDIF
RNU=1
RKA=PM(J)
DEN=(PM(J)*BESJP(RKA,RNU))*PMR
SUM=SUM+UME/DEN
14 CONTINUE
TR=(-2)*SUM
TRM=CABS(TR)
TRP=ATAN(TR)
22 SSM=CABS(SSI)
SSP=ATAN(SSI)
TI=SSI+TR
ATI=CABS(TI)
WRITE(3,18) F(O),IME,RAD,TCM,TCP,SSM,SSP,ATI,TIP
18 FORMAT(3X,I8,3X,I4,4X,F4.2,5X,F8.6,6X,F8.4,6X,F7.5,5X,F8.4,
+8X,F7.5,5X,F8.4/)
30 CONTINUE
STOP
END
C FUNCTION SUBPROGRAM 1
C DOUBLE PRECISION FUNCTION BESJP(X,P)
C SUBROUTINE BESSEL(BESJP,X,P)
C COMPUTATION OF BESSEL FUNCTION J(X,J) OF THE ORDER OF P
C LIMITATION X.GE.0.AND.P.GT.(-1)
C RETURNS THE VALUE ZERO IF X.LT.0.OR.P.LT.(-1).OR.IF(X.EQ.0.
C AND P.LT.0).OR.WHEN THE VALUE OF THE BESSEL FUNCTION WOULD CAUSE
C AN UNDER FLOW.
C
C DOUBLE PRECISION A,A1 AK,AL,ALOGUF,BL,Y2,DABS,DCOS,DEXP,DLOG,
+DSIN,DSQRT,EMPACH,FF,FI,P,PP,PN,QN,S,SIGN,U,UB,UU,U1,V,X,XB,
+XX,Y,Y1,PI
C INTEGER I,K,L,NP,NU,NUB,NUM
C THE CONSTANTS DEFINED IN THE FOLLOWING DATA STATEMENT ARE MACHINE
C DEPENDENT
C ALOGUF IS THE NATURAL LOGARITHM OF THE LARGEST MACHINE NUMBER.
C EMPACH IS THE SMALLEST POSITIVE NUMBER SO THAT (1+EMPACH) > 1.
C DATA ALOGUF/1.70D+02/
C DATA EMPACH/1.0D-16/
C DATA PI/3.14159265358979323846264338327950288D+00/
42 BESJP=0.0D+00
IF(X.EQ.0.0D+00.AND.P.EQ.0.0D+00)BESJP=1.0D+00
IF(X.LE.0.0D+00.OR.P.LE.(-1.0D+00))GO TO 110
XB=(-15.0D-01)*(DLOG(EMPACH))
IF(X.GE.XB.AND.P.LT.X)GO TO 60
NP=X-P
PP=NP
IF(NP.GT.0)U=P+PP+1.0D+00
IF(NP.LE.0)U=P
C COMPUTATION OF THE LOGARITHM OF THE GAMMA FUNCTION
UU=U
AL=0.0D+00

```

```

NUB=10
IF(EMPACH.LT.1.0D-17)NUB=50
UB=NUB
IF(U.GE.UB)GO TO 20
NU=U
L=NUB-NU
BL=L
UU=U+BL
S=1.0D+00
DO 10 K=1,L
AK=K
S=S*(U+AK)
10 CONTINUE
AL=DLOG(S)
20 A=2.5D-01*X*X/(U+1.0D+00)
XX=1.0D+00/(UU+1.0D+00)**2
F1=(((X/1.56D+02-6.91D+02/3.60360D+05)*XX+1.0D+00/1.188D+03)
+*XX-1.0D+00/1.680D+03)*XX+1.0D+00/1.260D+03)*XX-1.0D+00/3.6D+02)
+*XX+1.0D+00/1.2D+01)/(UU+1.0D+00)-AL
FF=-F1-A+U*DLOG(5.0D-01*X)+UU*(1.0D+00-DLOG(UU+1.0D+00))+1.0D+00
+-5.0D-01*DLOG(2.0D+00*PI*(UU+1.0D+00))
IF(-FF.GT.(ALOGUF-1.0D+01))GO TO 110
FF=DEXP(FF)
C EVALUATION OF SERIES EXPANSION
V=1.0D+00
Y1=0.0D+00
BESJP=1.0D+00
S=U-A
DO 30 I=2,200
AI=I
Y2=A*(Y1*(AI+AI-2.0D+00)-V*A)/(AI*(AI+U))
BESJP=BESJP+Y2
S=S+(U-A+AI)*Y2
IF(X.LT.1.0D-01.AND.DABS(Y2).LT.(1.0D-02*EMPACH))GO TO 40
IF((1.0D+01/EMPACH)*(U-A+AI)*(DABS(Y1)+DABS(Y2)).LT.DABS(S))GO TO
+40
V=Y1
Y1=Y2
30 CONTINUE
40 BESJP=BESJP*FF
IF(NP.LE.0)GO TO 110
C START OF BACKWARD RECURSION(WHEN X.LT.XB.AND.P.LT.X)
XX=2.0D+00/X
V=S*XX*FF
DO 50 K=1,NP
AK=K
Y=XX*(U-AK)*V-BESJP
BESJP=V
V=Y
50 CONTINUE
BESJP=V
GO TO 110
C COMPUTATION WHEN X.GE.XB.AND.P.LT.X
60 NUM=1

```

```

IF(P.GT.2.0D+00)NUM=2
NP=P
PP=NP
UU=P-PP+1.0D+00
IF(NUM.EQ.1)UU=P
DO 90 K=1,NUM
AK=K
U=UU+1.0D+00-AK
C HANKEL'S ASYMPTOTIC EXPANSION OF BESSEL FUNCTION
V=1.0D+00
U1=4.0D+00*U*U
XX=8.0D+00*X
PN=1.0D+00
QN=0.0D+00
SIGN=1.0D+00
AI=-1.0D+00
DO 70 I=1,100
AI=AI+2.0D+00
V=V*(U1-AK*AK)/(AI*XX)
IF(DABS(V).LT.EMPACH)GO TO 80
SIGN=-SIGN
70 CONTINUE
80 FI=X-(5.0D-01*U+2.5D-01)*PI
Y1=DSQRT(2.0D+00/(PI*X))*(PN*X)*(PN*DCOS(FI)-QN*DSIN(FI))
IF(NUM.EQ.1)Y2=Y1
90 CONTINUE
BESJP=Y2
IF(NUM.EQ.1)GO TO 110
C START OF FORWARD RECURSION(WHEN X.GT.2.AND.P.LT.X)
XX=2.0D+00/X
DO 100 K=2,NP
BESJP=XX*UU*Y2-Y1
UU=UU+1.0D+00
Y1=Y2
Y2=BESJP
100 CONTINUE
110 RETURN
END
C FUNCTION SUBPROGRAM BES(X) FOR CALCULATING THE BESSEL REAL
C AND BESSEL IMAGINARY .
C -----
C COMPLEX FUNCTION BES(X)
C -----
IF(Z.LE.1) GO TO 40
IF(Z.GT.1.AND.Z.LE.8) GO TO 60
IF(Z.GT.1) GO TO 70
C FIRST SLAB STARTS
40 BER=1.
BEI=0.
INF=6
DO 50 K=1,INF,1
FAC=1.
K2=2*K
DO 24 I=1,K2

```

```

24 FAC=FAC*I
   FAK2=FAC
   BER=BER+((-1)**K)*((Z*.25)**K2)/(FAK2**2)
   FACI=1:
   KD=2*K-1
   DO 26 I=1,KD
26 FACI=FACI*I
   FACIT=FACI
   BEI=BEI+((-1)**(K-1))*((Z*.25)**KD)/(FACIT**2)
50 CONTINUE
   BES=CMPLX(BER, BEI)
   RETURN
C SECOND SLAB STARTS
60 BER=1-64*(Z/8)**4+113.77777774*(Z/8)**8-32.3634565*(Z/8)**12
++2.641913976*(Z/8)**16-.08346906*(Z/8)**20+.00122552*(Z/8)**24
+-.00000901*(Z/8)**28
   BEI=16*(Z/8)**2-113.77777774*(Z/8)**6+72.8177775*(Z/8)**10
+-10.56765779*(Z/8)**14+.52185615*(Z/8)**18-.01103667*(Z/8)**22
++0.00011346*(Z/8)**26
   BES=CMPLX(BER, BEI)
   RETURN
C THIRD SLAB STARTS
70 PAI=22/7
   EPSI1=1.E-7
   EPSI2=3.E-7
   FK=SQRT(PAI/(2*X))
   GK=1/SQRT(2*PAI*X)
   FARG=-CMPLX(.707, .707)*X+THETA(-X)
   FRA=REAL(FARG)
   FIA=AIMAG(FARG)
   N=FIA/(2*PAI)
   FIA=FIA-N*2*PAI
   FX=FK*EXP(FRA)*CMPLX(COS(FIA), SIN(FIA))
   FR=REAL(FX)/PAI
   FI=AIMAG(FX)/PAI
   GARG=CMPLX(.707, .707)*X+THETA(X)
   GRA=REAL(GARG)
   GIA=AIMAG(GARG)
   M=GIA/(2*PAI)
   GIA=GIA-M*2*PAI
   GX=GK*EXP(GRA)*CMPLX(COS(GIA), SIN(GIA))
   BES=GX*(1+EPSI2)+CMPLX(-FI, FR)*(1+EPSI1)
   RETURN
END
C FUNCTION SUBPROGRAM 2
   COMPLEX FUNCTION THETA(X)
   COMPLEX CMPLX
43 TREAL=.0110486*(8/X)-.0000906*(8/X)**3-.0000252*(8/X)**4-.0000035
+(8/X)**5+.0000006*(8/X)**6
   TIMAG=-.3926994-.0110485*(8/X)-.0009765*(8/X)**2-.0000901*
+(8/X)**3-.00000009*(8/X)**4+.0000051*(8/X)**5+.0000019*(8/X)**6
   THETA=CMPLX(TREAL, TIMAG)
111 RETURN
   END

```

```

C   COMPUTER PROGRAM FOR THE DETERMINATION OF RADIAL AND TIME
C   DISTRIBUTION OF STRESS AT DIFFERENT TIME AFTER SWITCHING
C   AND STEADY-STATE STRESS.
C   -----
C   VARIABLES ARE FREQUENCY OF OPERATION , TIME AFTER SWITCHING
C   AND RADIAL DISTANCE R/R0.
C   -----
C   DIMENSION PX(200),PM(50)
C   COMMON JO,M,PM,F,R0
C   REAL MU
C   INTEGER FF,F
C   COMPLEX PX,PX1M,SUMX,TCD
C   OPEN(UNIT=1,STATUS='OLD',FILE='INPUT')
C   OPEN(UNIT=3,STATUS='NEW',FILE='OUTPUT')
C   PI=3.141592653
C   INPUTTING THE FREQUENCY.
C   READ(1,*) (FF(I),I=1,5)
C   WRITE(3,5)
5   FORMAT(3X,'TIME',5X,'R/R0',5X,'MAG.STRESS'/)
12  R0=.004
C   MU=4*PI*1.0E-07
C   DO 52 T=0,1000,200
C   DO 52 I=1,5
C   T=1000000, FOR STEADY-STATE 1 SEC AFTER SWITCHING IS
C   CONSIDERED.
C   DO 52 RAD=0.0,1,.2
C   A=0
C   FOR THE CALCULATION OF DIELECTRIC STRESS NO INTEGRATION IS
C   REQUIRED , FOR MAGNETIC STRESS INTEGRATION W.R.T DISTANCE
C   FROM THE AXIS IS NECESSARY BUT FOR STRESS DUE TO JOULE-
C   HEATING TIME INTEGRATION IS ESSENTIAL.
C   -----
C   INTEGRATION WITH RESPECT TO DISTANCE FROM THE AXIS STARTS.
C   RR=RAD*R0
C   X=A
C   N=100
C   DX=(RR-A)/N
C   MM=N+1
C   DO 25 K=1,MM
C   F=FF(I)
C   CALL STSC(X,T,TCD)
C   PX(K)=X*TCD
C   X=X+DX
25  CONTINUE
C   PX1M=PX(1)-PX(MM)
C   SUMX=0
C   DO 35 K=2,N,2
35  SUMX=SUMX+(2.0*PX(K)+PX(K+1))
C   SUMX=(2.0*SUMX+PX1M)*DX/3
C   PRINT *,1
C   CDX=CABS(SUMX)
C   IF (RR.EQ.0.)THEN
C   SMR=0.0
C   ELSE

```

```

SMR=MU*CDX*CDX/(2*RR*RR)
ENDIF
WRITE(3,7) T,RAD,SMR
7 FORMAT(3X,F5.0,5X,F4.2,5X,E10.4/)
52 CONTINUE
STOP
END
C SUBROUTINE FOR CALCULATION OF TIME AND TIME AND RADIAL
C DISTRIBUTION OF CURRENT.
SUBROUTINE STSC(R,TT,TI)
DIMENSION PM(50)
COMPLEX PMR,SUM,TR,DEN,SSI,TI
COMPLEX CMLX
REAL MUS,M
DATA PI/3.141592653
DATA MU/0.00001256
DATA SIGMA/3.58E+08
MUS=MU*SIGMA
C DETERMINATION OF STEADY-STATE CURRENT DENSITY
DO I=1,15
AF=2*PI*F(I)
M=SQRT(AF*MUS)
ROM=R0*M
TIM=T*1.0E-6
AM=AF*TIM
K=AM/(2*PI)
AM=AM-K*2*PI
R=RAD*R0
RM=M*R
SSI=(BES(RM)/BES(ROM))CEXP(AM)
C DETERMINATION OF TRANSIENT CURRENT DISTRIBUTION
SUM=CMLX(0.0,0.0)
DO 14 J=1,21
PMS=PM(J)*PM(J)
PRG=M*R0*R0
PMR=CMLX(PMS,PRG)
XE=((-(PM(J)/R0)**2)*(TIM/MUS))
IF (XE.LE.-170) THEN
EXE=0
ELSE
EXE=EXP(XE)
ENDIF
RKA=RAD*PM(J)
RNU=0
IF (RKA.EQ.0.)THEN
UME=EXE
ELSE
UME=BESJP(RKA,RNU)*EXE
ENDIF
RNU=1
RKA=PM(J)
DEN=(PM(J)*BESJP(RKA,RNU))*PMR
SUM=SUM+UME/DEN
14 CONTINUE

```

```

TR=(-2)*SUM
TI=SSI+TR
RETURN
END
C   FUNCTION SUBPROGRAM 1
C   DOUBLE PRECISION FUNCTION BESJP(X,P)
C   SUBROUTINE BESSEL(BESJP,X,P)
C   COMPUTATION OF BESSEL FUNCTIONJ(X,J) OF THE ORDER OF P
C   LIMITATION X.GE.0.AND.P.GT.(-1)
C   RETURNS THE VALUE ZERO IF X.LT.0.OR.P.LT.(-1).OR.IF(X.EQ.0.
C   AND P.LT.0).OR.WHEN THE VALUE OF THE BESSEL FUNCTION WOULD CAUSE
C   AN UNDER FLOW.
C
C   DOUBLE PRECISION A,A1 AK,AL,ALOGUF,BL,Y2,DABS,DCOS,DEXP,DLOG,
+DSIN,DSQRT,EMPACH,FF,FI,P,PP,PN,QN,S,SIGN,U,UB,UU,U1,V,X,XB,
+XX,Y,Y1,PI
C   INTEGER I,K,L,NP,NU,NUB,NUM
C   THE CONSTANTS DEFINED IN THE FOLLOWING DATA STATEMENT ARE MACHINE
C   DEPENDENT
C   ALOGUF IS THE NATURAL LOGARITHM OF THE LAGEST MACHINE NUMBER.
C   EMPACH IS THE SMALLEST POSITIVE NUMBER SO THAT (1+EPMACH) > 1.
C   DATA ALOGUF/1.70D+02/
C   DATA EMPACH/1.0D-16/
C   DATA PI/3.14159265358979323846264338327950288D+00/
42 BESJP=0.0D+00
IF(X.EQ.0.0D+00.AND.P.EQ.0.0D+00)BESJP=1.0D+00
IF(X.LE.0.0D+00.OR.P.LE.(-1.0D+00))GO TO 110
XB=(-15.0D-01)*(DLOG(EMPACH))
IF(X.GE.XB.AND.P.LT.X)GO TO 60
NP=X-P
PP=NP
IF(NP.GT.0)U=P+PP+1.0D+00
IF(NP.LE.0)U=P
C   COMPUTATION OF THE LOGARITHM OF THE GAMMA FUNCTION
UU=U
AL=0.0D+00
NUB=10
IF(EMPACH.LT.1.0D-17)NUB=50
UB=NUB
IF(U.GE.UB)GO TO 20
NU=U
L=NUB-NU
BL=L
UU=U+BL
S=1.0D+00
DO 10 K=1,L
AK=K
S=S*(U+AK)
10 CONTINUE
AL=DLOG(S)
20 A=2.5D-01*X*X/(U+1.0D+00)
XX=1.0D+00/(UU+1.0D+00)**2
F1(((((((XX/1.56D+02-6.91D+02/3.60360D+05)*XX+1.0D+00/1.188D+03)
+*XX-1.0D+00/1.680D+03)*XX+1.0D+00/1.260D+03)*XX-1.0D+00/3.6D+02)

```



```

+*XX+1.0D+00/1.2D+01)/(UU+1.0D+00)-AL
  FF=-F1-A+U*DLOG(5.0D-01*X)+UU*(1.0D+00-DLOG(UU+1.0D+00))+1.0D+00
+-5.0D-01*DLOG(2.0D+00*PI*(UU+1.0D+00))
  IF(-FF.GT.(ALOGUF-1.0D+01))GO TO 110
  FF=DEXP(FF)
C  EVALUATION OF SERIES EXPANSION
  V=1.0D+00
  Y1=0.0D+00
  BESJP=1.0D+00
  S=U-A
  DO 30 I=2,200
  AI=I
  Y2=A*(Y1*(AI+AI-2.0D+00)-V*A)/(AI*(AI+U))
  BESJP=BESJP+Y2
  S=S+(U-A+AI)*Y2
  IF(X.LT.1.0D-01.AND.DABS(Y2).LT.(1.0D-02*EMPACH))GO TO 40
  IF((1.0D+01/EMPACH)*(U-A+AI)*(DABS(Y1)+DABS(Y2)).LT.DABS(S))GO TO
+40
  V=Y1
  Y1=Y2
30  CONTINUE
40  BESJP=BESJP*FF
  IF(NP.LE.0)GO TO 110
C  START OF BACKWARD RECURSION(WHEN X.LT.XB.AND.P.LT.X)
  XX=2.0D+00/X
  V=S*XX*FF
  DO 50 K=1,NP
  AK=K
  Y=XX*(U-AK)*V-BESJP
  BESJP=Y
  V=Y
50  CONTINUE
  BESJP=V
  GO TO 110
C  COMPUTATION WHEN X.GE.XB.AND.P.LT.X
60  NUM=1
  IF(P.GT.2.0D+00)NUM=2
  NP=P
  PP=NP
  UU=P-PP+1.0D+00
  IF(NUM.EQ.1)UU=P
  DO 90 K=1,NUM
  AK=K
  U=UU+1.0D+00-AK
C  HANKEL'S ASYMPTOTIC EXPANSION OF BESSEL FUNCTION
  V=1.0D+00
  U1=4.0D+00*U*U
  XX=8.0D+00*X
  PN=1.0D+00
  QN=0.0D+00
  SIGN=1.0D+00
  AI=-1.0D+00
  DO 70 I=1,100
  AI=AI+2.0D+00

```

```

V=V*(U1-AK*AK)/(AI*XX)
IF(DABS(V).LT.EMPACH)GO TO 80
SIGN=-SIGN
70 CONTINUE
80 FI=X-(5.0D-01*U+2.5D-01)*PI
Y1=DSQRT(2.0D+00/(PI*X))*(PN*X)*(PN*DCOS(FI)-QN*DSIN(FI))
IF(NUM.EQ.1)Y2=Y1
90 CONTINUE
BESJP=Y2
IF(NUM.EQ.1)GO TO 110
C START OF FORWARD RECURSION(WHEN X.GT.2.AND.P.LT.X)
XX=2.0D+00/X
DO 100 K=2,NP
BESJP=XX*UU*Y2-Y1
UU=UU+1.0D+00
Y1=Y2
Y2=BESJP
100 CONTINUE
110 RETURN
END
C FUNCTION SUBPROGRAM BES(X) FOR CALCULATING THE BESSEL REAL
C AND BESSEL IMAGINARY .
C -----
C COMPLEX FUNCTION BES(X)
C -----
IF(Z.LE.1) GO TO 40
IF(Z.GT.1.AND.Z.LE.8) GO TO 60
IF(Z.GT.1) GO TO 70
C FIRST SLAB STARTS
40 BER=1.
BEI=0.
INF=6
DO 50 K=1,INF,1
FAC=1.
K2=2*K
DO 24 I=1,K2
24 FAC=FAC*I
FAK2=FAC
BER=BER+((-1)**K)*((Z*Z*.25)**K2)/(FAK2**2)
FACI=1.
KD=2*K-1
DO 26 I=1,KD
26 FACI=FACI*I
FACIT=FACI
BEI=BEI+((-1)**(K-1))*((Z*Z*.25)**KD)/(FACIT**2)
50 CONTINUE
BES=CMPLX(BER,BEI)
RETURN
C SECOND SLAB STARTS
60 BER=1-64*(Z/8)**4+113.77777774*(Z/8)**8-32.3634565*(Z/8)**12
++2.641913976*(Z/8)**16-.08346906*(Z/8)**20+.00122552*(Z/8)**24
+-.00000901*(Z/8)**28
BEI=16*(Z/8)**2-113.77777774*(Z/8)**6+72.8177775*(Z/8)**10
+-10.56765779*(Z/8)**14+.52185615*(Z/8)**18-.01103667*(Z/8)**22

```

```

++ .00011346*(Z/8)**26
BES=CMPLX(BER,BEI)
RETURN
C   THIRD SLAB STARTS
70  PAI=22/7.
    EPSI1=1.E-7
    EPSI2=3.E-7
    FK=SQRT(PAI/(2*X))
    GK=1/SQRT(2*PAI*X)
    FARG=-CMPLX(.707,.707)*X+THETA(-X)
    FRA=REAL(FARG)
    FIA=AIMAG(FARG)
    N=FIA/(2*PAI)
    FIA=FIA-N*2*PAI
    FX=FK*EXP(FRA)*CMPLX(COS(FIA),SIN(FIA))
    FR=REAL(FX)/PAI
    FI=AIMAG(FX)/PAI
    GARG=CMPLX(.707,.707)*X+THETA(X)
    GRA=REAL(GARG)
    GIA=AIMAG(GARG)
    M=GIA/(2*PAI)
    GIA=GIA-M*2*PAI
    GX=GK*EXP(GRA)*CMPLX(COS(GIA),SIN(GIA))
    BES=GX*(1+EPSI2)+CMPLX(-FI,FR)*(1+EPSI1)
    RETURN
    END
C   FUNCTION SUBPROGRAM 2
    COMPLEX FUNCTION THETA(X)
    COMPLEX CMPLX
43  TREAL=.0110486*(8/X)-.0000906*(8/X)**3-.0000252*(8/X)**4-.0000035
    +(8/X)**5+.0000006*(8/X)**6
    TIMAG=-.3926994-.0110485*(8/X)-.0009765*(8/X)**2-.0000901*
    +(8/X)**3-.00000009*(8/X)**4+.0000051*(8/X)**5+.0000019*(8/X)**6
111 THETA=CMPLX(TREAL,TIMAG)
    RETURN
    END

```

REFERENCES:

- [1] House H.E. and Tuttle P.D., "Current carrying capacity of ACSR". A.I.E.E trans., vol. PAS. 77, pp. 1169-77, Feb 1958.
- [2] Davidson, G.A., Donoho, T.E., Landrieu, P.R.H., McElhaney, R.T., and Saeger, J.H., "Short-time thermal ratings for bare overhead conductors", IEEE trans; Vol. PAS -88, No. 3. pp. 194-199, March 1969.
- [3] Wong, T.V., Findlay, J.A., and McMurtrie, A.N., "An on-line method for transmission Ampacity evaluation," IEEE trans., Vol. PAS-101, No.2, Feb. 1982.
- [4] Black, W.Z., and Byrd, W.R., "Real-time Ampacity model for overhead lines", IEEE tranbs., Vol. PAS-102, No.7, pp. 2289- 2293, July 1983.
- [5] Stratton, J.A. " Electromagnetic theory", McGraw-hill book Co., Inc. NY & LONDON 1941. pp. 83- 103
- [6] Begg, R.K., "Calculation of electromechanical stress distribution in insulators using finite element method", M.Sc.Engg. Thesis, B.U.E.T. Dhaka. pp. 68-72, May 1987.

- [7] Collin, R.E., "Foundations of Microwave engineering", McGraw-hill Kogakusha, Ltd. pp. 31-33,1966.
- [8] Ramo, S.,Whinnery, J.R. and Vanduzer, T. , "Fields and Waves in Communication Electronics", John Wiley and Sons, Inc. New York, 1965, pp. 291-293.
- [9] Pipes, L.A. , Harvill, L.R. ,"Applied Mathematics for Engineers and Physicists", Third Edition, McGraw-hill book Co. Ltd. , pp. 424-426,1970.
- [10] McLachlan, " Bessel functions for Engineers", 2nd Edition, Oxford at the Clarendon press, 1961, pp. 138.
- [11] William, D. Stevenson Jr. " Elements of Power system analysis", 2nd Edition, Mcgraw-Hill Book Co. Inc. Kogakusha Co. Ltd. Tokyo, 1962 , pp 84-85.
- [12] Dekker, Adrianus, J., "Electrical Engineering Materials", Prentice-Hall of India , New Delhi-110001. 1977, pp. 151.
- [13] British standard 215: Part 1: 1970 specification for Aluminium conductors and Aluminium conductors steel reinforced for overhead power transmission line. pp. 11.
- [14] Distribution Planning Guide, Bangladesh Power Development Board, Dhaka , 1980 , pp. 6-7.

- [15] Rao, Sunil S., "Switchgear and Protection", Khanna Publishers. New Delhi 110006, 1982, pp. 305-308.
- [16] Lester Fink and Kjell Carlsen; " Operating under stress and Strain", IEEE Spectrum, March 1978, pp. 48-50.
- [17] Dekker, A.J., " Electrical Engineering Materials", Prentice-Hall of India, New Delhi-110001, 1977, pp.110
- [18] Simms, J.R., " Overvoltage Protection of Gas Insulated Substations", Power Engineering Journal, July 1987, No.4, IEE, pp. 215-222.
- [19] Weedy, B.M., " Electric Power Systems", 3rd Edition. John Wiley and Sons, Chichester, December 1984, pp. 357-359.

